Naval Research Laboratory

Washington, DC 20375-5320

NRL/MR/6930--19-9852

Reflectance-Based Sensing: Post-Evaluation Analysis of Sensor Responses

Brandy J. White
Jeffrey S. Erickson

Laboratory for the Study of Molecular Interfacial Interactions
Center for Bio/Molecular Science & Engineering

Anthony P. Malanoski

Laboratory for Biosensors and Biomaterials
Center for Bio/Molecular Science & Engineering

Martin H. Moore

Laboratory for the Study of Molecular Interfacial Interactions
Center for Bio/Molecular Science & Engineering

March 28, 2019

REPORT DOCUMENTATION PAGE

Form Approved
OMB No. 0704-0188

1. REPORT DATE *(DD-MM-YYYY)*
28-03-2019

2. REPORT TYPE
Memorandum Report

3. DATES COVERED *(From - To)*
4/01/2018 - 01/16/2018

4. TITLE AND SUBTITLE
Reflectance-Based Sensing: Post-Evaluation Analysis of Sensor Responses

5a. CONTRACT NUMBER

5b. GRANT NUMBER

5c. PROGRAM ELEMENT NUMBER

6. AUTHOR(S)
Brandy J. White, Jeffrey S. Erickson, Anthony P. Malanoski, and Martin H. Moore

5d. PROJECT NUMBER

5e. TASK NUMBER

5f. WORK UNIT NUMBER
69-6594

7. PERFORMING ORGANIZATION NAME(S) AND ADDRESS(ES)
Naval Research Laboratory
4555 Overlook Avenue, SW
Washington, DC 20375-5344

8. PERFORMING ORGANIZATION REPORT NUMBER
NRL/MR/6930--19-9852

9. SPONSORING / MONITORING AGENCY NAME(S) AND ADDRESS(ES)
Office of Naval Research
One Liberty Center
875 North Randolph Street, Suite 1425
Arlington, VA 22203-1995

10. SPONSOR / MONITOR'S ACRONYM(S)
NRL - 6.2

11. SPONSOR / MONITOR'S REPORT NUMBER(S)

12. DISTRIBUTION / AVAILABILITY STATEMENT
DISTRIBUTION STATEMENT A: Approved for public release; distribution is unlimited.

13. SUPPLEMENTARY NOTES

14. ABSTRACT
Here, we report on NRL analysis of data collected during independent evaluation of a prototype reflectance sensing device (version 2.08) and the device associated algorithms. The presented evaluation uses variations within the applied algorithm as well as a manual approach. Discussion of target identification based on these results is also offered.

15. SUBJECT TERMS
Chemical Warfare Agent, Reflectance Based Sensing, Prototype Device, Porphyrin, Colorimetric, Environmental Sensor, Chemical Sensor

16. SECURITY CLASSIFICATION OF: a. REPORT	b. ABSTRACT	c. THIS PAGE	17. LIMITATION OF ABSTRACT	18. NUMBER OF PAGES	19a. NAME OF RESPONSIBLE PERSON
Unclassified Unlimited	Unclassified Unlimited	Unclassified Unlimited	Unclassified Unlimited	72	Brandy J. White

19b. TELEPHONE NUMBER *(include area code)*
(202) 404-6100

Standard Form 298 (Rev. 8-98)
Prescribed by ANSI Std. Z39.18

This page intentionally left blank.

CONTENTS

This page intentionally left blank.

FIGURES

TABLES

EXECUTIVE SUMMARY

In October 2012, the Center for Bio/Molecular Science and Engineering at the Naval Research Laboratory (NRL) began an effort intended to develop wireless sensor networks for real-time monitoring of airborne targets across a broad area. The goal was to apply the spectrophotometric characteristics of porphyrins and metalloporphyrins in a colorimetric array for detection and discrimination of changes in the chemical composition of environmental air samples. The effort encompasses hardware, software, and firmware development as well as development of algorithms for identification of event occurrence and discrimination of targets. Here, we report on NRL analysis of data collected during evaluation of a prototype device (version 2.08) and algorithm by US Army RDECOM Edgewood Chemical Biological Center at the direction of the Joint Project Manager for Nuclear, Biological and Chemical Contamination Avoidance (JPM NBC CA; Solicitation Number W911SR-18-R-CVCA) in support of the Compact Vapor Chemical Agent Detector (CVCAD) program.

This page intentionally left blank.

INTRODUCTION

The Center for Bio/Molecular Science and Engineering at the US Naval Research Laboratory has an ongoing effort focused on development of wireless sensor networks for real-time monitoring of changes in environmental air composition. In order to achieve this aim, small, highly portable, chemical sensors are desired that offer autonomous and long term function. The larger approach was to combine a group of sensors (rather than a single point device) to provide information over a region of interest. Theoretical work has illustrated the potential benefits inherent in using chemical sensor arrays, rather than single devices, for obtaining early warning of threats as well as in gathering information on target distributions and plume movement. [1] The approach employed here uses semi-specific indicators that are differentially responsive across classes of targets rather than using specific sensors or indicators for each target. [2] The color changes in porphyrin and metalloporphyrin indicators upon interaction with targets provide the basis of the detection approach. The use of response profiles across multiple indicators offers the potential for a unique signature or "fingerprint," providing resolution of targets to a class of chemicals and/or to a specific identification depending on the particular array of indicators used. Tracking of reflectance based color changes can be accomplished using low cost, commercially available sensor chips. We have reported on indicator behavior and initial prototype devices previously (Figure 1). [1, 2, 3, 4, 5]

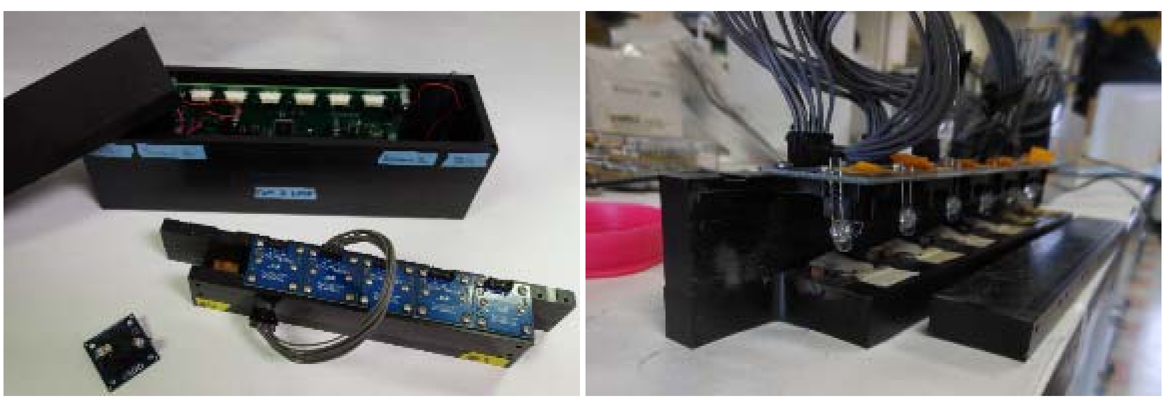

Fig. 1 — The prototype device includes six color sensing breakout boards, a custom control board, fans, and indicator supports with custom housing. The device used for these evaluations required external power and was controlled by a laptop computer.

In addition to hardware, software, and firmware components, a complete system requires development of an algorithm for identifying event occurrence and interpreting indicator responses. Our focus has been on development of sensors for simultaneous monitoring of multiple targets. [1, 2, 5] The ongoing effort has prompted significant exploration of methods to process information from arrays of indicators in order to mitigate the shortcomings of individual elements and to obtain a rapid consensus result from the large amount of available information. While several array based technologies have been developed, they typically require intense data processing (image processing or spectrophotometric analysis), increasing cost and power requirements. This prototype uses a simplified information stream, the reflectance intensity of

Manuscript approved March 6, 2019.

the indicator elements reported as red, green, and blue color values. We have demonstrated selection of effective arrays for specific targets as well as the basic concepts in device utilization. [1, 2] The use of reflectance responses lowers cost and power requirements for the devices. We have established a detection algorithm to support the device. [4, 5] The algorithm effectively compensates for general background interference. It is also computationally simple, keeping device power and memory requirements to a minimum. [4, 5]

For the complete system evaluated under this study, NRL supplied the prototype sensor device with six color sensing breakout boards. LEDs from these boards are aligned to the center of a target placed 25.4 mm away from the board through the use of a custom designed indicator support. The breakout boards are sequentially mounted onto the top rails of this sample holder (machined from chemically resistant Delrin). Paper supported porphyrin indicator coupons bearing six different metalloporphyrins are mounted at the bottom of the holder. Once assembled, the sample holder forms a rectangular tube. Airflow through this tube at is driven by fans, with one mounted at each end. A housing (also Delrin) contains the sample holder; the fans; and a home-built circuit board, providing power management, data acquisition, on-board flash memory, and control of the individual sensors. Custom software (written in LabWindows) was provided to start and stop each experiment and to download data from the instrument. While the device can function autonomously, it was used in conjunction with the laptop (USB connection) for all experiments under this study. Data was acquired by the laptop in real time with reporting on event detection provided within the laptop interface.

METHODS

The original prototype reflectance instrument developed by NRL utilized low cost, commercially available color sensing breakout boards from Parallax, Inc. (model TCS3200-DB, Rocklin, CA), providing a color light-to-frequency integrated circuit from AMS (model TCS3200, Plano, TX), a pair of white LEDs, and an adjustable lens. [1] The device output consists of a stream of digital pulses proportional to the intensity of the color being measured. A custom printed circuit board (PCB) interfaces with and controls six of the commercial color sensors. Communications between the instrument and the computer are via USB; power is supplied through a DC barrel jack. A LabWindows developed software-based graphical user interface (GUI) communicates with the PCB firmware through simple ASCII commands.

The prototype sensor device used here is a slightly modified version of the previously reported NRL device (v2.08). [1, 2, 3, 4, 5] Like that prototype, the heart of this instrument is the TCS-3200-DB breakout board (Parallax) (Figure 1). Airflow through the sample tube at 2.7 CFM is provided by two small 5 VDC fans (Orion Fans, model #OD2510-05HB), one mounted at each end.

The detection algorithm used to identify the occurrence of events has been described previously. [4, 5] A detailed description with implementation approaches is provided in a recent NRL report. [3] Figure 2 provides pseudocode describing this algorithm. The algorithm used with the prototype type in the evaluations described here varies from that described previously on three points. First, the algorithm was incorporated into the LabWindows GUI for real-time analysis and event reporting. This is the first use of the device in this manner. Previously, all algorithm use was in post-experiment offline data analysis. Second, for these trials, it was desired that instrument warm-up time be dramatically reduced as compared to all prior work. The algorithm first populates background windows prior to function with the time duration dependent on sampling increment (total number of points, rather than a time interval). With data collected at 30 s increments, it is necessary to have 120 points for a stable initial condition (Background) with 20 additional points to fill the detection windows (Active and Snap). In order to fill this background buffer, the first 15 minutes of data was entered into the data matrix four times for each data point. The raw data files, therefore, have the same data at 0, 30, 60, and 90 s – the data collected at time 0 s. The data at 120, 150, 180, and 210 s is all the same, the data collected at the 30 s time point. At the 3600 s time entry (900 s), the data resumes the normal pattern of one point collected every 30 s. In the images provided here, this replication of data points has been removed, and the time course has been corrected to reflect actual times. Finally, the conditions for ending positive event identification were changed. The global cooldown was changed from 60 min (120 points) to 5 min (10 points) and the buffering period for the global event was changed from 5 min (10 points) to 1 min (2 points).

It should be noted, unless they are taken from the experiment log, timestamps throughout this document refer to those reported in files provided as prototype device output. Data file time stamps are based on the laptop clock.

We have previously reported on the impact of integration time and sampling interval in the performance noted for these prototype devices (Figure 3). [4, 5] The conditions established for use here were 500 ms integration with a 30 s sampling interval. While this set of conditions will not provide the highest specificity (400 ms preferred), it was expected to provide the greatest sensitivity. Given the targets list used for these trials and the lack of prior data on these targets, it was felt that a greater chance of positive response would be preferred over the higher specificity that may be achieved using 400 ms integration. It should be noted, initial data under this study was collected at 100 ms integration with a 5 s sampling increment. This is not a preferable set of conditions as it is likely to yield both low specificity and low sensitivity. The conditions used can be verified in the header information of the data files. Files Parallax_temp_1.txt through Parallax_temp_8.txt, encompassing the pretest data and all SO_2 and phosgene exposures, were completed with these parameters.

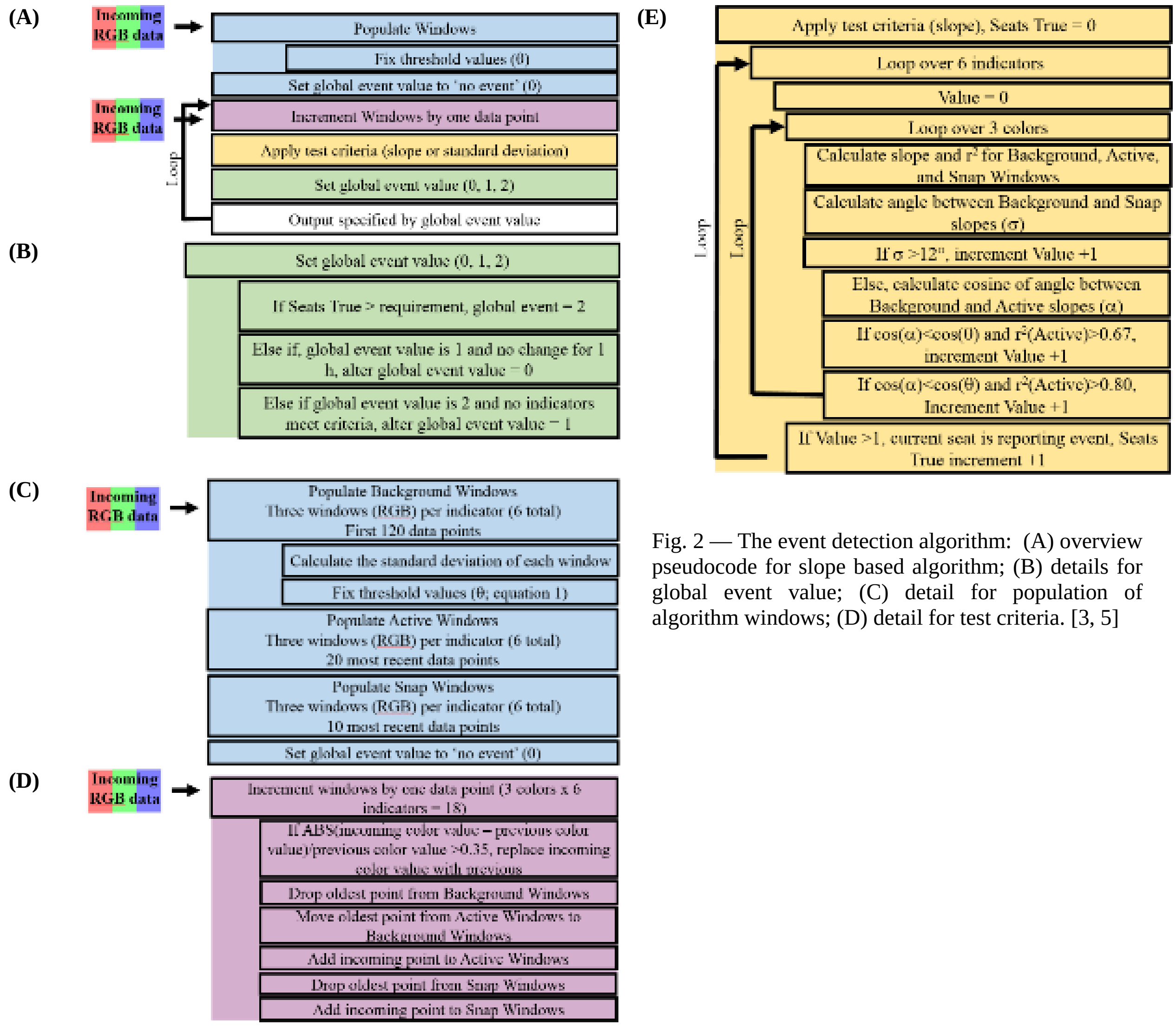

Fig. 2 — The event detection algorithm: (A) overview pseudocode for slope based algorithm; (B) details for global event value; (C) detail for population of algorithm windows; (D) detail for test criteria. [3, 5]

Silver (AgN_4TPP) and zinc (ZnN_4TPP) variants of meso-tetra(4-aminophenyl) porphine (CAS 22112-84-1) and gold (AuDIX), yttrium (YDIX), and thallium (TlDIX) variants of Deuteroporphyrin IX bis ethylene glycol (CAS 6239456-72-5) were prepared by reflux as previously reported. [1, 2] Paper supported porphyrin indicators were prepared using a dip and dry technique. [2, 5] For a 5 x 33 cm swatch, 0.4 mM porphyrin in water (total volume 6 mL) was used. The paper support (WypAll X60) was pulled through this solution and allowed to dry slightly before being pulled through the solution again. This was repeated until all porphyrin solution had been deposited (typically three cycles). Samples were then dried at 100°C before storing in the dark in sealed plastic bags. All six component coupons used under this evaluation were identical with the sequence from seat 1 to seat 6 within the device as follows: N_4TPP, AgN_4TPP, ZnN_4TPP, AuDIX, TlDIX, YDIX.

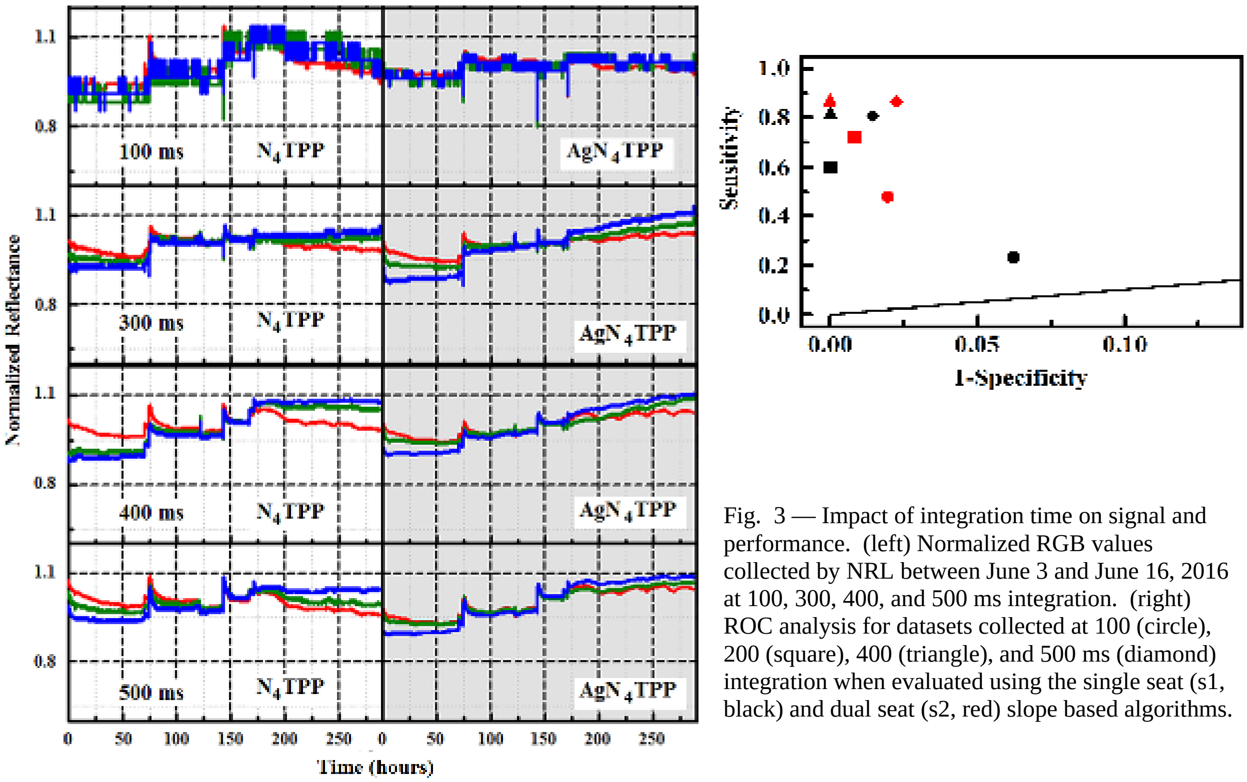

Fig. 3 — Impact of integration time on signal and performance. (left) Normalized RGB values collected by NRL between June 3 and June 16, 2016 at 100, 300, 400, and 500 ms integration. (right) ROC analysis for datasets collected at 100 (circle), 200 (square), 400 (triangle), and 500 ms (diamond) integration when evaluated using the single seat (s1, black) and dual seat (s2, red) slope based algorithms.

RESULTS

In all presented datasets, initiation of exposures is indicated by dashed black lines. These lines are marked at the start of the chemical stream rather than for the time of chamber equilibrium. Gray shaded areas of the graph indicate that the device is in a positive reporting condition based on post-experiment, offline data analysis; green regions are used to indicate the specific indicators involved in the event.

Pretest data is provided in Figures 4, 5, 6, and 7. No details were provided for collection of this data or positive control exposures completed during this time. Temperature and humidity data were not included. In the absence of these details, little analysis can be completed. The characteristic noise levels for 100 ms integration data collection are apparent. The device otherwise appears to be functioning normally.

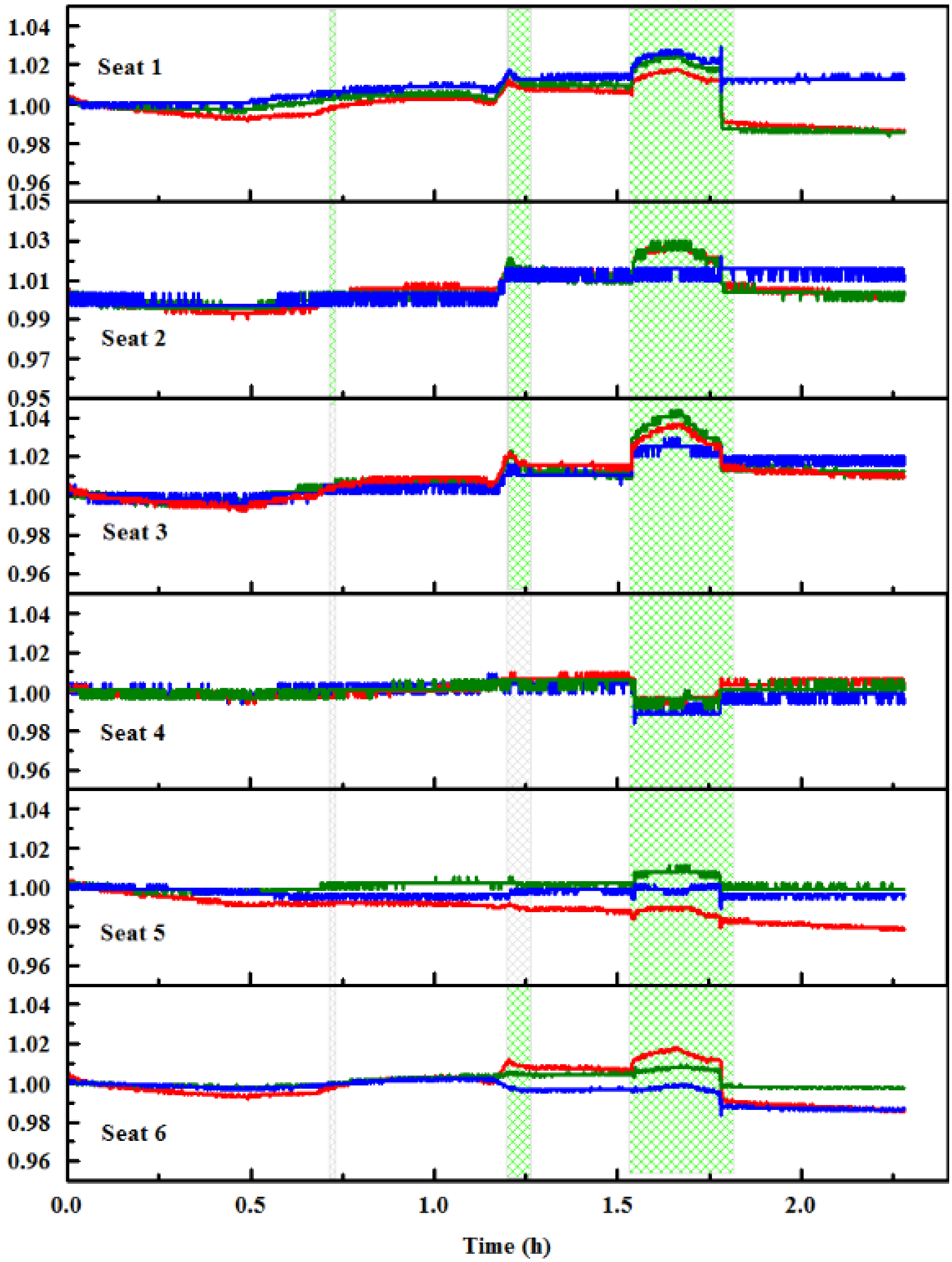

Fig. 4 — Pre-test Data. This data was collected on 29 October 2018 between 13:30 and 15:47. No information was provided for exposures or positive control tests during this period. No humidity data was collected. Collected at 100 ms with a 5 s sampling increment. Filename: parallax_temp_1.txt

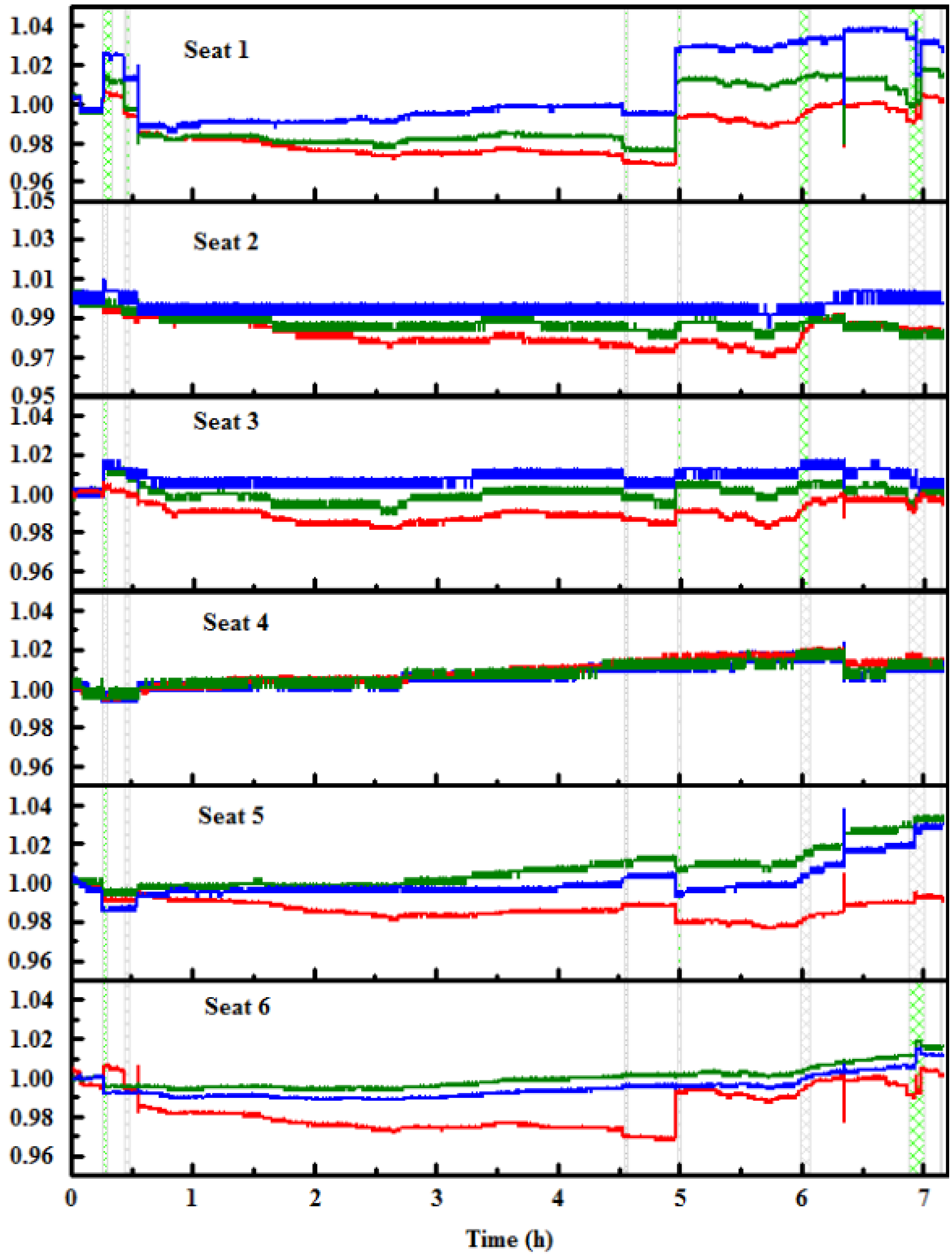

Fig. 5 — Pre-test Data. This data was collected on 31 October 2018 between 08:36 and 15:46. No information was provided for exposures or positive control tests during this period. No humidity data was collected. Collected at 100 ms with a 5 s sampling increment. Filename: parallax_temp_2.txt

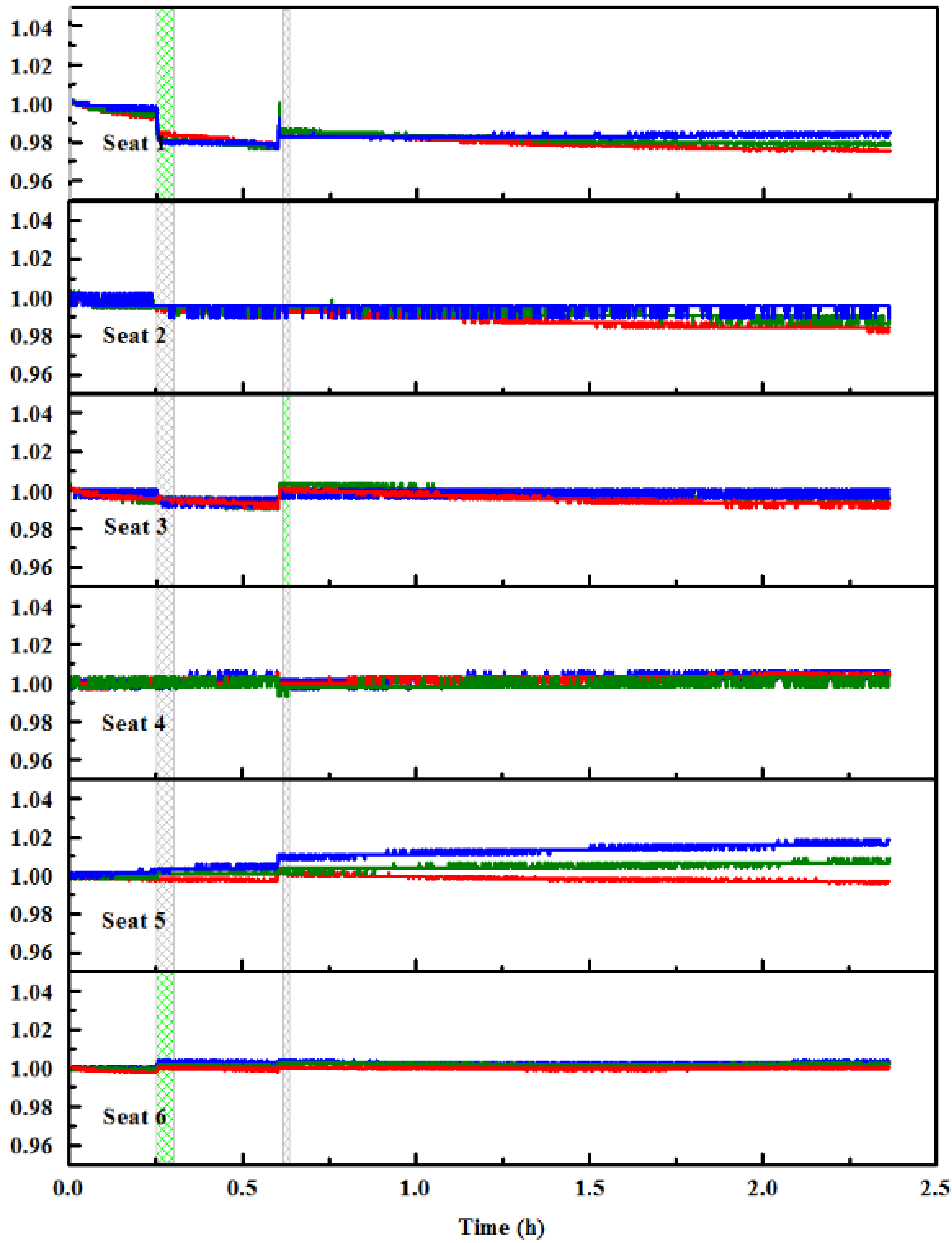

Fig. 6 — Pre-test Data. This data was collected on 05 November 2018 between 13:05 and 15:27. No information was provided for exposures or positive control tests during this period. No humidity data was collected. Collected at 100 ms with a 5 s sampling increment. Filename: parallax_temp_3.txt

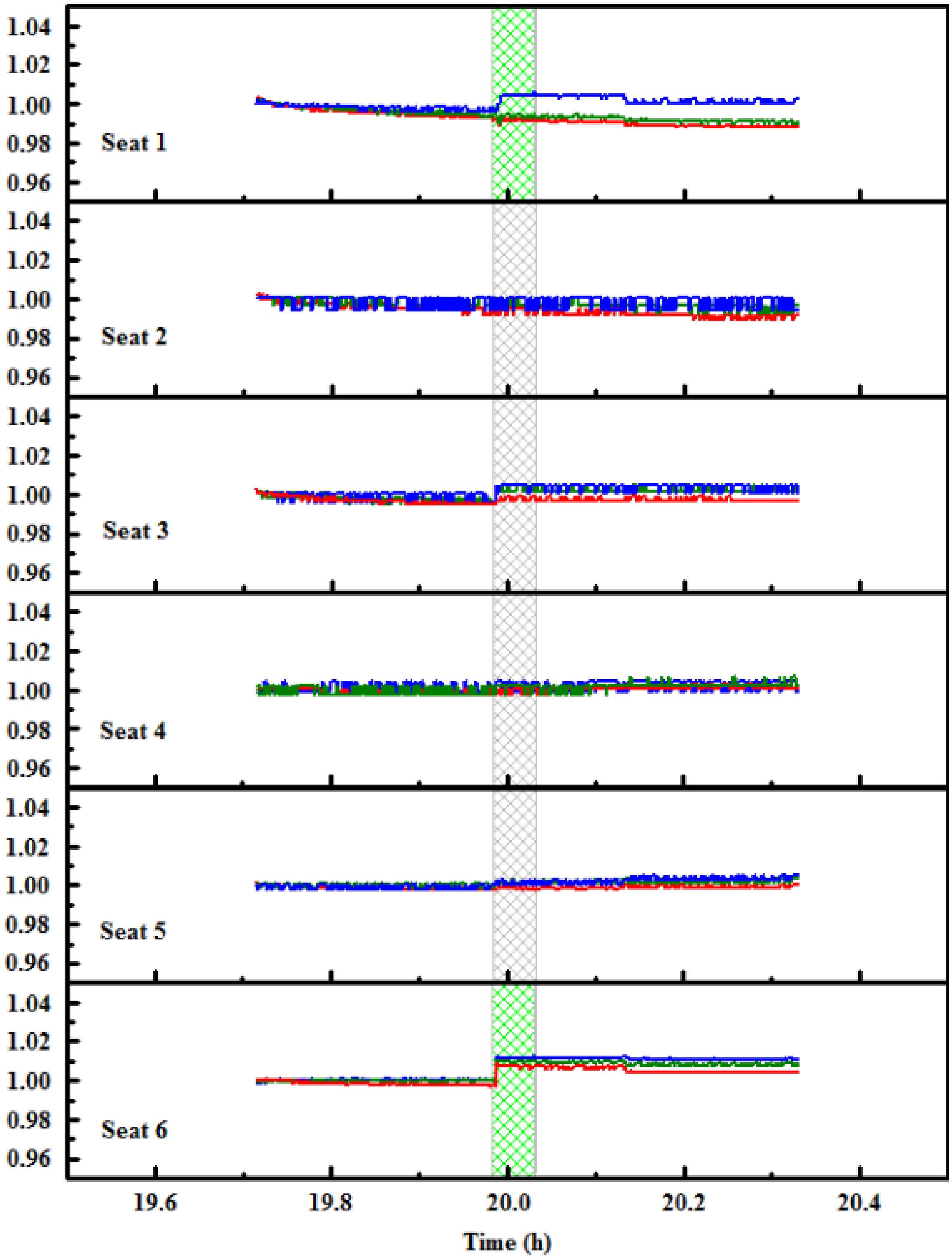

Fig. 7 — Pre-test Data. This data was collected on 06 November 2018 between 08:48 and 09:25. No information was provided for exposures or positive control tests during this period. No humidity data was collected. Collected at 100 ms with a 5 s sampling increment. Filename: parallax_temp_4.txt

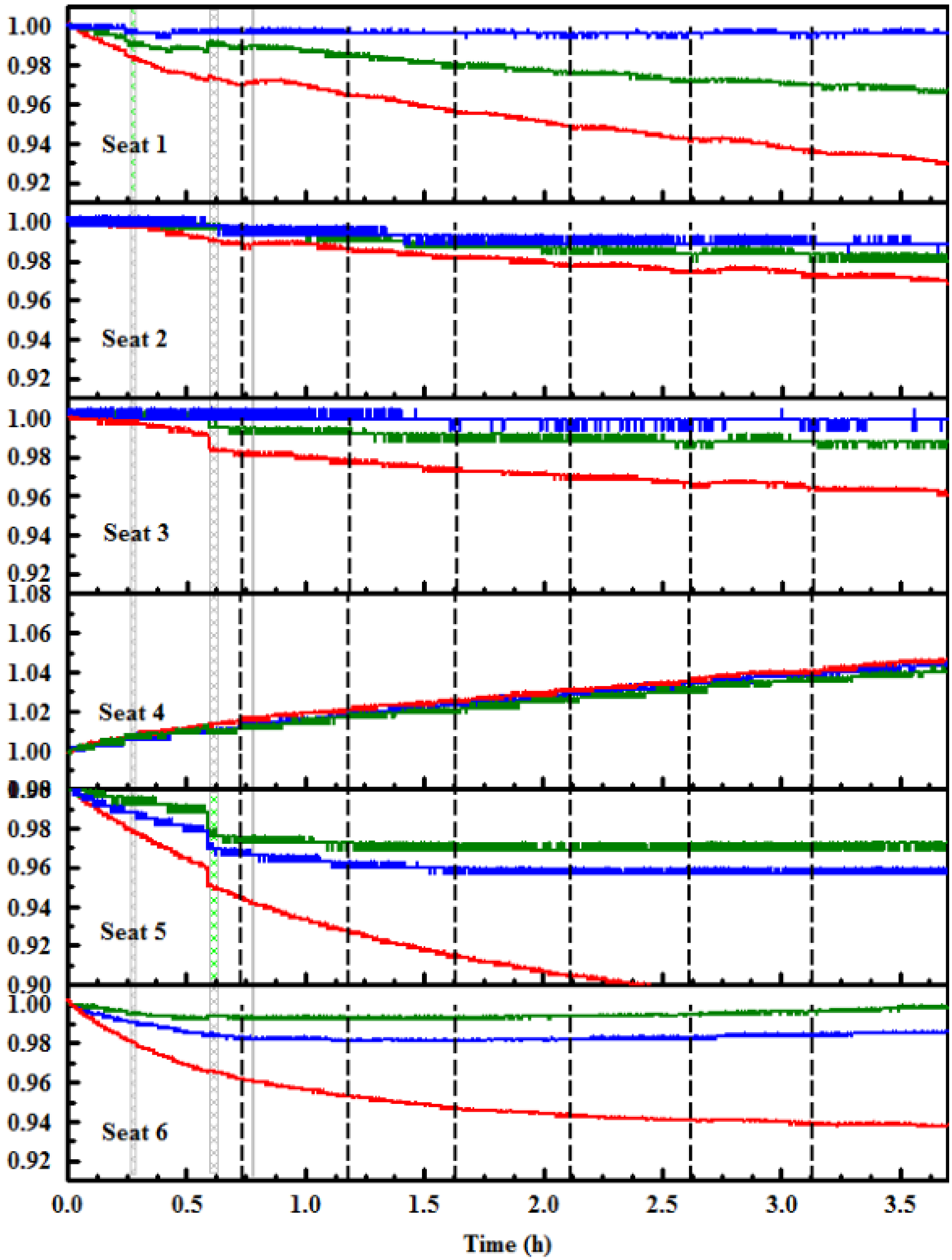

Fig. 8 — SO_2 Exposures. This data was collected on 06 November 2018 between 10:13 and 13:55. Dashed lines indicate the beginning of chemical stream flow, 1.5 ppm SO_2. Humidity and temperature are provided in Figure 9. Collected at 100 ms with a 5 s sampling increment. Filename: parallax_temp_5.txt

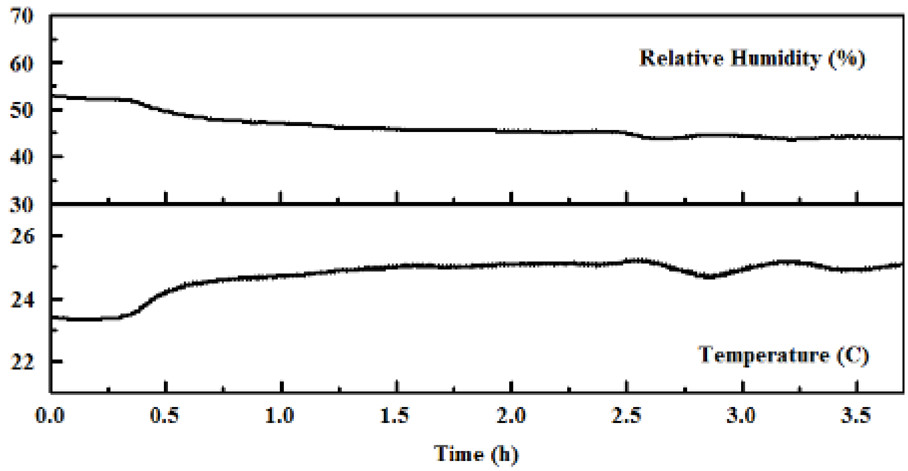

Fig. 9 — SO_2 Exposures. The temperature and humidity trends provided here were those observed during collection of data presented in Figure 8 from 06 November 2018 between 10:13 and 13:55.

SO_2 exposures used 1.5 (Figure 8) and 30 ppm (Figure 10) levels. These exposures used the 100 ms integration with a 5 s sampling increment. For the low target concentration, only a single positive response was associated with SO_2 exposure. It is unclear whether the reported responses prior to target exposures were the result of a positive control test or represent noise. The positive response window beginning at 0.6 h may be related to the sudden change in temperature and humidity at that time. With the low signal provided by 100 ms integration, it is difficult to make any further determinations from this dataset. The data from high concentration SO_2 exposures of Figure 10 suffer from the same limitations, also using the 100 ms integration time. Early positive response windows again appear to be associated with changes in temperature and humidity, but this may be coincidental. Table 1 provides a response summary. Where appropriate, the time to response has been calculated based on times noted in the Experiment Log for beginning of chemical stream start as well as for the time at which the chamber reached equilibrium.

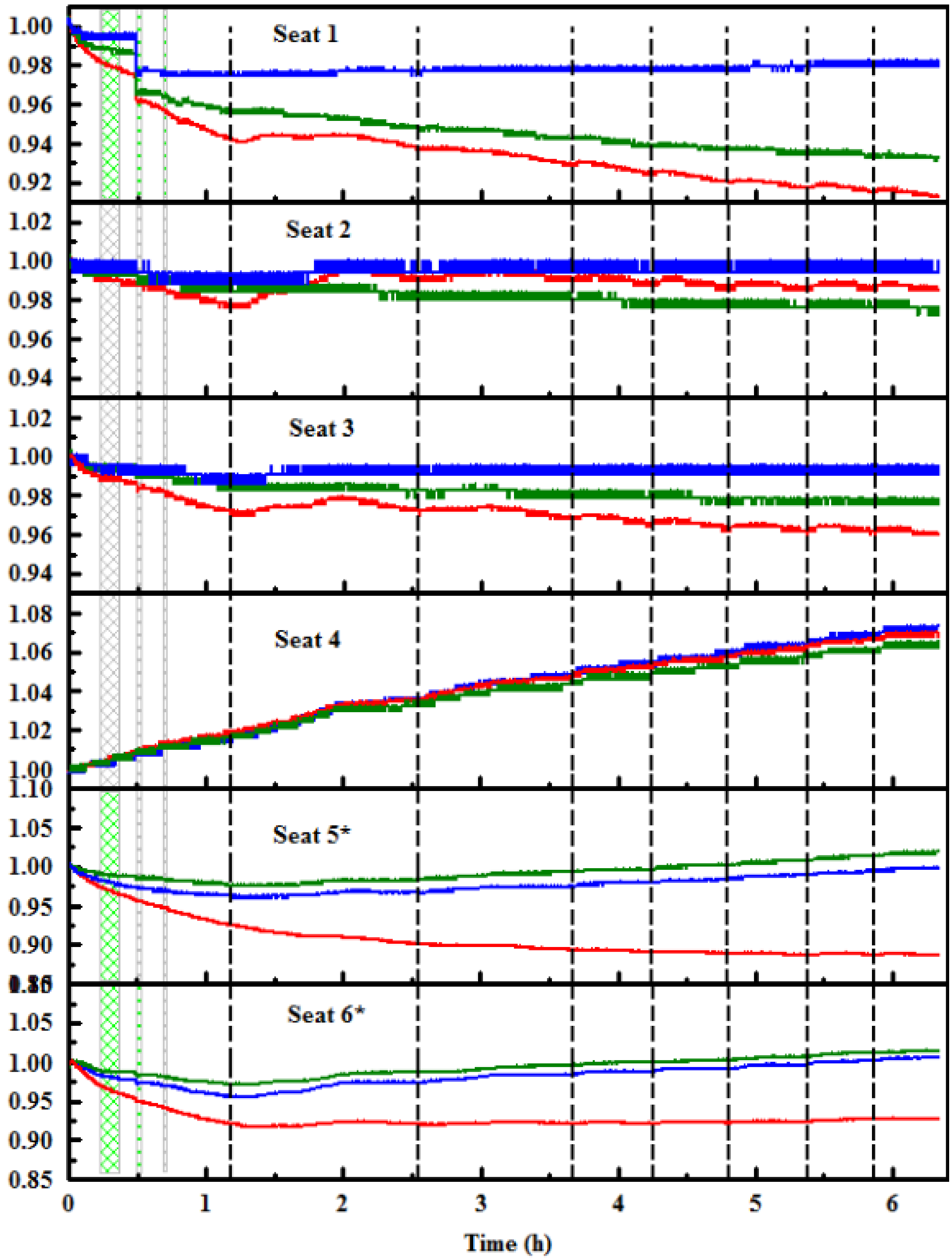

Fig. 10 — SO_2 Exposures. This data was collected on 07 November 2018 between 10:15 and 16:35. Dashed lines indicate the beginning of chemical stream flow, 30 ppm SO_2. Humidity and temperature are provided in Figure 11. Collected at 100 ms with a 5 s sampling increment. Filename: parallax_temp_6.txt

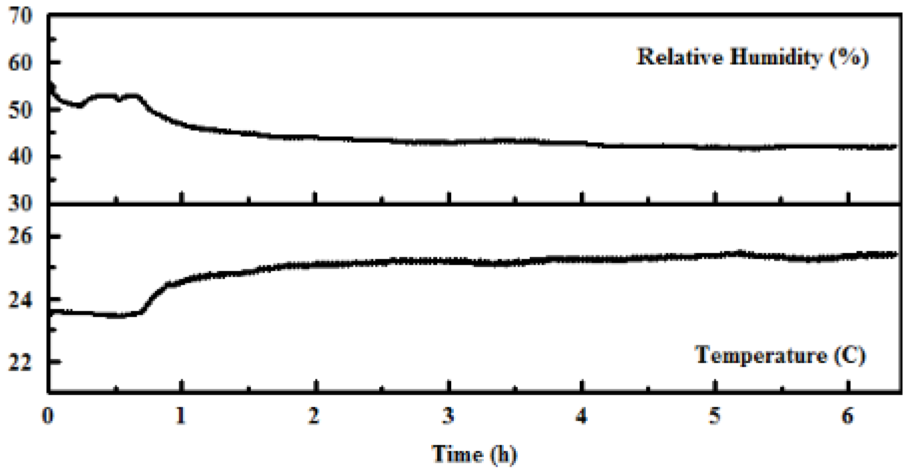

Fig. 11 — SO_2 Exposures. The temperature and humidity trends provided here were those observed during collection of data presented in Figure 10 for 07 November 2018 between 10:15 and 16:35.

Phosgene exposures used 1.2 (Figure 12) and 7.4 ppm (Figure 13) levels. These exposures used the 100 ms integration parameter with a 5 s sampling increment. As noted for the SO_2 datasets, there are positive responses early in the run, prior to beginning exposures. For the low target concentration, there are two initial exposures that lack an ETO (referee) concentration, the prototype response to these exposures was at seat 1 only. Exposures three and four of the series have referee concentrations at 1.5 ppm and show responses at seats 1, 2, and 5. Exposure five has a referee concentration at 2 ppm and shows positive responses at seats 1, 2, 3, and 5. Exposure six is also at 2 ppm; though movement can be seen in the data, it was less than that required for a positive response. This would be expected to result in detection at the higher integration setting (500 ms); however, the changes upon exposure for the remaining two cycles (1.5 ppm) are of smaller intensity. The indicators were likely saturating or becoming damaged at this point in the cycle.

Similar behaviors are noted in the high concentration phosgene data (Figure 14). The initial 7.5 ppm (referee) exposure produces a large change at seats 1, 2, 3, and 5. Subsequent exposures at 2.5, 3, and 3.5 ppm produce changes at seats 1, 2, and 3 that would likely yield positive responses for the 500 ms parameter with the 3.5 ppm exposures producing positive responses through the end of the cycle. Table 1 provides a response summary.

Table 1 – Algorithm Performance, SO_2 and Phosgene at 100 ms

Target	Duration (h)	Exposures	Events	Exposure Associated	Avg Time to Response (min)$^{\gamma}$	Avg Time to Response (min)*
SO2, 1.5 ppm	3.70	6	3	1	-5	3
SO2, 30 ppm	6.33	7	3	0		
Phosgene, 1.2 ppm	5.40	8	9	6	-6	3
Phosgene, 7.4 ppm	6.50	8	8	5	-8	2

*Time to response calculated based on algorithm output from chamber equilibrium time. $^{\gamma}$ Time to response calculated based on algorithm output from chemical stream start.

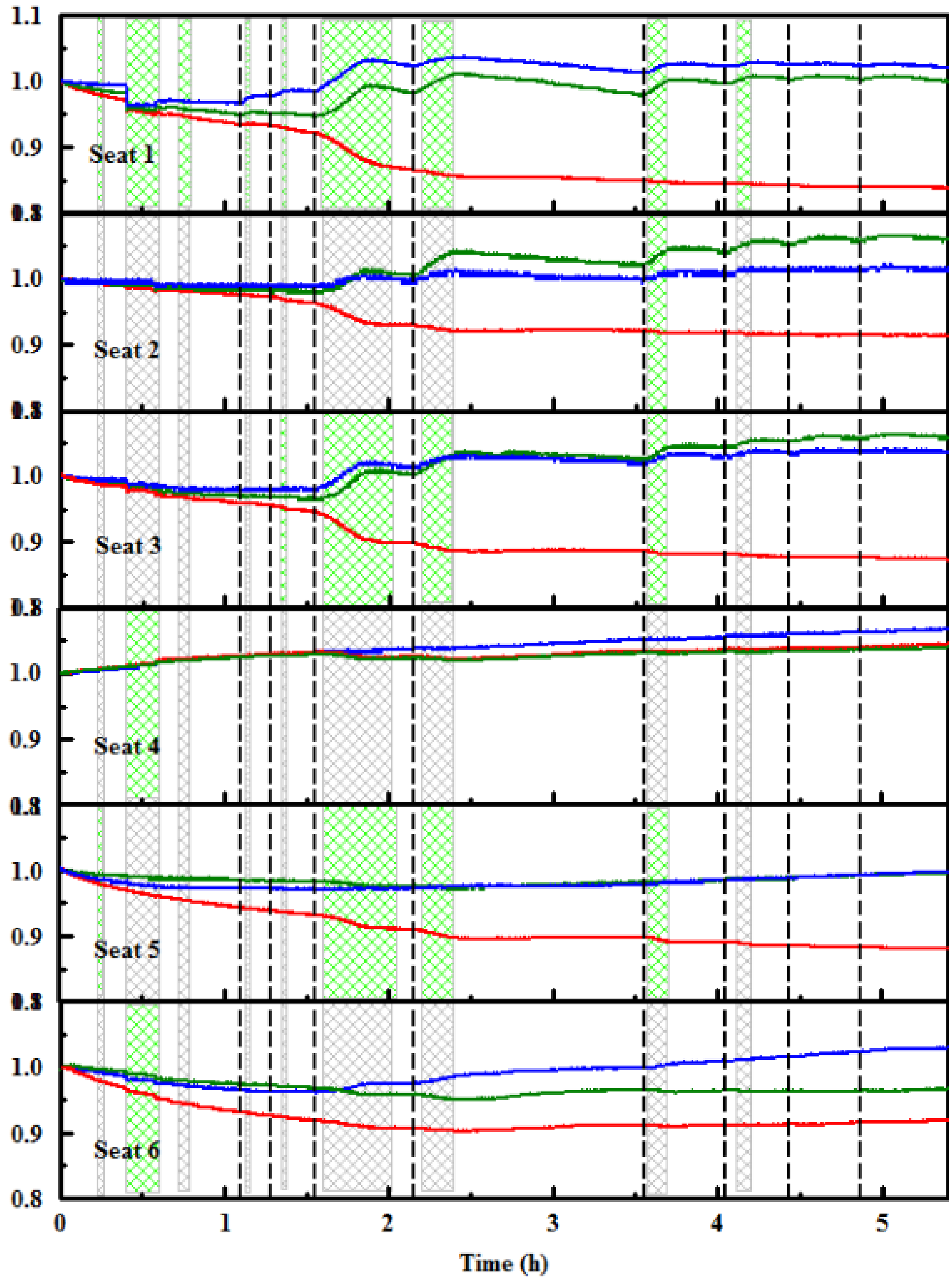

Fig. 12 — Phosgene Exposures. This data was collected on 13 November 2018 between 09:20 and 14:44. Dashed lines indicate the beginning of chemical stream flow, 1.2 ppm phosgene. Humidity and temperature are provided in Figure 14. Collected at 100 ms with a 5 s sampling increment. Filename: parallax_temp_7.txt

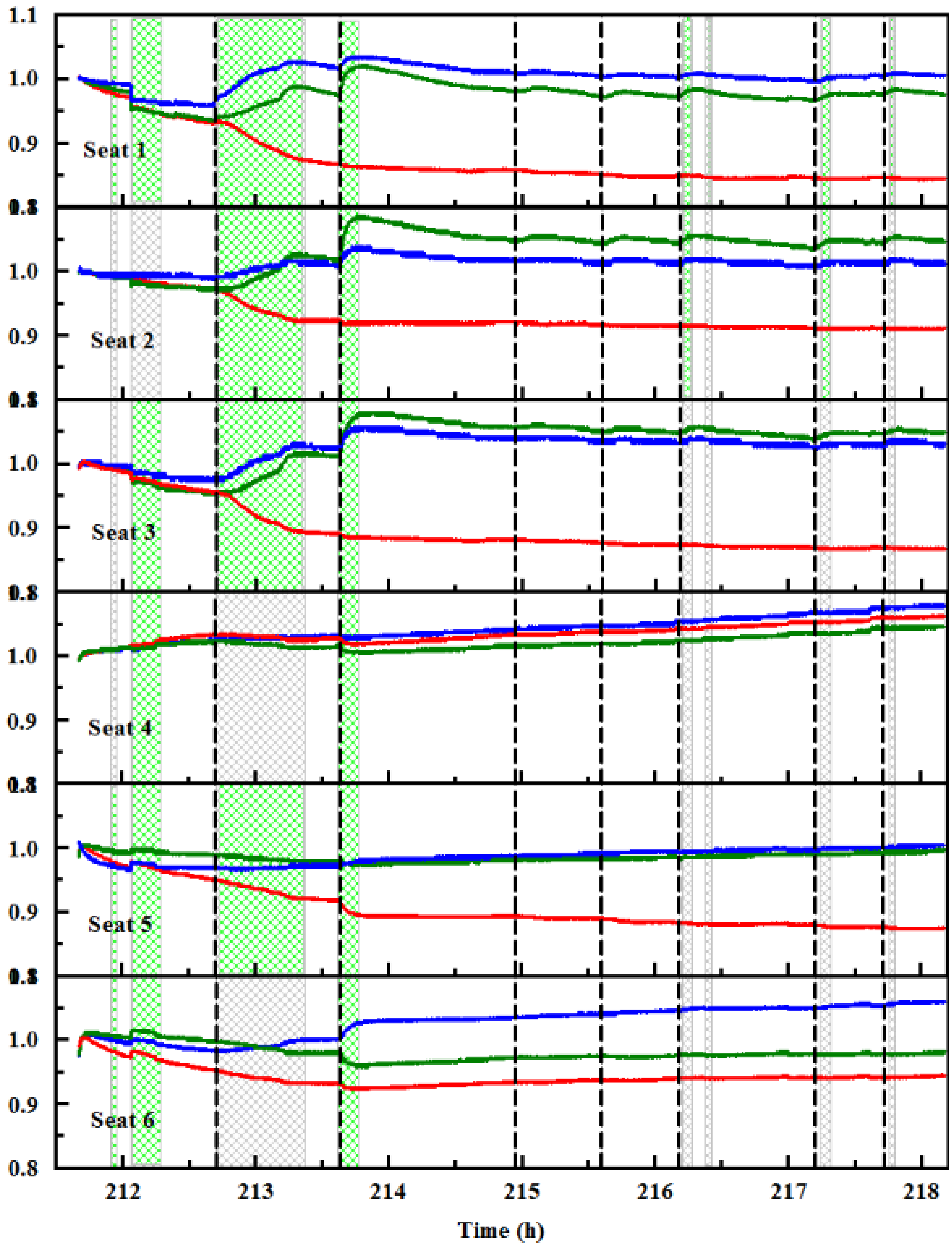

Fig. 13 — Phosgene Exposures. This data was collected on 14 November 2018 between 08:46 and 15:26. Dashed lines indicate the beginning of chemical stream flow, 7.4 ppm phosgene. Humidity and temperature are provided in Figure 15. Collected at 100 ms with a 5 s sampling increment. Filename: parallax_temp_8.txt

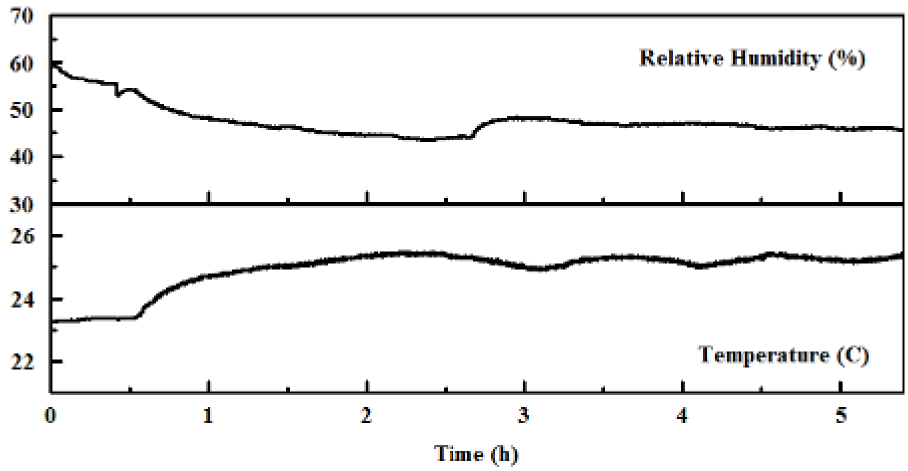

Fig. 14 — Phosgene Exposures. The temperature and humidity trends provided here were those observed during collection of data presented in Figure 12 collected on 13 November 2018 between 09:20 and 14:44.

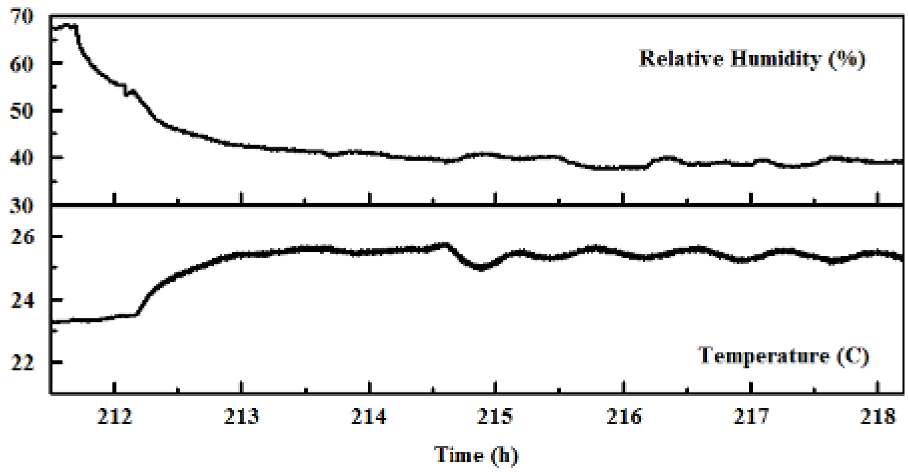

Fig. 15 — Phosgene Exposures. The temperature and humidity trends provided here were those observed during collection of data presented in Figure 13 collected on 14 November 2018 between 08:46 and 15:26.

Ethylene oxide exposures used 78 (Figure 16 and 17) and 361 ppm (Figure 19) levels. These exposures used 500 ms integration with a 30 s sampling increment. As noted for the datasets above, there are events identified early in the data collection, prior to beginning of exposures. The cause is unclear; further discussion of this point is provided in the Discussion. Referee concentrations for the exposures in Figure 16 were 77.5, aborted, 88, 88, and 86.5 ppm. An event was triggered for the fourth exposure on seats 1 and 3, no other responses were noted. The second day of 78 ppm exposures (Figure 17) included two aborted runs and exposures at 82.5 and 79.5 ppm. No alarms in response to target exposure were noted. High concentration ethylene oxide exposures (Figure 19) were completed at 350 to 420 ppm and produced no positive responses. Table 2 provides a response summary. Where appropriate, the time to response has been calculated based on times noted in the Experiment Log for beginning of chemical stream start as well as for the time at which the chamber reached equilibrium.

Table 2 – Algorithm Performance, Ethylene Oxide at 500 ms

Target	**Duration (h)**	**Exposures**	**Events**	**Exposure Associated**	**Avg Time to Response (min)$^{\gamma}$**	**Avg Time to Response (min)***
Ethylene oxide, 78 ppm	6.05	5	5	1	-1	2
Ethylene oxide, 78 ppm	4.25	4	3	0		
Ethylene oxide, 361 ppm	6.73	6	2	0		

*Time to response calculated based on algorithm output from chamber equilibrium time. $^{\gamma}$ Time to response calculated based on algorithm output from chemical stream start.

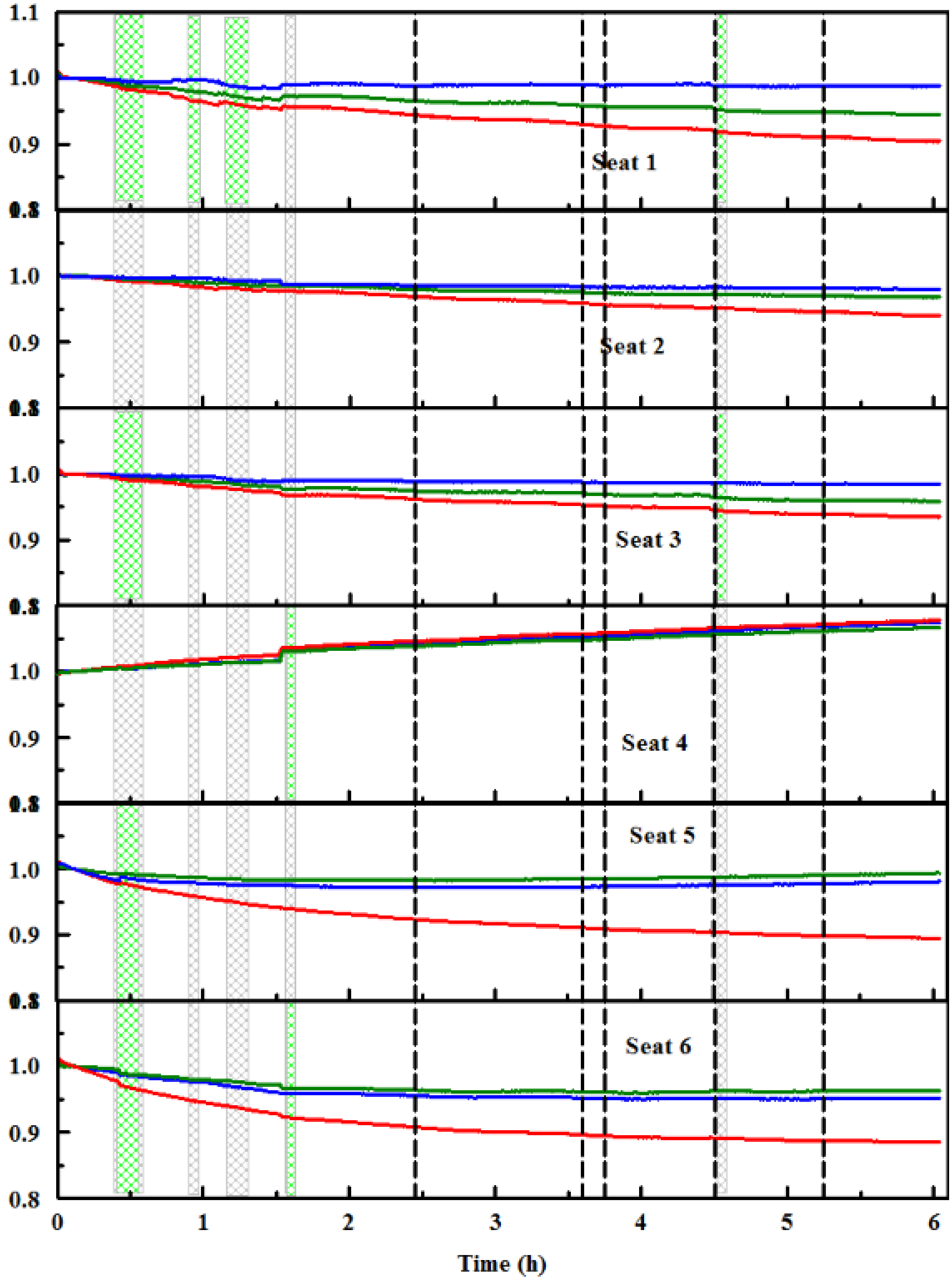

Fig. 16 — Ethylene Oxide Exposures. This data was collected on 19 November 2018 between 09:38 and 15:41. Dashed lines indicate the beginning of chemical stream flow, 78 ppm ethylene oxide. Humidity and temperature are provided in Figure 18. Filename: parallax_temp_9.txt

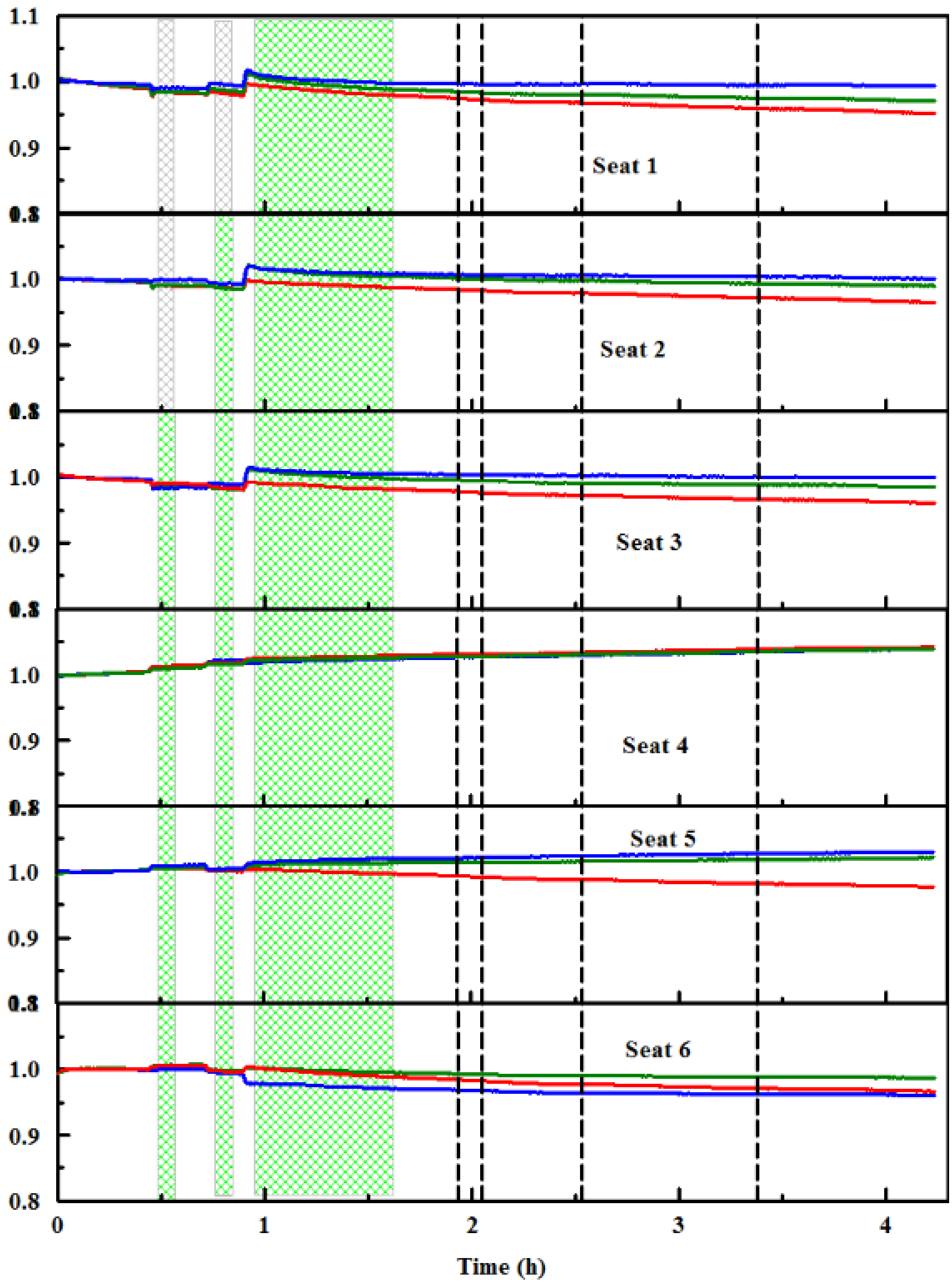

Fig. 17 — Ethylene Oxide Exposures. This data was collected on 20 November 2018 between 08:45 and 13:00. Dashed lines indicate the beginning of chemical stream flow, 78 ppm ethylene oxide. Humidity and temperature are provided in Figure 18. Filename: parallax_temp_10.txt

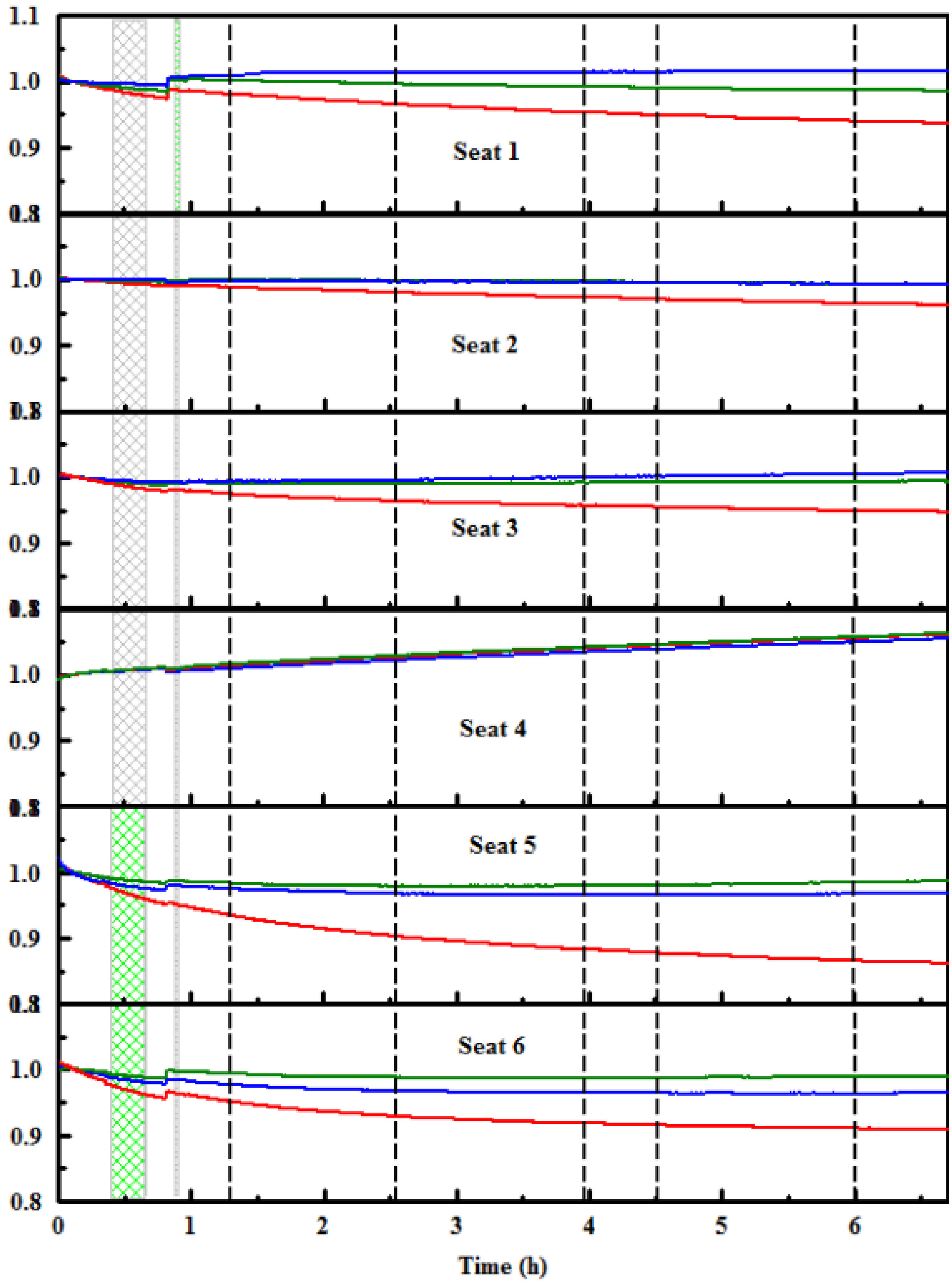

Fig. 18 — Ethylene Oxide Exposures. This data was collected on 26 November 2018 between 09:18 and 16:02. Dashed lines indicate the beginning of chemical stream flow, 361 ppm ethylene oxide. Humidity and temperature are provided in Figure 20. Filename: parallax_temp_11.txt

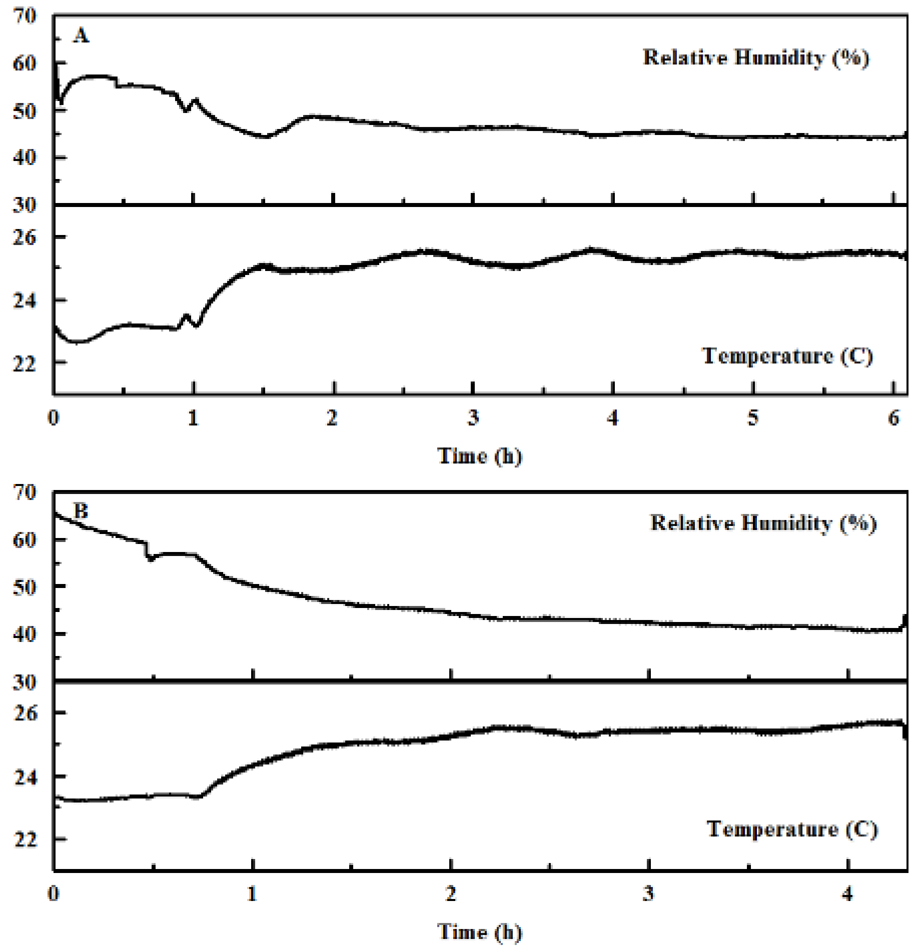

Fig. 19 — Ethylene Oxide Exposures. The temperature and humidity trends provided here were those observed during collection of data presented in Figures 16 and 17 collected on (A) 19 November 2018 between 08:46 and 15:26 and (B) 20 November 2018 between 08:45 and 13:00.

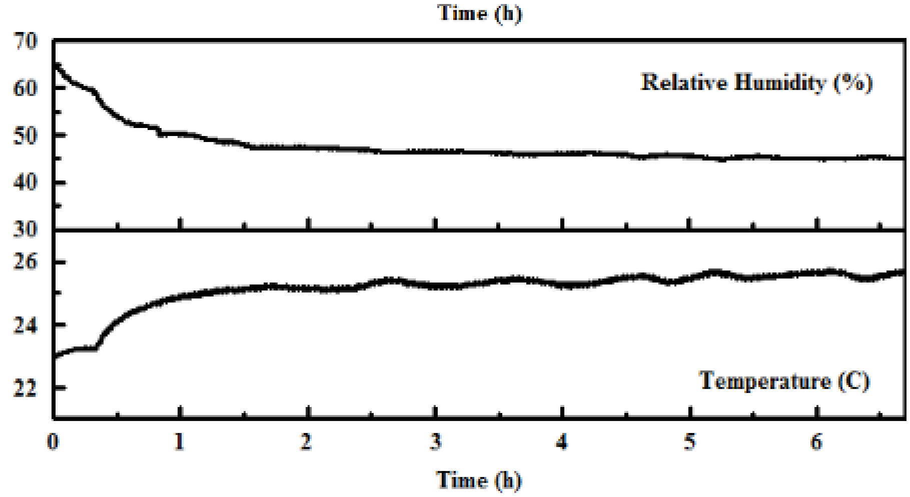

Fig. 20 — Ethylene Oxide Exposures. The temperature and humidity trends provided here were those observed during collection of data presented in Figure 18 collected on 26 November 2018 between 09:18 and 16:02.

On November 28, an issue was reported. The device was giving a time out error and would not communicate with the laptop. While attempting to reset the device to address this issue, component failure was noted based on the absence of indicator light illumination on the main board (#1). It was determined that the power plug connection had been damaged. The main control board was replaced with a one-to-one component swap to address this issue (#2). On 30 November, additional issues were reported (Figure 21) with the device reporting data that was unrelated to expected reflectance values. Troubling shooting a similar board was undertaken by NRL. It was found that the MIC5219 power supply that goes into the

Parallax boards was the wrong part on the device supplied. The part was supplied by Mouser Electronics with packaging that indicated 5 V. Under a microscope, 3.3 can be seen on the part. A probe of the output voltage lines indicated +3.3 V. It was found that, while boards from an older build correctly used the +5 V component, newer devices had the +3.3 V part. The main control board was again replaced (#3, 04 December); a board from the older build was used. During installation of the new board, the connector for seat 1 was torqued off of the control board. This board (#3), measuring only seats 2 through 6, was used for data collection on 04 December. Another board was supplied (#4) to replace #3; it was installed on 06 December. On 12 December, following Cl_2 exposures, this board failed (#4). The failure was likely a result of corrosion on the main board; it is not isolated from the targets. The previous board (#3) was reinstalled on 13 December for use during the remainder of the trails.

Between the original device failure (#1) on 28 November and installation of the new functional board (#3), collection of data for GB exposures was completed. This data is exclusively noise (Figure 22).

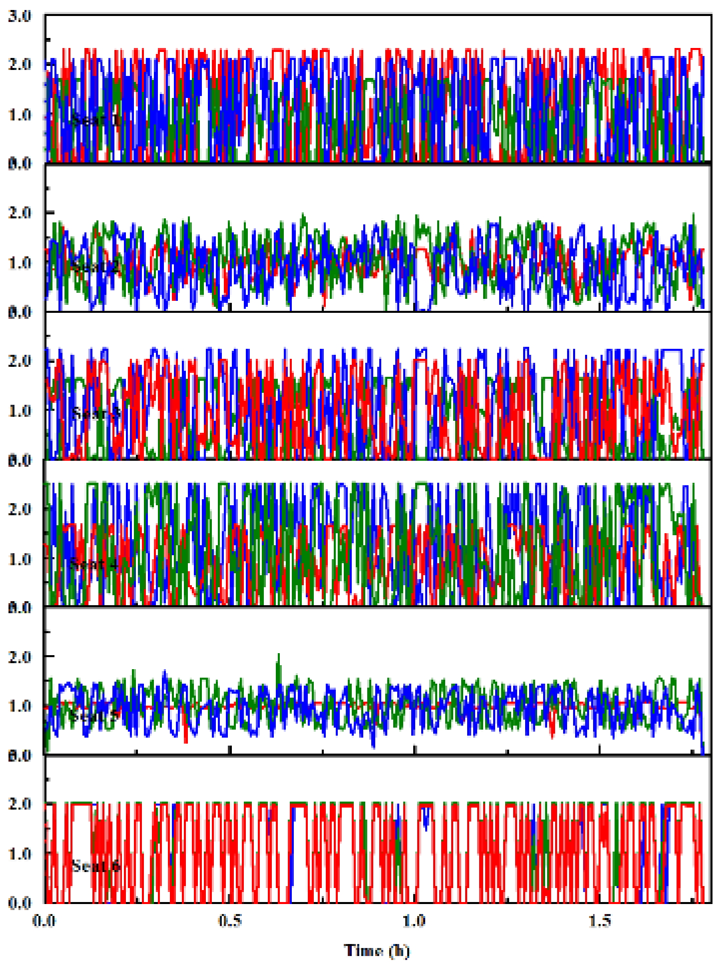

Fig. 21 — Post Board Swap. This data was collected on 30 November 2018 between 09:44 and 12:16. Filename: parallax_temp_16.txt

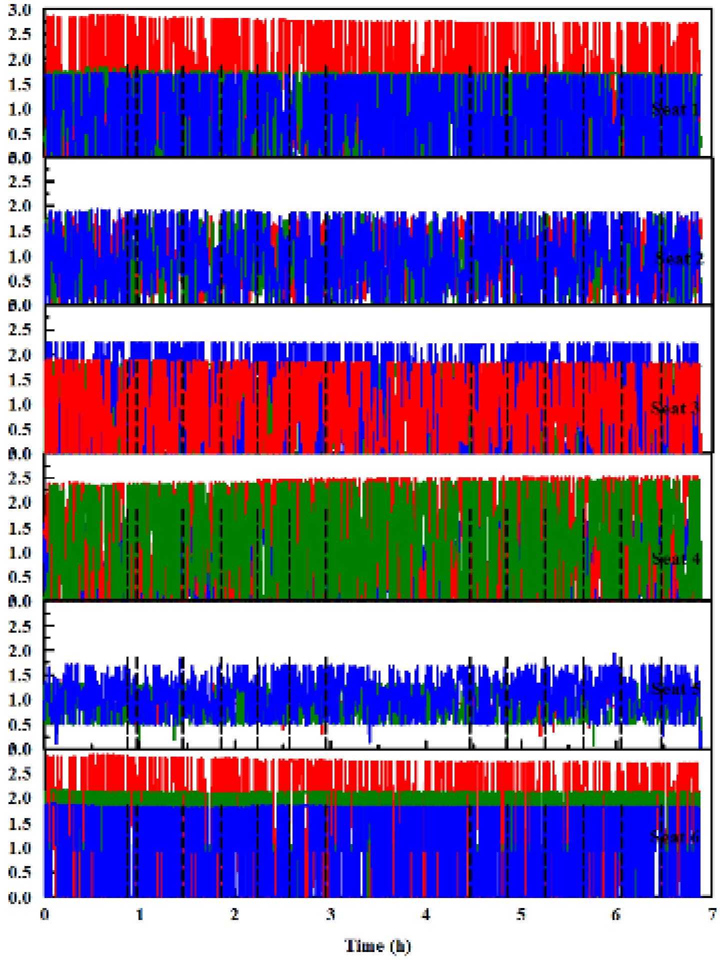

Fig. 22 — GB Exposures. This data was collected on 03 December 2018 between 08:37 and 16:15. Dashed lines indicate the beginning of chemical stream flow, 0.14 and 0.22 mg/m^3 GB. Humidity and temperature are provided in Figure 23. Filename: parallax_temp_19.txt

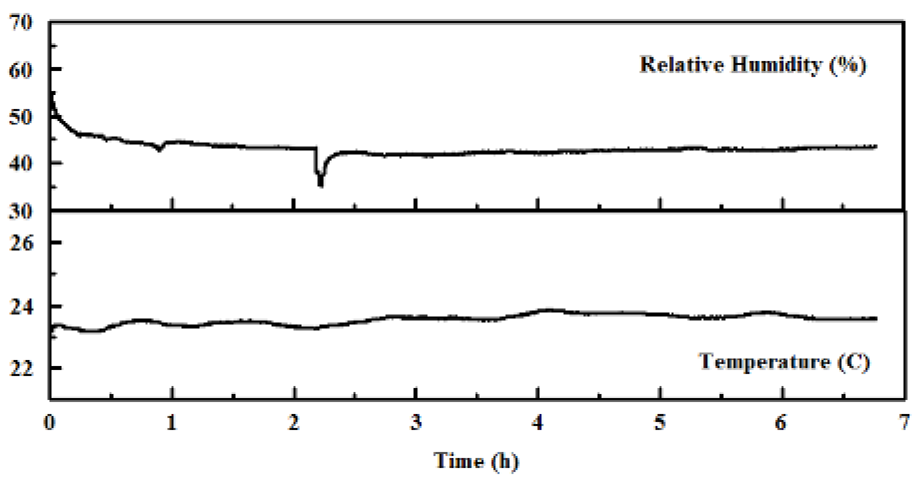

Fig. 23 — GB Exposures. The temperature and humidity trends provided here were those observed during collection of data presented in Figure 22 collected on 03 December 2018 between 08:37 and 16:15.

Up to this point, NRL's post experiment data analysis agreed with that reported in real-time during the trial. For the Simple Green exposure cycle (Figure 24), the experiment log indicates that an event was triggered early in the trial and that it failed to clear through much of the early part of the trail. Positive responses were, as a result, indicated for three of the six exposures. The device generated log of events for this trial indicates a different set of responses. Offline analysis provides a similar series to that of the device generated log with some variation on the seats involved. Table 3 provides a summary of these sets of responses. The experiment immediately following this cycle, exposures to GB with Simple Green, did not yield these types of discrepancies (Table 4).

Post experiment analysis (Table 3 & Figure 24) indicates short duration early events, as noted for other experiment cycles, followed by two positive responses to Simple Green exposures. Both responses are associated with seat 4. The third exposure was completed while the device was alarming to the second exposure, but exposures four through six did not produce a response by the device. There is a large response that can be seen in the figure just before 1.5 h (Figure 24). While this is not associated with a recorded event, it shows the distinct form expected for a target response. The experiment log has an entry prior to the first exposure that is simply H2 with no times or additional information. This H2 occurs here and a single time in the GB only dataset. Because this device was not functioning during collection of GB data, there is no point of comparison for this large change. For the GB exposures completed with Simple Green, seats 5 and 6 indicated several times prior to the first exposure. Following that time period, a positive indication was given for only the first GB exposure. This response involved all of the seats except 5. In the graph, this response can be distinctly seen at the 2 hour mark. Algorithm summaries are provided in Table 5. Where appropriate, the time to response has been calculated based on times noted in the Experiment Log for beginning of chemical stream start as well as for the time at which the chamber reached equilibrium.

Table 3 – Simple Green Exposures and Event Indication. Exposure begin and end times reflect initiation of the chemical stream (not chamber equilibrium) and equilibrium of the chamber to no compound, respectively.

Type	**Begin**		**End**		**Seats**
Start	12:30				
Post Experiment		12:54		12:57	5, 6
Device Log		12:55		12:55	5
Post Experiment		13:18		13:25	2, 4, 6
Device Log		13:20		13:25	2, 4
Post Experiment		14:12		14:16	2, 3, 4
Device Log		14:12		14:25	2, 3, 4
Exposure	14:32		14:37		
Post Experiment		14:33		14:46	4
Device Log		14:33		14:46	4
Experiment Log		14:37		>14:51	
Exposure	14:51		14:56		
Experiment Log		14:56		>15:04	
Device Log		14:56		15:06	4
Post Experiment		14:56		15:06	4
Exposure	15:05		15:11		
Experiment Log		15:06		15:13	
Exposure	15:22		15:27		
Exposure	15:37		15:50		
Exposure	15:51		15:58		
End			16:02		

Table 4 – GB with Simple Green Exposures and Event Indication. Exposure begin and end times reflect initiation of the chemical stream (not chamber equilibrium) and equilibrium of the chamber to no compound, respectively.

Type	**Begin**		**End**		**Seats**
Start	08:43				
Post Experiment		9:07		9:22	5, 6
Device Log		9:08		9:22	5, 6
Post Experiment		9:35		9:36	6
Device Log		9:35		9:36	6
Device Log		9:43		10:02	6
Post Experiment		10:00		10:02	6
Post Experiment		10:13		10:17	6
Experiment Log		<10:17		?	
Device Log		10:13		10:17	5
Exposure	10:17		10:43		
Post Experiment		10:45		10:48	1, 2, 3, 4, 6
Device Log		10:45		10:48	1, 2, 3, 4, 6
Experiment Log		10:47		10:56	
Exposure	11:11		11:12		
Exposure	11:36		11:38		
Exposure	13:12		13:14		
Exposure	13:43		13:45		
Exposure	14:04		14:05		
Exposure	14:33		14:37		
End			15:12		

Table 5 – Algorithm Performance, GB and Simple Green at 500 ms

Target	**Duration (h)**	**Exposures**	**Events**	**Exposure Associated**	**Avg Time to Response (min)$^{\gamma}$**	**Avg Time to Response (min)***
Simple Green	3.53	6	5	3	4	3
GB, 0.22 mg/m^3 with Simple Green	6.48	7	5	1	--	4

*Time to response calculated based on algorithm output from chamber equilibrium time. $^{\gamma}$ Time to response calculated based on algorithm output from chemical stream start. -- indicates unavailable data.

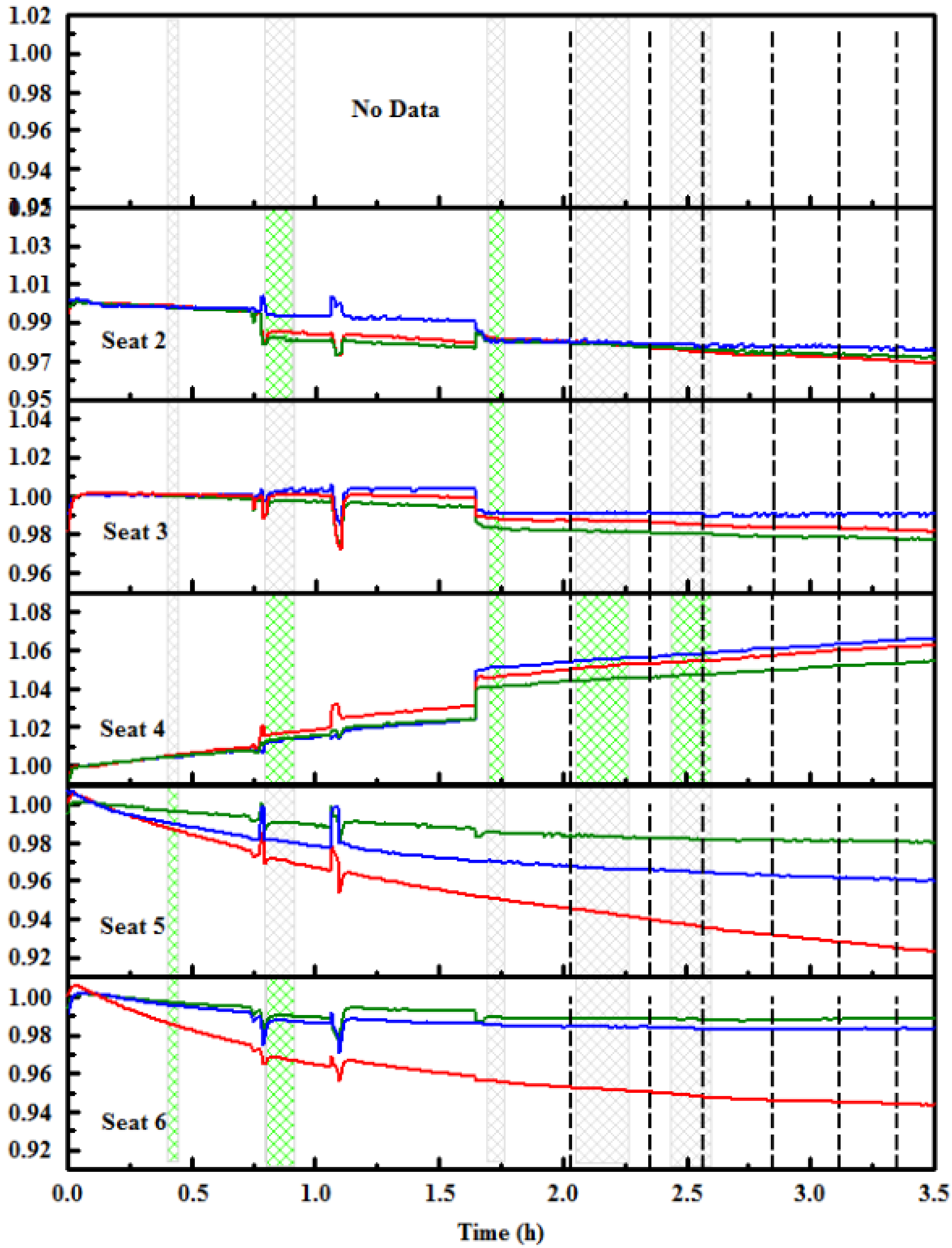

Fig. 24 — Simple Green Exposures. This data was collected on 04 December 2018 between 12:30 and 16:02. Dashed lines indicate the beginning of chemical stream flow from headspace. Humidity and temperature are provided in Figure 25. Filename: parallax_temp_21.txt

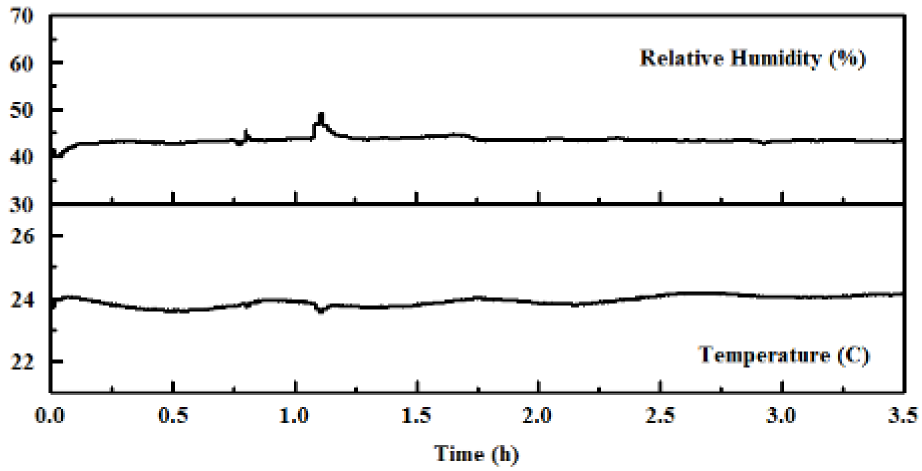

Fig. 25 — Simple Green Exposures. The temperature and humidity trends provided here were those observed during collection of data presented in Figure 24 collected on 04 December 2018 between 12:30 and 16:02.

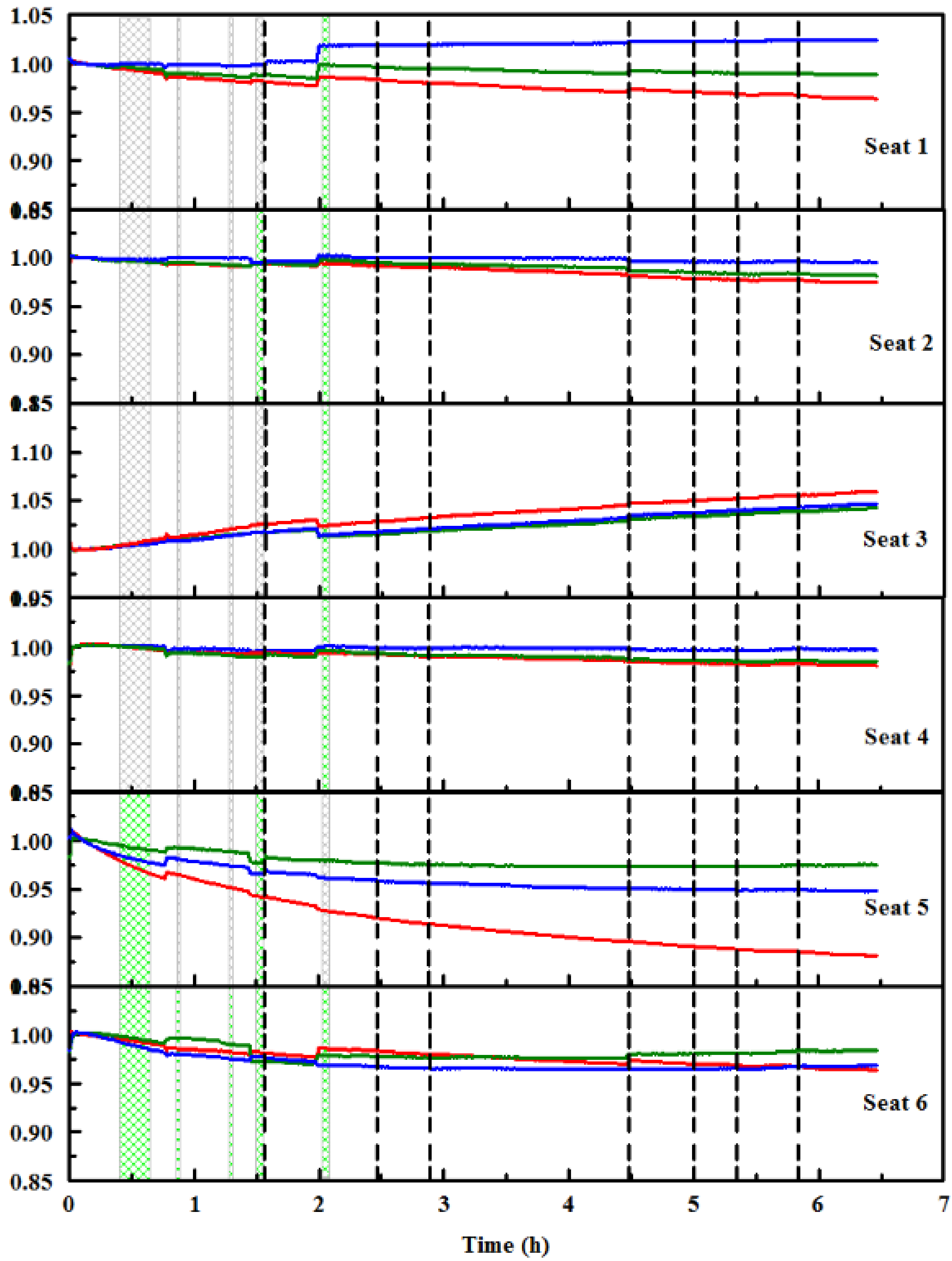

Fig. 26 — GB with Simple Green Exposures. This data was collected on 06 December 2018 between 08:43 and 15:12. Dashed lines indicate the beginning of chemical stream flow, 0.22 mg/m^3 GB. Humidity and temperature are provided in Figure 26. Filename: parallax_temp_22.txt

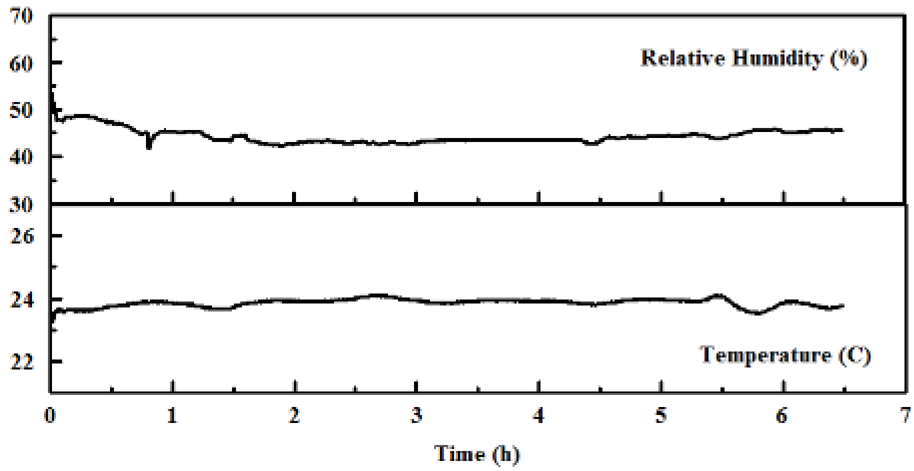

Fig. 27 — GB with Simple Green Exposures. The temperature and humidity trends provided here were those observed during collection of data presented in Figure 25 collected on 06 December 2018 between 08:43 and 15:12.

Reported results for HD exposures again show discrepancies between the experiment logs and the algorithm reports. Here, the Device Log and Post Experiment analysis are identical, so the device log was omitted (Tables 6 & 7). The time variations of 1 or 2 minutes are not significant. Without recorded start and stop times for the devices, the time axis for the data is estimated based on the laptop clock. Start times are obtained from the raw data file header while stop times are estimated based on the total number of points in the file at a nominal 30 s increment. The point that is concerning here are the larger discrepancies, for example, between 15:12 and 15:49 in the high concentration HD exposures (Table 7) and the additional positive response at the end of the run. Because we have completed limited evaluations of this real-time software reporting function at NRL, we have little insight into what produced this behavior, especially given the absence of these events in the device log.

Table 6 – Low concentration HD Exposures (1.2 mg/m^3) and Event Indication. Exposure begin and end times reflect initiation of the chemical stream (not chamber equilibrium) and equilibrium of the chamber to no compound, respectively.

Type	**Begin**		**End**		**Seats**
Start	10:47				
Post Experiment		11:11		11:18	5, 6
Post Experiment		11:51		11:56	6
Post Experiment		12:02		12:13	1, 5, 6
Post Experiment		12:20		12:26	1, 4
Post Experiment		12:52		13:01	4
Exposure	13:07		13:17		
Exposure	13:33		13:40		
Post Experiment		13:56		13:59	3, 4
Exposure	14:07		14:15		
Exposure	14:45		14:52		
Exposure	15:15		15:21		
Exposure	15:42		15:49		
End			16:26		

Table 7 – High concentration HD Exposures (2.5 mg/m^3) and Event Indication. Exposure begin and end times reflect initiation of the chemical stream (not chamber equilibrium) and equilibrium of the chamber to no compound, respectively.

Type	**Begin**		**End**		**Seats**
Start	09:38				
Post Experiment		10:02		10:15	4, 5, 6
Post Experiment		10:24		10:28	1, 3
Exposure	11:22		12:00		
Exposure	13:20		14:04		
Post Experiment		13:21		13:24	4
Post Experiment		13:36		13:39	2, 3, 6
Post Experiment		13:55		13:56	5
Post Experiment		14:05		14:09	5, 6
Exposure	14:16		14:40		
Post Experiment		15:07		15:46	1, 2, 3, 4, 5, 6
Exposure	15:12		15:36		
Experiment Log		15:31		15:32	
Experiment Log		15:34		15:36	
Experiment Log		15:40		15:49	
Exposure	15:50		16:15		
Post Experiment		15:53		15:57	4
Experiment Log		15:55		16:04	
Post Experiment		16:05		16:07	4
Experiment Log		16:06		16:14	
Post Experiment		16:16		16:20	3,4
Experiment Log		16:17		16:26	
Exposure	16:26		14:48		
Post Experiment		16:30		16:45	1, 3, 4, 5, 6
Experiment Log		16:31		16:52	
Exposure	16:50		17:20		
Post Experiment		17:01		17:07	4
Experiment Log		17:03		17:10	
Post Experiment		17:15		17:20	3, 4, 5
Experiment Log		17:16		17:23	
Experiment Log		17:19		17:26	
End			17:34		

Low concentration HD exposures (1.2 mg/m^3) did not produce associated responses (Figure 28). Responses for high concentration HD exposures (2.5 mg/m^3) were noted for 5 of the 7 exposures, excluding the first and third exposures. The first exposure in this series had a peak concentration of 2.7 mg/m^3. The second, on the other hand, has a listed peak of 19 mg/m^3 with the remaining exposures peaking between 2.7 and 2.9 mg/m^3. There is also a sharp, short duration change in humidity noted at 15:06, just before the fourth exposure (Figure 30). All of the seats were impacted by this change. Prior work with these device optimized the algorithm for use in the changing outdoor environment in which humidity changes occur much more slowly. These changes do not interfere with analysis. Here, the humidity in the chamber dropped from 43% to 26% in 4 min returning to 43% over the following 11 min. This change resulted in the early alarm reported in the experiment log. The subsequent response to target can be observed in the graph of the data (Figure 29). Algorithm summaries are provided in Table 8. Where appropriate, the time to response has been calculated based on times noted in the Experiment Log for beginning of chemical stream start as well as for the time at which the chamber reached equilibrium.

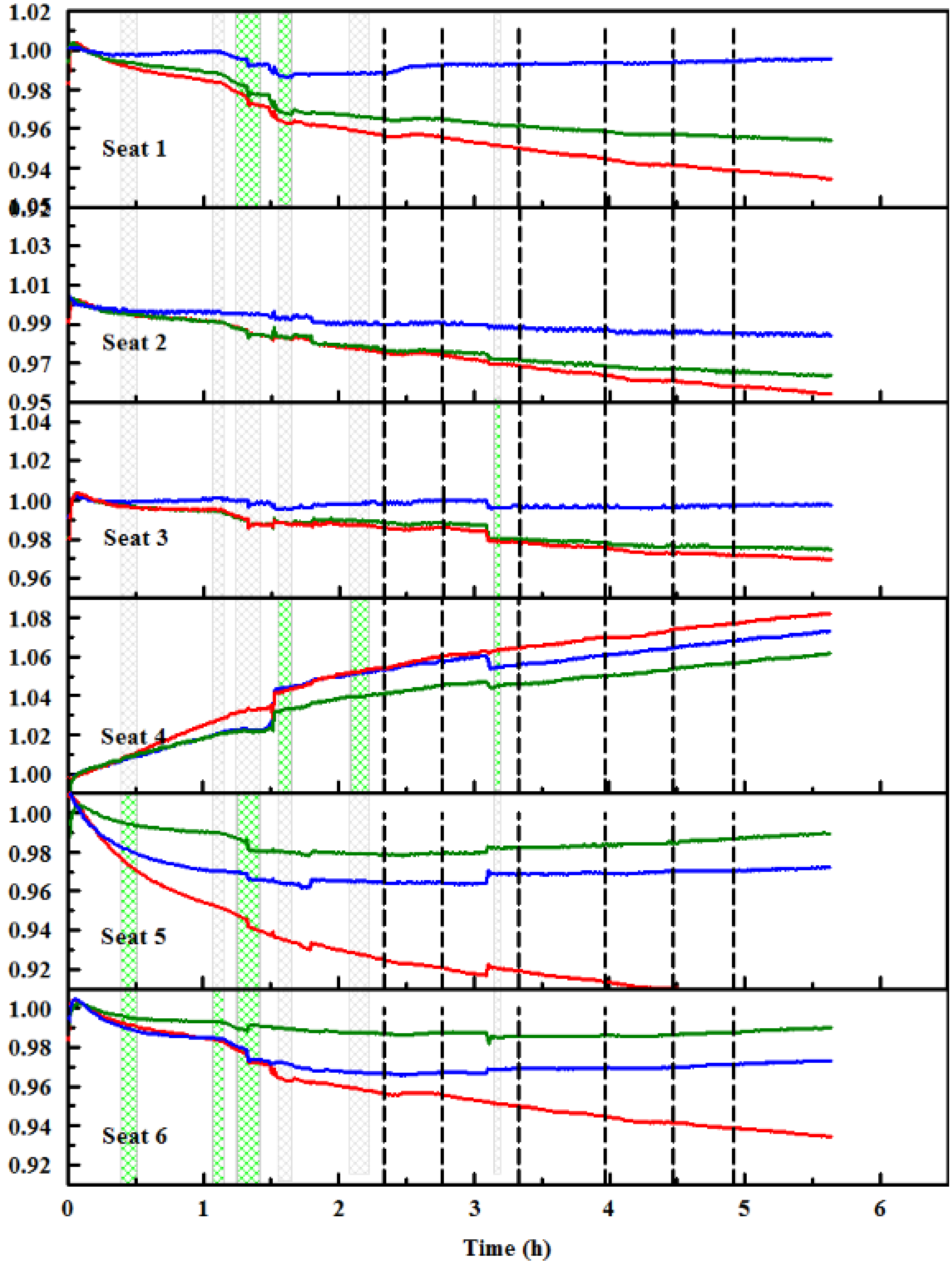

Fig. 28 — HD Exposures. This data was collected on 07 December 2018 between 10:47 and 16:26. Dashed lines indicate the beginning of chemical stream flow, 1.2 mg/m^3 HD. Humidity and temperature data were not provided for this date. Filename: parallax_temp_23.txt

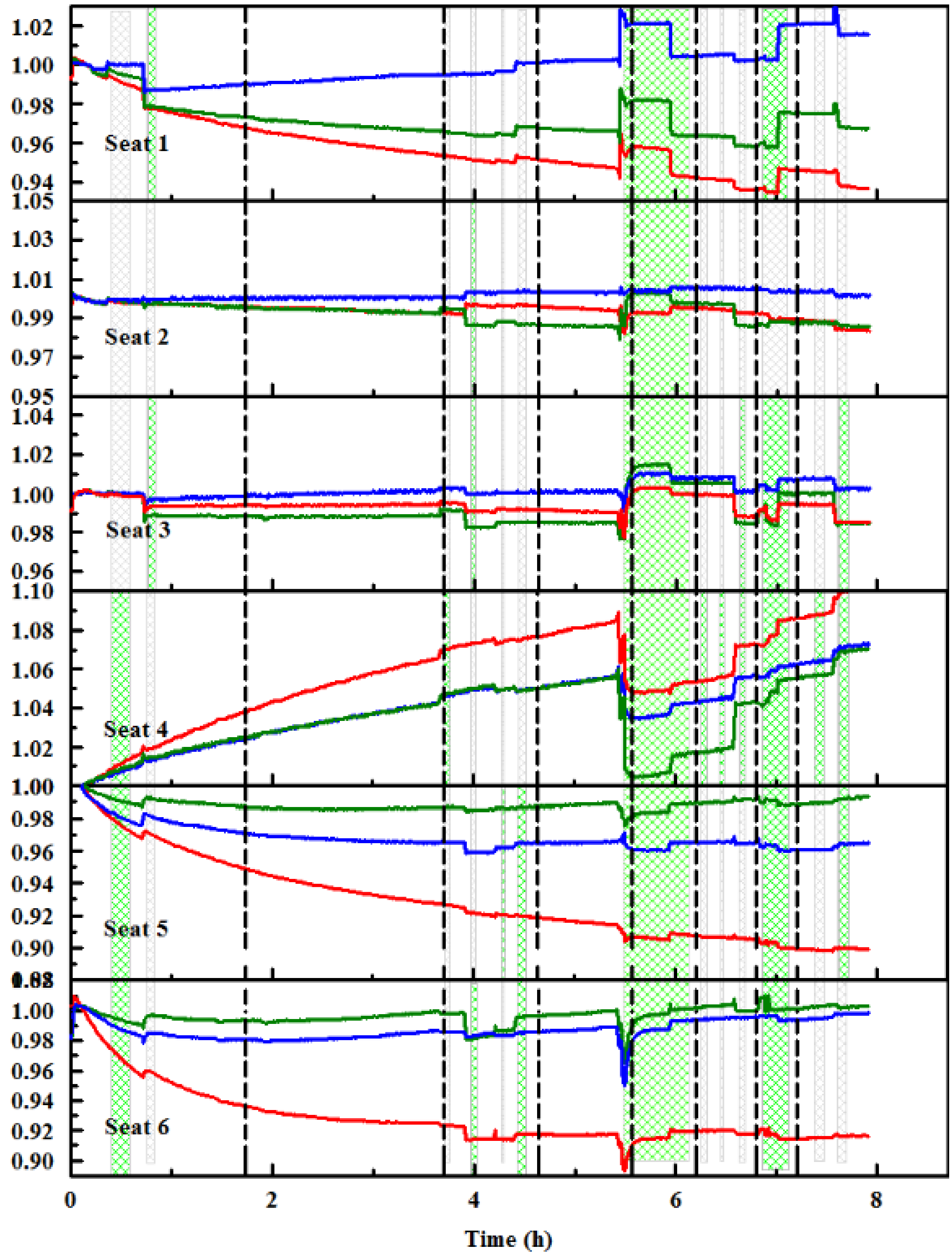

Fig. 29 — HD Exposures. This data was collected on 10 December 2018 between 09:38 and 17:34. Dashed lines indicate the beginning of chemical stream flow, 2.5 mg/m^3 HD. Humidity and temperature are provided in Figure 30. Filename: parallax_temp_24.txt

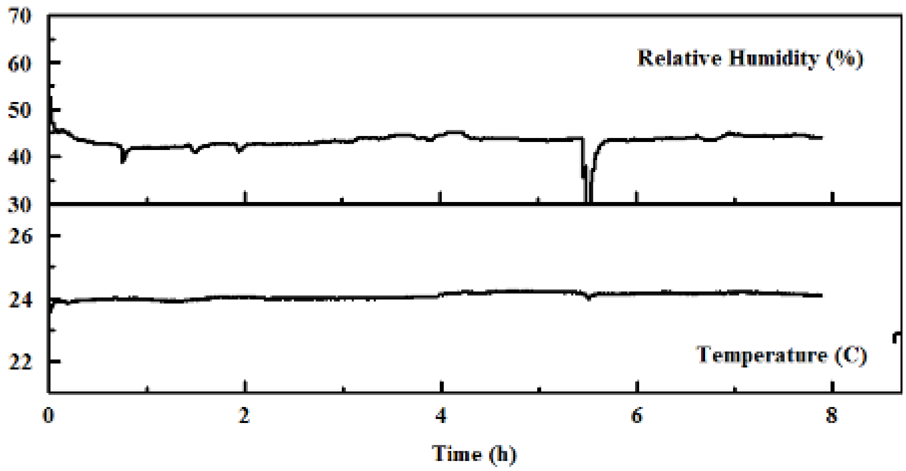

Fig. 30 — HD Exposures. The temperature and humidity trends provided here were those observed during collection of data presented in Figure 29 from 10 December 2018 between 09:38 and 17:34.

Table 8 – Algorithm Performance, HD and Cl_2 at 500 ms

Target	Duration (h)	Exposures	Events	Exposure Associated	Avg Time to Response (min)$^{\gamma}$	Avg Time to Response (min)†
HD, 1.2 mg/m^3	5.65	6	6	0		
HD, 2.5 mg/m^3	7.93	7	13	5	1	-5
Cl_2, 5 ppm	4.95	6	6	6	6	1
Cl_2, 100 ppm*	6.92	7	6	7	3	1

*Device failure after 5 exposures. $^{\gamma}$ Time to response calculated based on algorithm output from chemical stream start. †Time to response calculated based on algorithm output from chamber equilibrium time.
-- indicates unavailable data.

Behaviors during Cl_2 exposures at 5 and 100 ppm are provided in Figures 31 and 32. With algorithm summaries provided in Table 8. This dataset again shows discrepancies between the experiment log, the device log, and post experiment analysis. Table 9 provides a summary of these results while Figure 33 offers another representation of the data for comparison. Responses to the first four low concentration Cl_2 exposures were reported by all of the logs. In the case of the algorithm (device log and post experiment processing), the first exposure (7 ppm) resulted in a sharp change in reflectance. The event identification condition was met from that point through the next three exposures. Changes in reflectance can be seen in the graph of the data (Figure 31). The remaining two exposures produced clean on / off responses. The final exposure of Figure 31 was at 100 ppm and also resulted in event identification.

The initial exposure of the 12 December data was collected at the high Cl_2 concentration and produced a dramatic change in the reflectance for seats 1, 2, 4, and 6 of the array with smaller changes at seats 3 and 5. Subsequent exposures produced much smaller responses across the array. Here again, the device was in alarm condition from the first exposure until after the second. Exposures three and four produced clean on / off responses. Around the time of the fifth exposure (10:55; 2.75 h) the device began to show signs of failure with full failure by 11:22 (3.23 h). Post experiment analysis ceases to report prior to the final exposures at 11:22 and 11:43. All data after device failure should be disregarded. The device was reset after the experiment ending at 11:50. The data collected after that point (parallax_temp_28.txt; Figure 35) shows complete failure with the possible exception of seat 3.

Table 9 – Low concentration Cl_2 Exposures (5 ppm) and Event Indication. Exposure begin and end times reflect initiation of the chemical stream (not chamber equilibrium) and equilibrium of the chamber to no compound, respectively. Data file includes one high concentration exposure.

Type	**Begin**		**End**		**Seats**
Start	10:27				
Post Experiment		10:51		11:02	5, 6
Device Log		10:52		11:00	5
Post Experiment		11:12		11:34	1
Exposure	13:13		13:35		
Post Experiment		13:23		15:22	1, 2, 3, 4, 5, 6
Device Log		13:23		15:22	1, 2, 3, 4, 5, 6
Experiment Log		13:24		?	
Exposure	14:09		14:23		
Experiment Log		14:15		14:45	
Exposure	14:40		15:01		
Experiment Log		14:47		15:17	
Exposure	15:12		15:39		
Experiment Log		15:20		15:39	
Post Experiment		15:41		15:48	6
Device Log		15:41		15:48	6
Exposure	16:10		16:21		
Post Experiment		16:15		16:25	1, 2, 3, 5, 6
Device Log		16:15		16:25	1, 2, 3, 5, 6
Experiment Log		16:17		16:30	
Exposure	16:31		16:44		
Post Experiment		16:36		16:41	1
Device Log		16:36		16:41	1
Experiment Log		16:37		16:44	
Exposure (100 ppm)	16:50		>16:54		
Post Experiment		16:55		17:21	1, 2, 3, 5, 6
Device Log		16:55		17:22	1, 2
Experiment Log		16:55		?	
Stop			17:22		

Table 10 – High concentration Cl_2 Exposures (100 ppm) and Event Indication. Exposure begin and end times reflect initiation of the chemical stream (not chamber equilibrium) and equilibrium of the chamber to no compound, respectively.

Type	**Begin**		**End**		**Seats**
Start	08:08				
Post Experiment		08:32		08:44	5, 6
Device Log		08:33		08:44	5, 6
Post Experiment		08:57		09:01	2, 3, 4
Device Log		08:57		09:01	2, 3, 4
Exposure	09:09		09:28		
Post Experiment		09:10		10:18	1, 2, 3, 4, 5, 6
Device Log		09:10		10:18	1, 2, 3, 4, 5, 6
Experiment Log		09:13		?	
Exposure	09:51		10:10		
Experiment Log		10:00		10:26	
Exposure	10:22		10:40		
Post Experiment		10:25		10:52	1, 2, 4, 5, 6
Device Log		10:25		10:52	1, 2, 4, 5, 6
Experiment Log		10:26		?	
Exposure	10:55		11:06		
Post Experiment		10:59		11:08	1, 2
Device Log		10:59		11:08	1, 2
Experiment Log		11:09		11:11	
Exposure	11:22		11:33		
Device Log		11:26		11:50	4
Experiment Log		11:27		11:36	
Exposure	11:43		>11:47		
Experiment Log		11:44		11:48	
Experiment Log		11:49		?	
Stop			11:50		

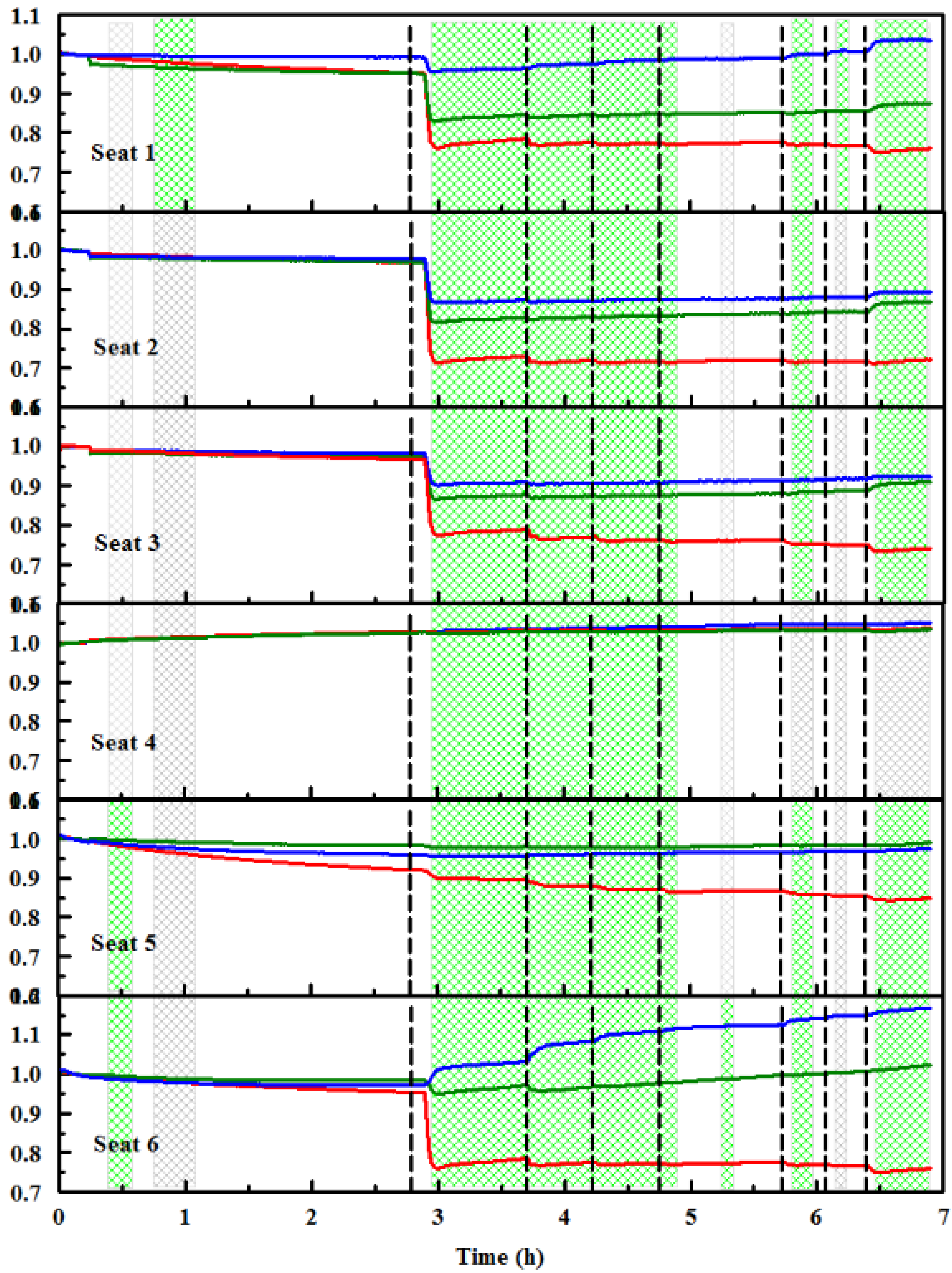

Fig. 31 — Cl_2 Exposures. This data was collected on 11 December 2018 between 10:27 and 17:22. Dashed lines indicate the beginning of chemical stream flow, 5 and 100 (final exposure) ppm Cl_2. Humidity and temperature are provided in Figure 31. Filename: parallax_temp_26.txt

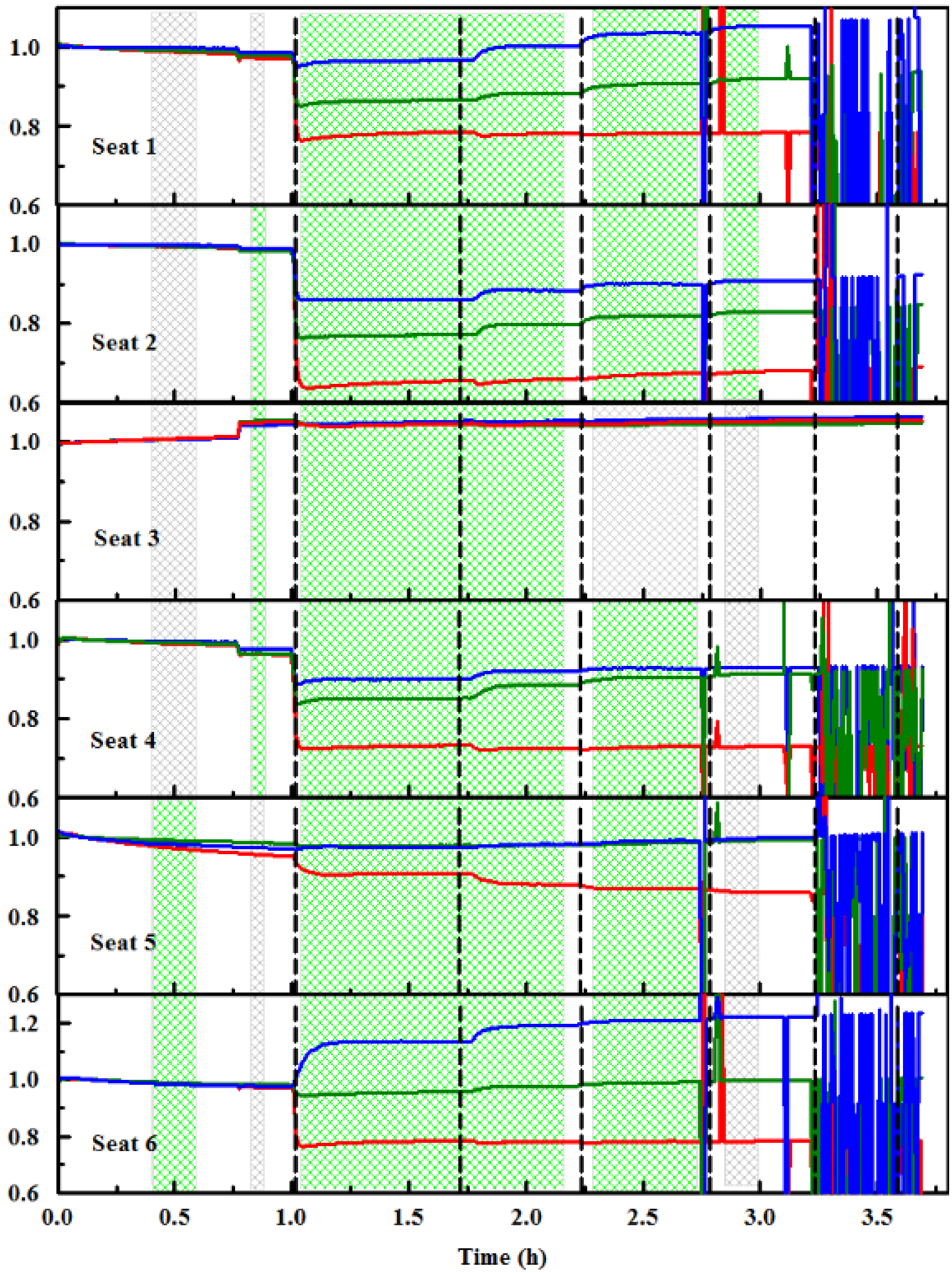

Fig. 32 — Cl_2 Exposures. This data was collected on 12 December 2018 between 08:08 and 11:50. Dashed lines indicate the beginning of chemical stream flow, 100 ppm Cl_2. Humidity and temperature data were not provided for this date. Filename: parallax_temp_27.txt

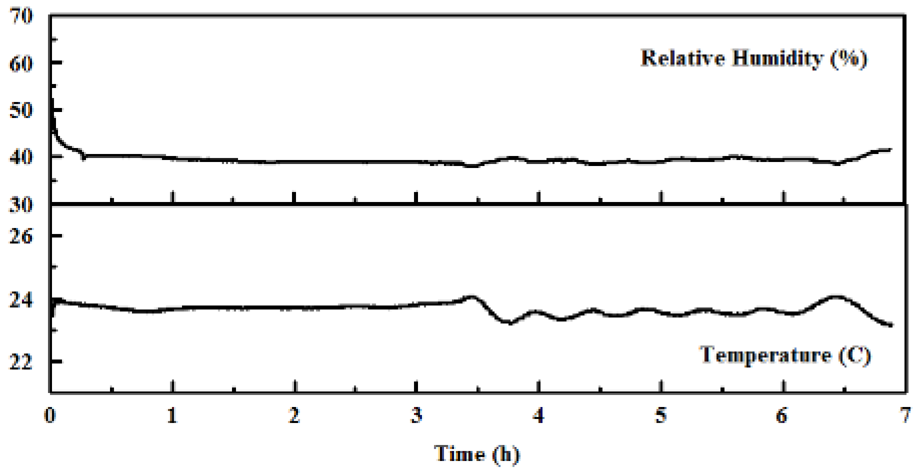

Fig. 33 — Cl_2 Exposures. The temperature and humidity trends provided here were those observed during collection of data presented in Figure 30 collected on 11 December 2018 between 10:27 and 17:22.

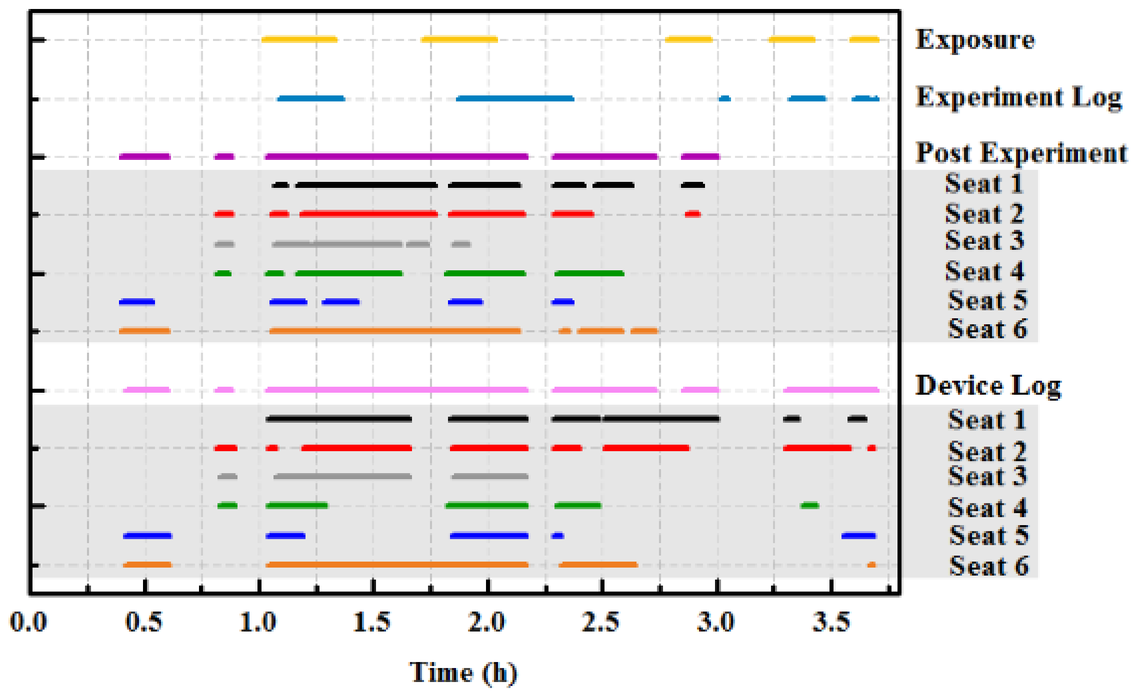

Fig. 34 — Cl_2 Exposures. The information provided here compares the time courses for exposures and the experiment log to the algorithm reporting via both the device log and post experiment data processing. Here, both the overall event indication (purple and pink) and the event indication for each seat are provided.

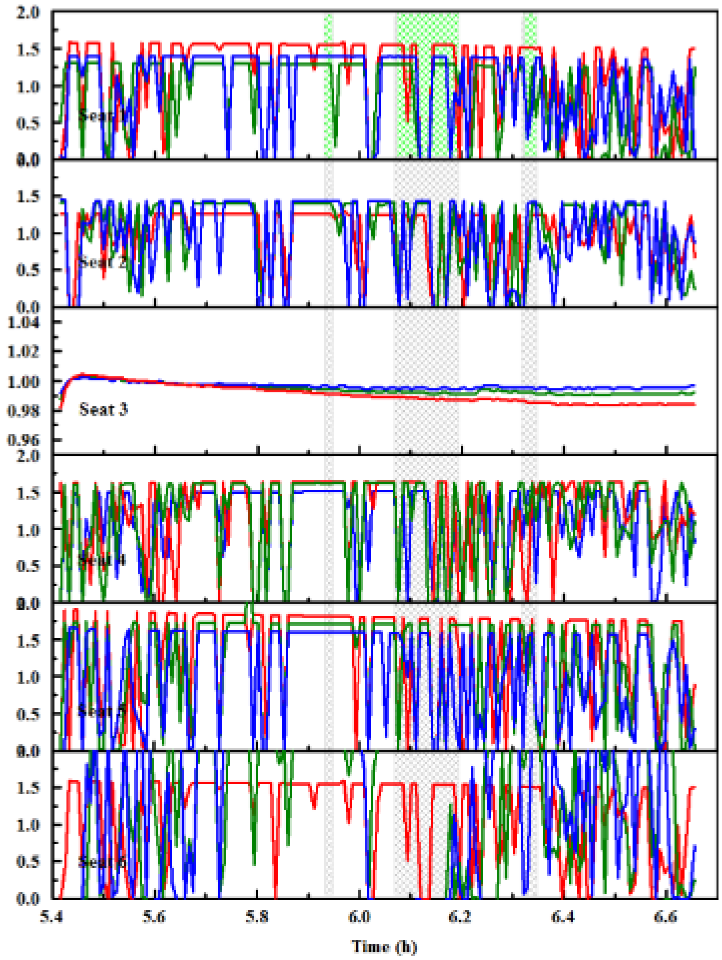

Fig. 35 — Post Cl_2 Exposure. This data was collected on 12 December 2018 between 13:33 and 14:48. Humidity and temperature data were not provided for this date. Filename: parallax_temp_28.txt

Because of the board failure during Cl_2 exposures, the main control board was again exchanged. This time the board with the missing seat 1 connector was used (#3). The remaining data, therefore, report for only five indicators, seats 2 through 6. Device behaviors during VX exposures at 0.013 and 0.022 mg/m^3 are provided in Figure 36. With algorithm summaries provided in Table 11. This dataset shows no responses to target exposure. Based on the trends in the collected reflectance data, the device (5 seats) appears to be functioning properly. Figure 38 provides device responses during exposure to Simulant at 0.013 and 0.022 mg/m^3; algorithm summaries are provided in Table 11. Again, no responses to exposures were noted. Seat 3 failed at the beginning of this cycle of exposures. The other four seats (2, 4, 5, 6) appear to be functioning normally throughout.

Table 11 – Algorithm Performance, VX and simulant at 500 ms

Target	Duration (h)	Exposures	Events	Exposure Associated
VX, 0.013 mg/m^3	10.68	6	2	0
VX, 0.022 mg/m^3		6	0	0
Simulant, 0.013 mg/m^3	11.32	6	1	0
Simulant, 0.022 mg/m^3		6	0	0

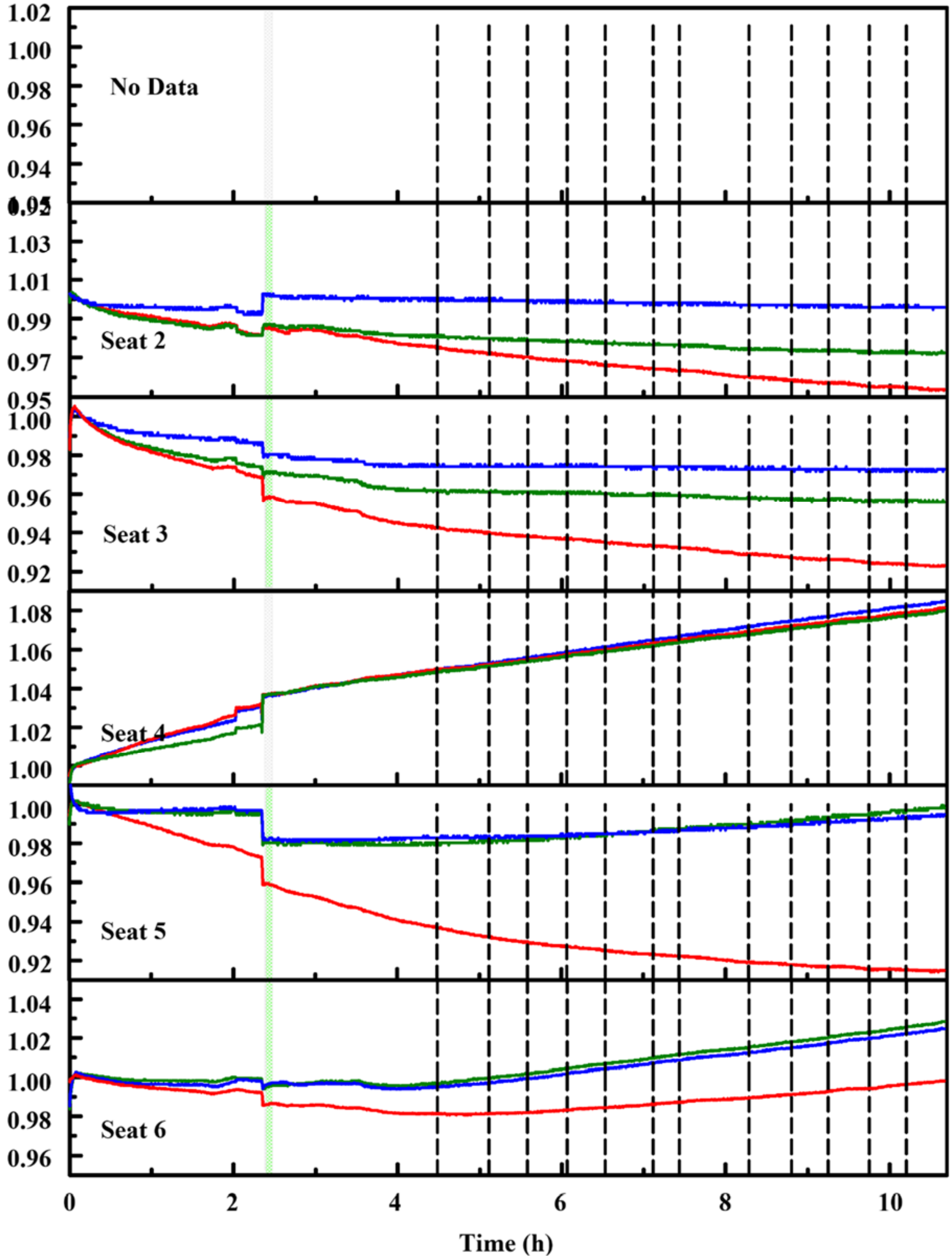

Fig. 36 — VX Exposures. This data was collected on 13 December 2018 between 08:25 and 19:06. Dashed lines indicate the beginning of chemical stream flow, 0.013 and 0.022 mg/m^3 VX. Humidity and temperature are provided in Figure 35. Filename: parallax_temp_30.txt

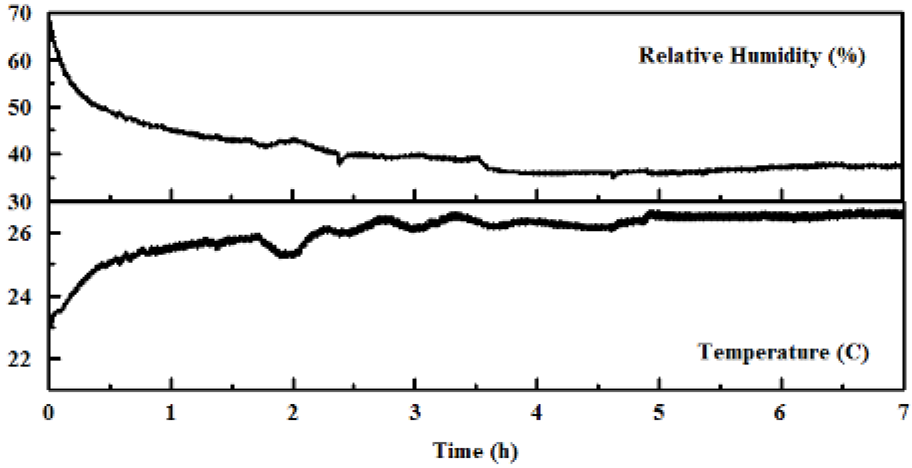

Fig. 37 — VX Exposures. The temperature and humidity trends provided here were those observed during collection of data presented in Figure 36 collected on 13 December 2018 between 08:25 and 19:06.

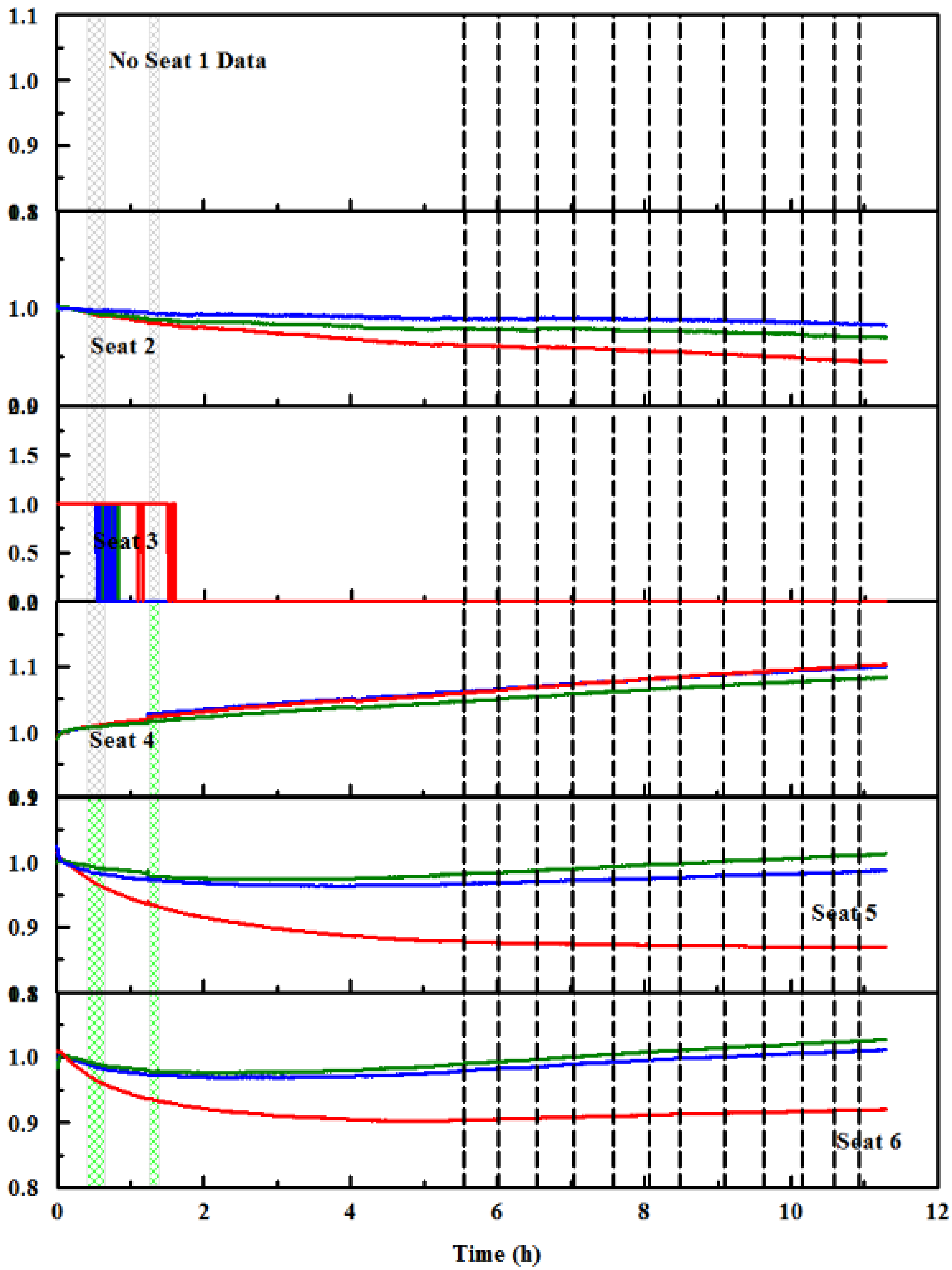

Fig. 38 — Simulant Exposures. This data was collected on 14 December 2018 between 08:15 and 19:34. Dashed lines indicate the beginning of chemical stream flow, 0.013 and 0.022 mg/m^3 Simulant. Humidity and temperature are provided in Figure 39. Filename: parallax_temp_31.txt

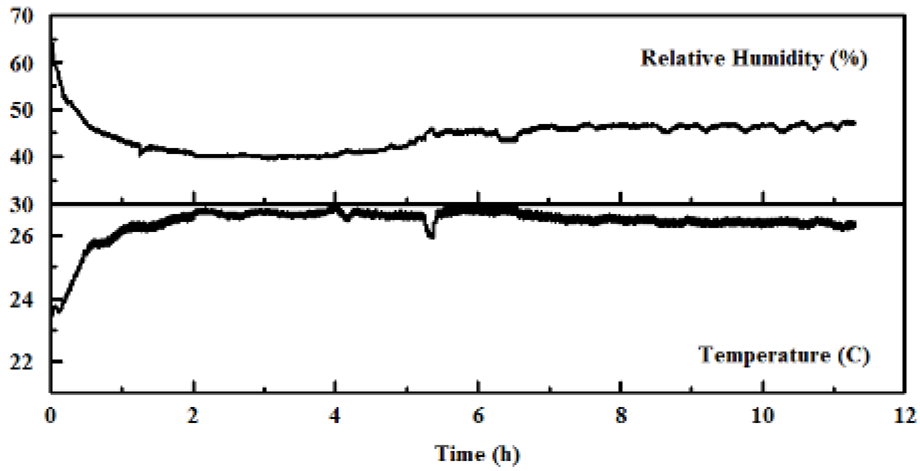

Fig. 39 — VX Exposures. The temperature and humidity trends provided here were those observed during collection of data presented in Figure 38 collected on 14 December 2018 between 08:15 and 19:34.

DISCUSSION

Across the 500 ms datasets (Table 12), there is a recurring event at ~1500 s (0.42 h). It is typically associated with seat 5 or seats 5 and 6. Given the changes made to the way our Background, Active, and Snap Windows (Figure 2) are populated in this implementation of the algorithm, 1500 s is the first time point at which detection can begin – the 25 minute warmup period is complete and all windows are populated. It should be noted that the fans of the NRL prototype were used to circulate the air within the test setup – air flow was initiated by starting data collection with the NRL device. In looking at the humidity data provided with the datasets, most of them show a steep change in humidity through the first hour while the test chamber equilibrates. In Figure 39, for example, the humidity begins at 64.1%, decreasing to 43.8% over the first hour. (Figure 40 provides a different type of plot distinctly shows this change.) The Background window for the algorithm is, therefore, populated by data reflecting the rapid humidity change. This changing slope leads to an event trigger as the algorithm comes online. At 5700 s (1.58 h), the sliding windows have been completely turned over, with the original data replaced by data collected between 1500 and 5700 s. It should be noted, however, that the threshold angles for each color and seat are fixed by the first 120 points in the matrix; this is the only calculation of those values for a given use cycle. Because this calculation is used to define the sensitivity of the algorithm, this may have a negative impact on the performance of the algorithm throughout the use cycle. This first 120 points is also used for the only calculation of the associated standard deviation values.

Table 12 – Early Reported Event. Times reported by Device Log.

File	Start	Time (s)	Duration (s)	Seats	Figure
parallax_temp_9	09:38 11/19	1500	890	1, 3, 5, 6	16
parallax_temp_10*	08:45 11/20	1770	330	5, 6	17
parallax_temp_11	09:18 11/26	1500	900	5, 6	18
parallax_temp_21	12:30 12/04	1500	230	5	24
parallax_temp_22	08:43 12/06	1500	940	5, 6	26
parallax_temp_23	10:47 12/07	1500	620	5	28
parallax_temp_24	08:53 12/10	1500	920	4, 5, 6	29
parallax_temp_26	10:27 12/11	1500	510	5	31
parallax_temp_27	08:08 12/12	1500	690	5, 6	32
parallax_temp_30	08:25 12/13	N/A			36
parallax_temp_31	08:15 12/14	1500	840	5, 6	38

As described above, the device and algorithms used for these evaluations were originally developed for application to long term, autonomous environmental monitoring. In prior reports, we have discussed differences in long sampling increment (30 s) and short increment (5 s) data collection. For the type of short duration, repetitive events used for the evaluations conducted here, short duration data would have been preferable, allowing for quicker window population and shorter times for return to non-event status. Unfortunately, the v2.08 device does not support simultaneous interrogation of the six indicators; they are sequentially sampled. The result is that the time required to sample, write, and switch limits the sampling rate to the 30 s increment for any integration longer than 100 ms. As shown in Figure 3, the noise in data collected at this integration level is significantly higher. Using the current algorithm parameters with 100 ms data results in a number of false positive events; false positive reporting can be controlled only through loss in sensitivity. The TCS3414 version of the color sensing chip offers the potential for simultaneous sampling. This type of device is under consideration for follow-on prototype generations. Beyond simply increasing the sampling interval, it may be of interest to use a dynamic sampling interval in some situations. For example, the device samples at a 30 s or even 1 min increment until an event is triggered. The trigger switches the sampling rate to a shorter duration until conditions for event end are met or based on some other criteria. This could be used to both shorten the necessary cool down condition and to provide more data points within the event cycle.

The array elements used for these evaluations were selected based on prior characterization by NRL. [1, 2, 4, 5] Targets previously considered include alcohols, phosgene, hydrochloric acid, sulfuric acid, dimethyl methylphosphonate (DMMP), diazinon, sulfur dioxide, nitric oxide, and cyanogen chloride as well as others of less relevance to the current work. Because of our extensive prior use of alcohols as surrogate targets, ethanol was used as a positive control (system check) during the work described here. N_4TPP, AgN_4TPP, ZnN_4TPP, TlDIX, and YDIX have been used in the majority of our published work on the development of the prototypes and algorithms. They have also been evaluated against the targets used in our unpublished work directed at expansion of the library of responses and development of identification algorithms. The AuDIX element used in seat 4 is the single new indicator used for this work. This seat has been AgDIX in our prior published work. Based on unpublished phosgene characterization and results from hydrochloric acid exposures [2], this element was expected to provide improved differential responses across the array for the targets considered here.

As shown in Table 13, the device was responsive to the compounds with chlorine bearing structures, phosgene, HD, and Cl_2. Based on prior work with HCl, phosgene, and cyanogen chlorine, this was expected. Previous work indicated that the N_4TPP, AgN_4TPP, and ZnN_4TPP indicators would react strongly to phosgene with little response by the YDIX and TlDIX indicators. The AuDIX indicator was included specifically because of responsiveness to HCl in prior evaluations. Sulfur dioxide responses have been evaluated previously by NRL as well. The YDIX indicator was expected to respond and provide differentiation from phosgene responses. Because 100 ms integration was used, determinations cannot be made on this point.

Evaluations with diazinon and DMMP provided responses by the YDIX and TlDIX indicators; they were expected to similarly respond to GB challenge. Here, only a single response was noted for the GB with Simple Green (all indicators except TlDIX); mixtures of Simple Green with the pesticides have not been previously evaluated. In the absence of the GB data, it is difficult to provide discussion of this result. AuDIX was responsive to Simple Green; this interaction had not been previously evaluated. This indicator did respond to the mixture as did several other indicators, but only to a single instance. N_4TPP data was available only for the mixture; not for either pure compound. Given the limited available information, conclusions regarding target discrimination cannot be made.

Table 13 – Response Summary from Device Log Events.

Target	Events	N_4TPP	AgN_4TPP	ZnN_4TPP	AuDIX	TlDIX	YDIX
Sulfur dioxide (low)	6	0	0	0	0	0	0
Sulfur dioxide (high)	7	0	0	0	0	0	0
Phosgene (low)	8	6	1	4	0	3	0
Phosgene (high)	7	3	3	2	1	2	1
Ethylene oxide (low)	9	1	0	1	0	0	0
Ethylene oxide (high)	6	0	0	0	0	0	0
GB (low)	7	No Data					
GB (high)	6						
Simple Green	6	-†	0	0	3	0	0
GB with Simple Green	7	1	1	1	1	0	1
HD (low)	6	0	0	0	0	0	0
HD (high)	7	4	2	4	5	4	4
Cl_2 (low)	6	6	5	5	4	5	5
Cl_2 (high)*	5	5	5	3	4	5	5
VX (low)	6	-†	0	0	0	0	0
VX (high)	6	-†	0	0	0	0	0
Simulant (low)	6	-†	0	0	-γ	0	0
Simulant (high)	6	-†	0	0	-γ	0	0

*Exposures after device failure have been omitted. †Completed with five indicators due to board damage. γCompleted with four indicators due to board damage.

ADDITIONAL DATA ANALYSIS

As described in the sections above, a slope based algorithm is used for identification of event occurrence. The development of the algorithm was guided by the original goals of the NRL project; long term monitoring using a computationally simple method, minimizing device costs and energy usage. It was intended that the device respond rapidly but no consideration was made for startup time as the application was for a device continuously monitoring. In the implementation used here, there are 120 points (60 min) in the Background window and 20 points (10 min) in the Active window. The 120 point Background window is intended to provide a smooth, slowly changing slope. This should capture any device drift over time as well as changes resulting from diurnal and environmental changes. The Active window (20 points) provides a faster changing slope that will respond to chemical presence, while the shorter Snap window (10 points) is used to capture large, rapid changes. Comparing the Active and Snap windows to the slowly changing Background window provides the discrimination needed for identification of an event. Figure 40 provides a comparison of the slope over time for a single seat calculated using varied numbers of points. As shown in Figure 40, varying the number of points in the slope calculation has a significant impact on the resulting slope behaviors. The 20 point Active window used here provides a compromise point between speed of response, sensitivity, and false positives. If a longer delay in response can be tolerated for an application, a longer window (say 40 points) provides the option of using a more sensitive threshold for triggering an event. An alternative is to use a shorter sampling increment during data collection. This would allow for population of a 40 point buffer in a shorter amount of time, providing the smoother slope without impacting speed of response. Recall, this is not a possibility with the current hardware.

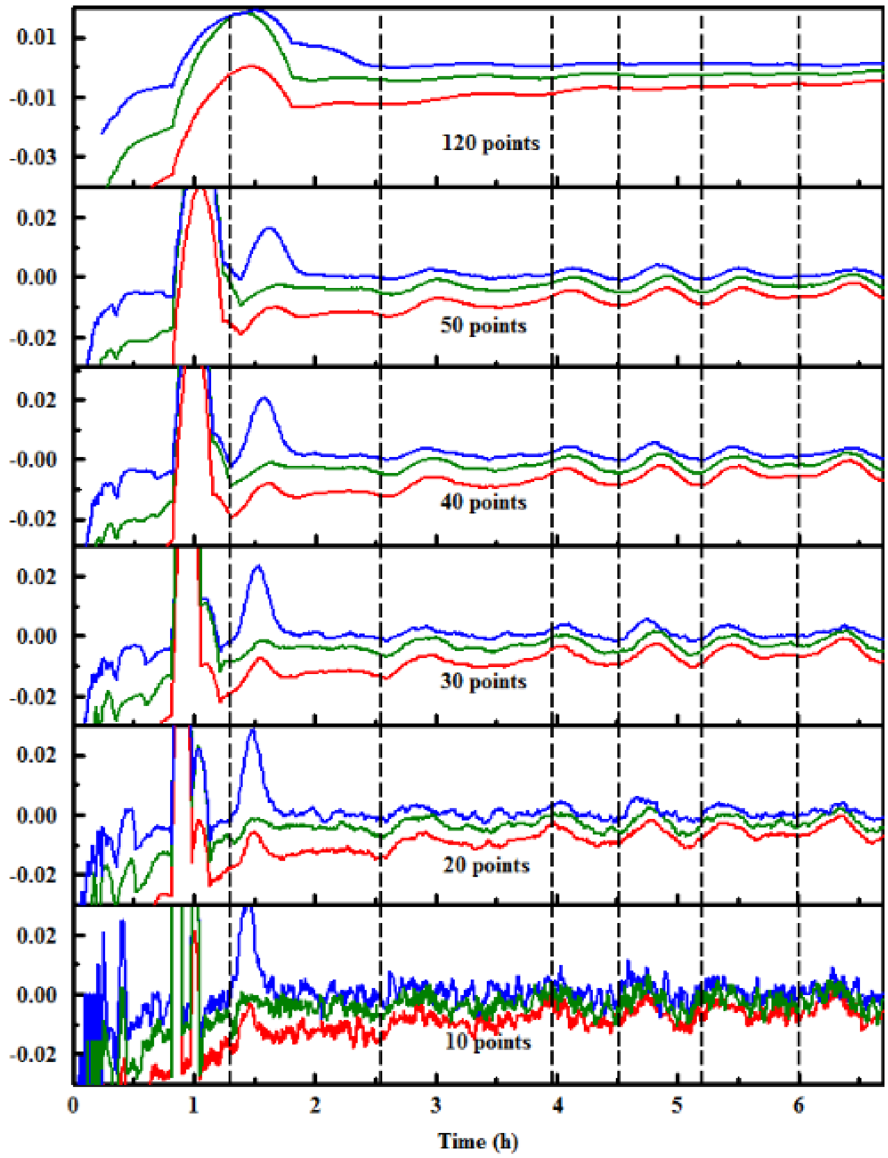

Fig. 40 — Slope Calculation, Varied Total Points. Prior to slope calculation, intensity values are normalized to the first intensity value for each color of each indicator. This uses the seat 1 (N_4TPP) data collected on 26 November 2018 between 09:18 and 16:02. Dashed lines indicate the beginning of chemical stream flow, 361 ppm ethylene oxide. Filename: parallax_temp_11.txt.

Alteration of the current or development of a new detection algorithm without sufficient datasets risks overtraining where the device and algorithm have been tuned to respond well under test conditions that may not accurately reflect real application use. The data generated during this test of the prototype is not sufficient for generation of a new automated algorithm. The intrinsic response of the device can, however, be examined more closely by looking at slopes over time for the experimental data collected under this study. This is a manual investigation, but can provide a better idea of the possible response profiles that the current algorithm implementation was not designed to capture. As shown in Figure 41, responses to Cl_2 exposures become clear for data plotted in this form. The calls made by the algorithm during the experiment indicated positive responses for these exposures. Post experiment analysis indicated the involvement of all seats for exposures 1 through 4, all seats excepting #4 for exposures 5 and 7, and only seat #1 for exposure 6 (Figure 31). From the slopes plotted in Figure 41, the responses of all seats with the exception of seat 4 are distinct for all exposures. Seat 4 responses can be seen. They are, however, significantly smaller than those of any other indicator.

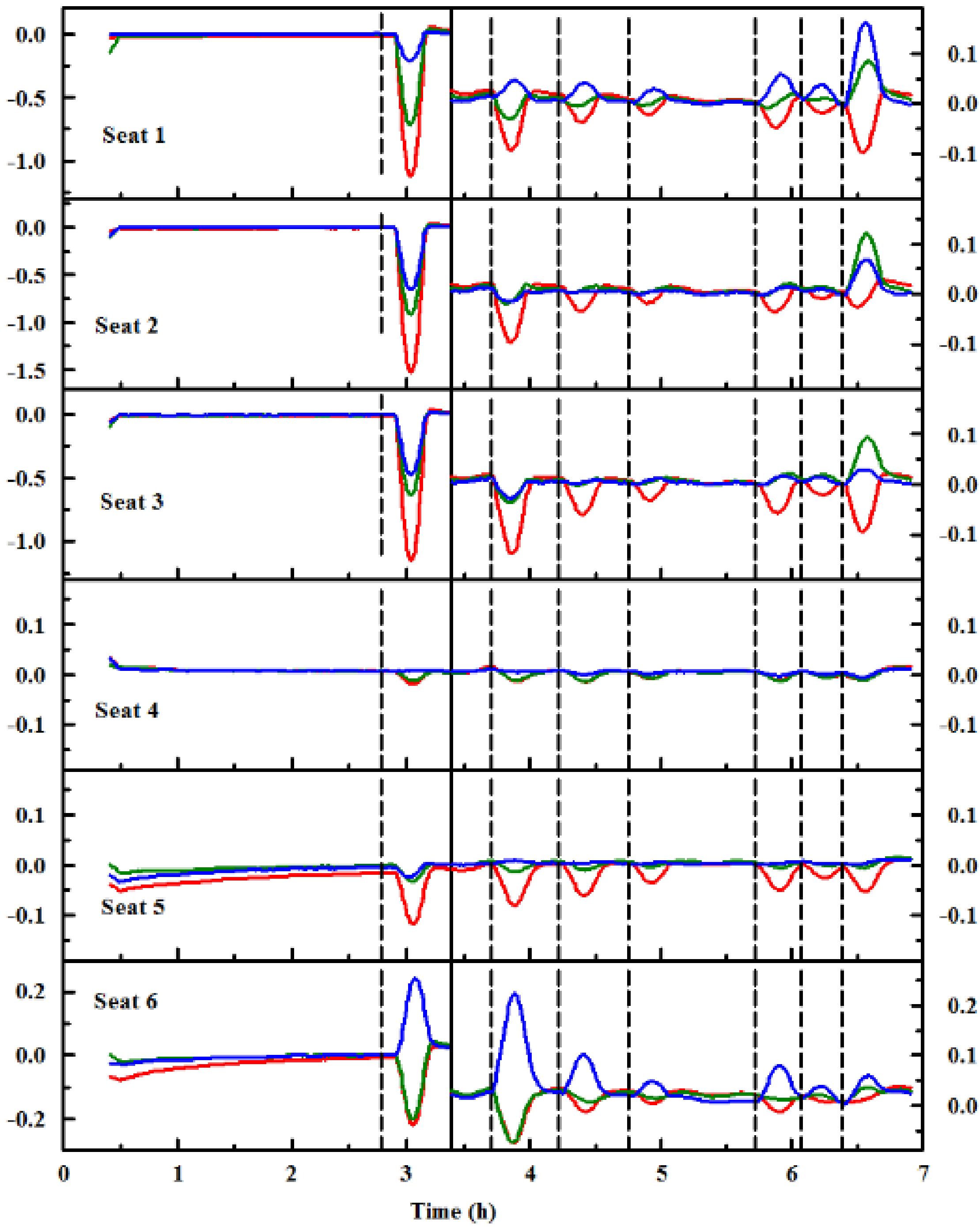

Fig. 41 — Slopes for Cl_2 Exposures. Here, a 30 point sliding window is applied to calculation of the slope – similar to the Active Window calculation using 15 min rather than 10 min of data. Prior to slope calculation, intensity values are normalized to the first intensity value for each color of each indicator. This data was collected on 11 December 2018 between 10:27 and 17:22. Dashed lines indicate the beginning of chemical stream flow, 5 and 100 (final exposure) ppm Cl_2. Filename: parallax_temp_26.txt

Figures 42 and 43 present the slopes calculated based on data collected during sulfur dioxide exposures. Recall, this data was collected at 100 ms integration with a 5 s increment. These parameters are less than optimal for this type of experimentation, and they tend to produce poor performance in combination with the algorithm implementation used here. In the figures, a 120 point (10 min) sliding window has been used. This window provides the same time duration as that used by the onboard algorithm with the data collected at the 30 s sampling increment. In Figure 42, responses to the first exposure are somewhat conflated with the changing environmental conditions. Seats 1, 2, 3, and 6, however, show a clear response pattern to the sequence of exposures. Figure 43 also shows the overlap between initial changing conditions and the first high concentration exposure. For the remaining exposures, the response pattern (seats 1, 2, 3, and 6) can be observed. At this higher concentration, responses from seats 4 and 5 can also been seen.

Figures 44 and 45 present the slopes calculated based on data collected during phosgene exposures. This data was also collected at 100 ms integration with a 5 s increment. The 120 point sliding window has again been applied. The experiment log does not provide referred concentrations for the first two exposures (Figure 44). The response is more distinct beginning at exposure 3 with seats 1, 2, and 3 showing strong responses, seats 5 and 6 showing weak responses, and seat 4 providing insignificant changes. In Figure 45, the high concentration of the first exposure (27 ppm) produces a very large change across seats 1, 2, and 3 as well as significant changes in 4, 5, and 6. A referee concentration is not provided for the second exposure, but large changes are noted across the expected indicators. For the remaining exposures, seats 1, 2, and 3 continue to provide distinct responses. Seats 5 and 6, on the other hand, are providing minimal response. This diminishing response is likely a result of damage caused to the indicator materials by the first two excessively high concentrations.

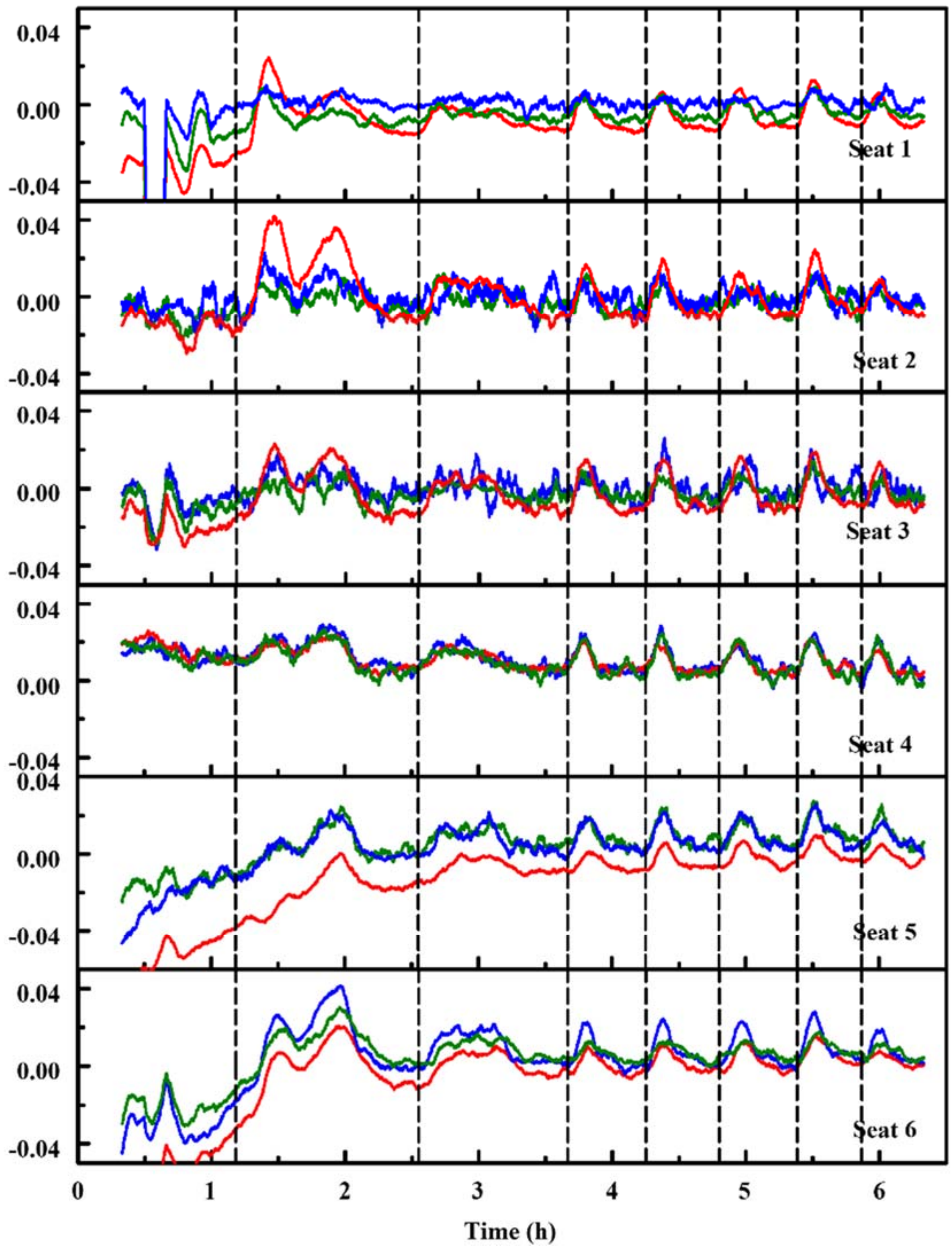

Fig. 42 — Slopes for SO_2 Exposures. This data was collected on 06 November 2018 between 10:13 and 13:55. Here, a 120 point sliding window is applied to calculation of the slope - 10 min of data. Prior to slope calculation, intensity values are normalized to the first intensity value for each color of each indicator. Dashed lines indicate the beginning of chemical stream flow, 1.5 ppm SO_2. Collected at 100 ms with a 5 s sampling increment. Filename: parallax_temp_5.txt

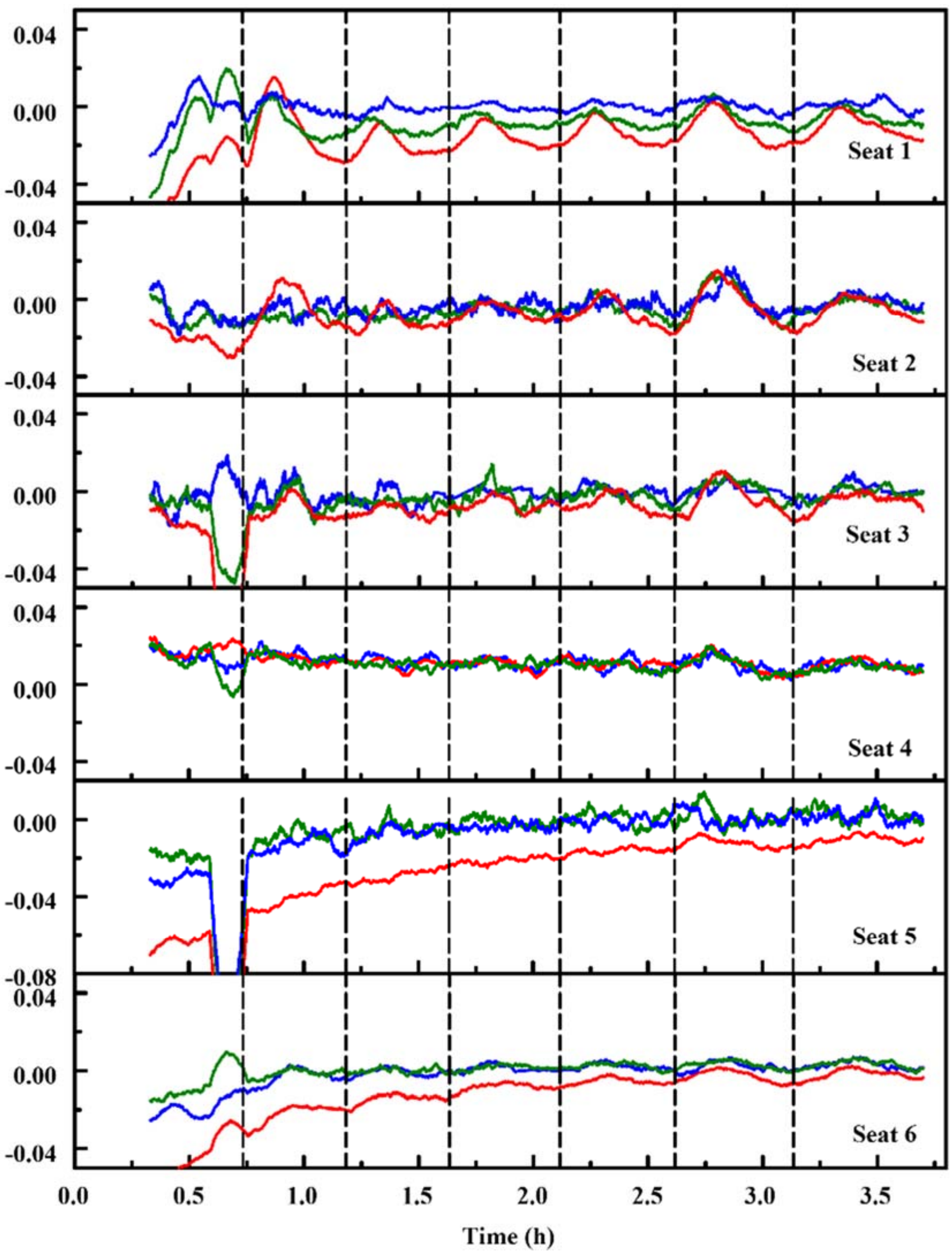

Fig. 43 — Slopes for SO_2 Exposures. This data was collected on 07 November 2018 between 10:15 and 16:35. Here, a 120 point sliding window is applied to calculation of the slope - 10 min of data. Prior to slope calculation, intensity values are normalized to the first intensity value for each color of each indicator. Dashed lines indicate the beginning of chemical stream flow, 30 ppm SO_2. Collected at 100 ms with a 5 s sampling increment. Filename: parallax_temp_6.txt

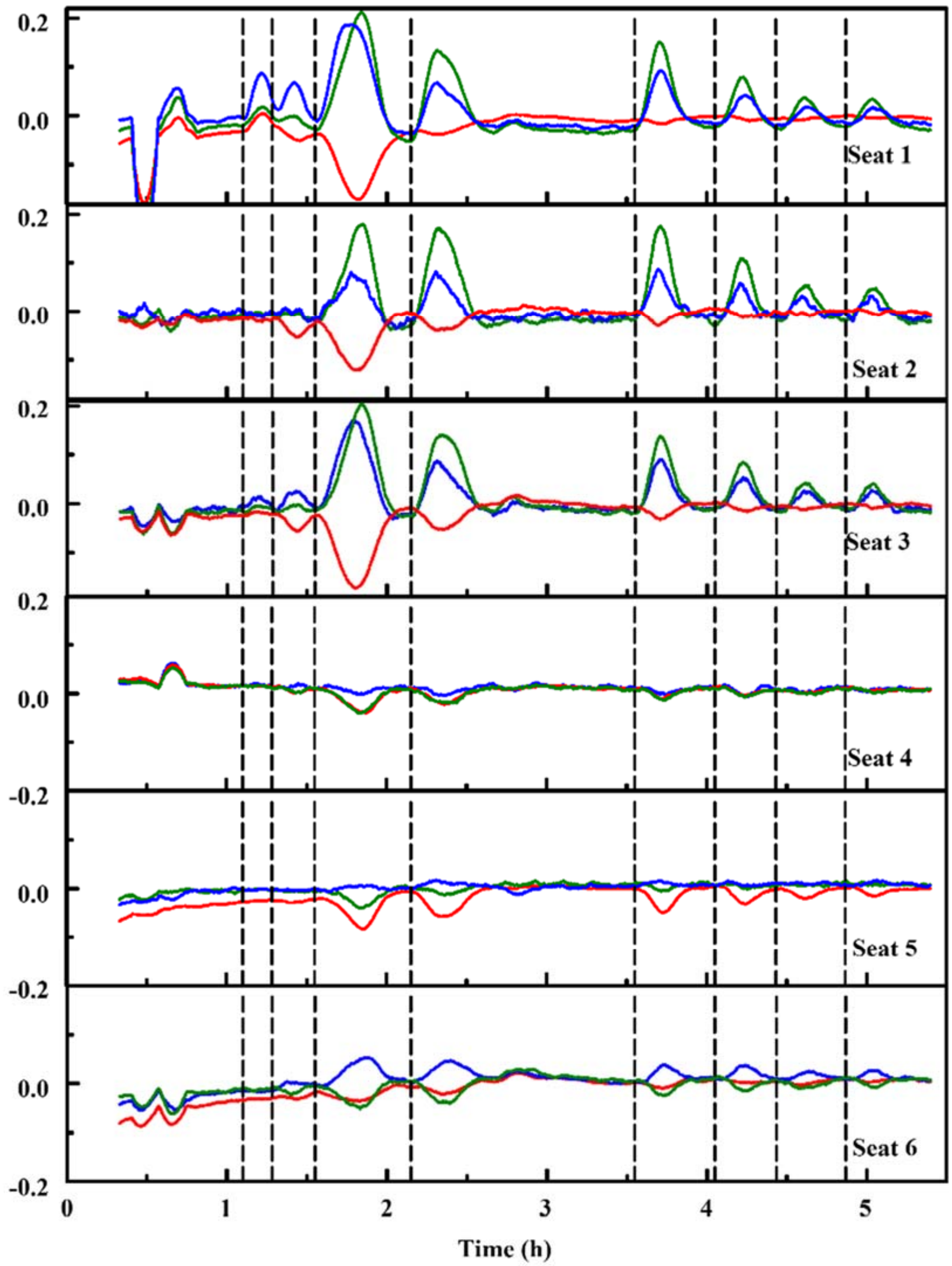

Fig. 44 — Slopes for Phosgene Exposures. This data was collected on 13 November 2018 between 09:20 and 14:44. Here, a 120 point sliding window is applied to calculation of the slope - 10 min of data. Prior to slope calculation, intensity values are normalized to the first intensity value for each color of each indicator. Dashed lines indicate the beginning of chemical stream flow, 1.2 ppm phosgene. Collected at 100 ms with a 5 s sampling increment. Filename: parallax_temp_7.txt

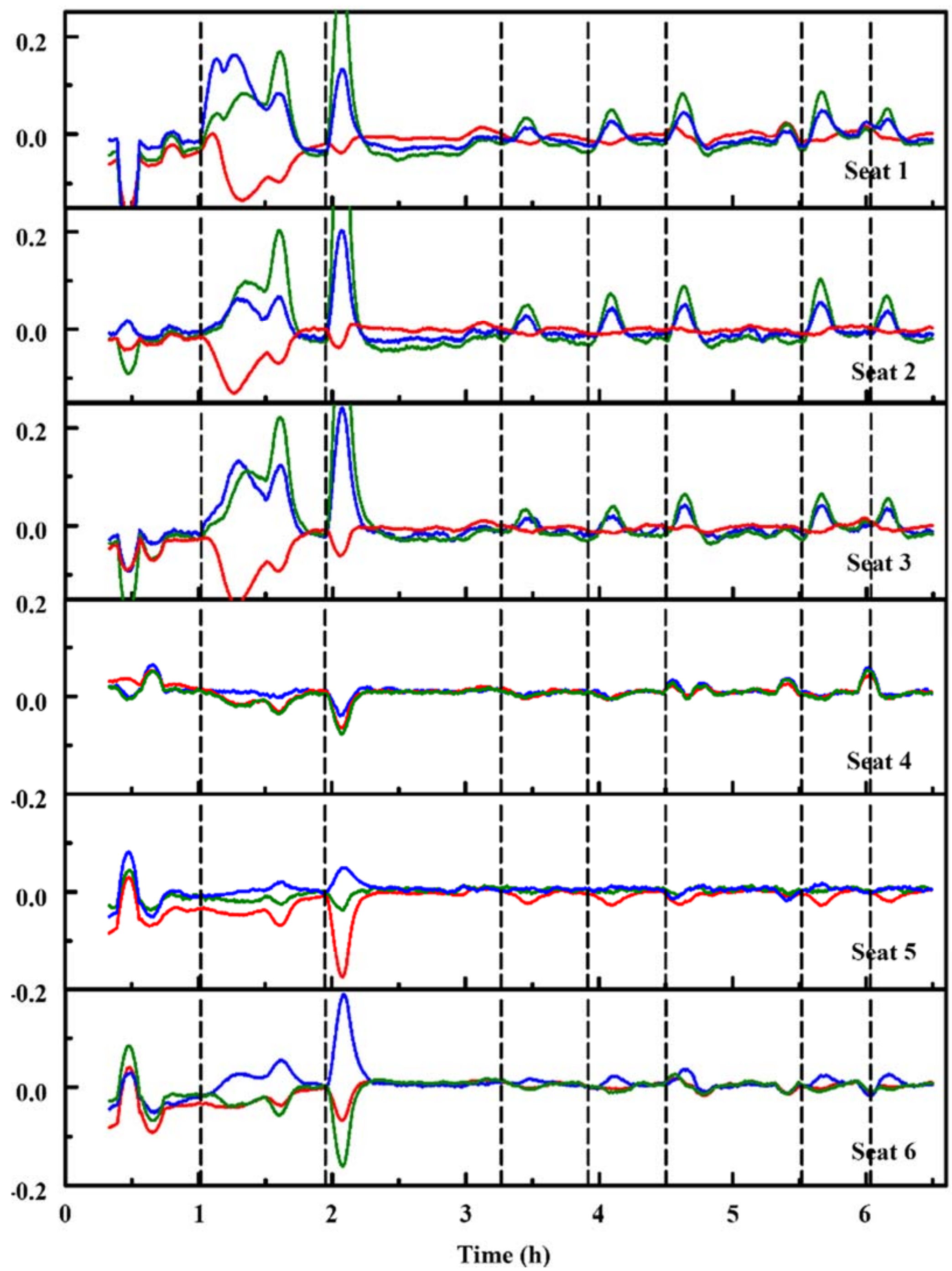

Fig. 45 — Slopes for Phosgene Exposures. This data was collected on 14 November 2018 between 08:46 and 15:26. Here, a 120 point sliding window is applied to calculation of the slope - 10 min of data. Prior to slope calculation, intensity values are normalized to the first intensity value for each color of each indicator. Dashed lines indicate the beginning of chemical stream flow, 7.4 ppm phosgene. Collected at 100 ms with a 5 s sampling increment. Filename: parallax_temp_8.txt

Figures 46, 47, and 48 present the slopes calculated based on data collected during ethylene oxide exposures. The low concentration produced very little response in the device (Figures 46 and 47). The response to the first of the high concentration exposures (Figure 48) is complicated by the ongoing equilibration of the chamber. The remaining exposures produced a characteristic response on seats 1, 2, 3, and 5 with a smaller response on seat 6.

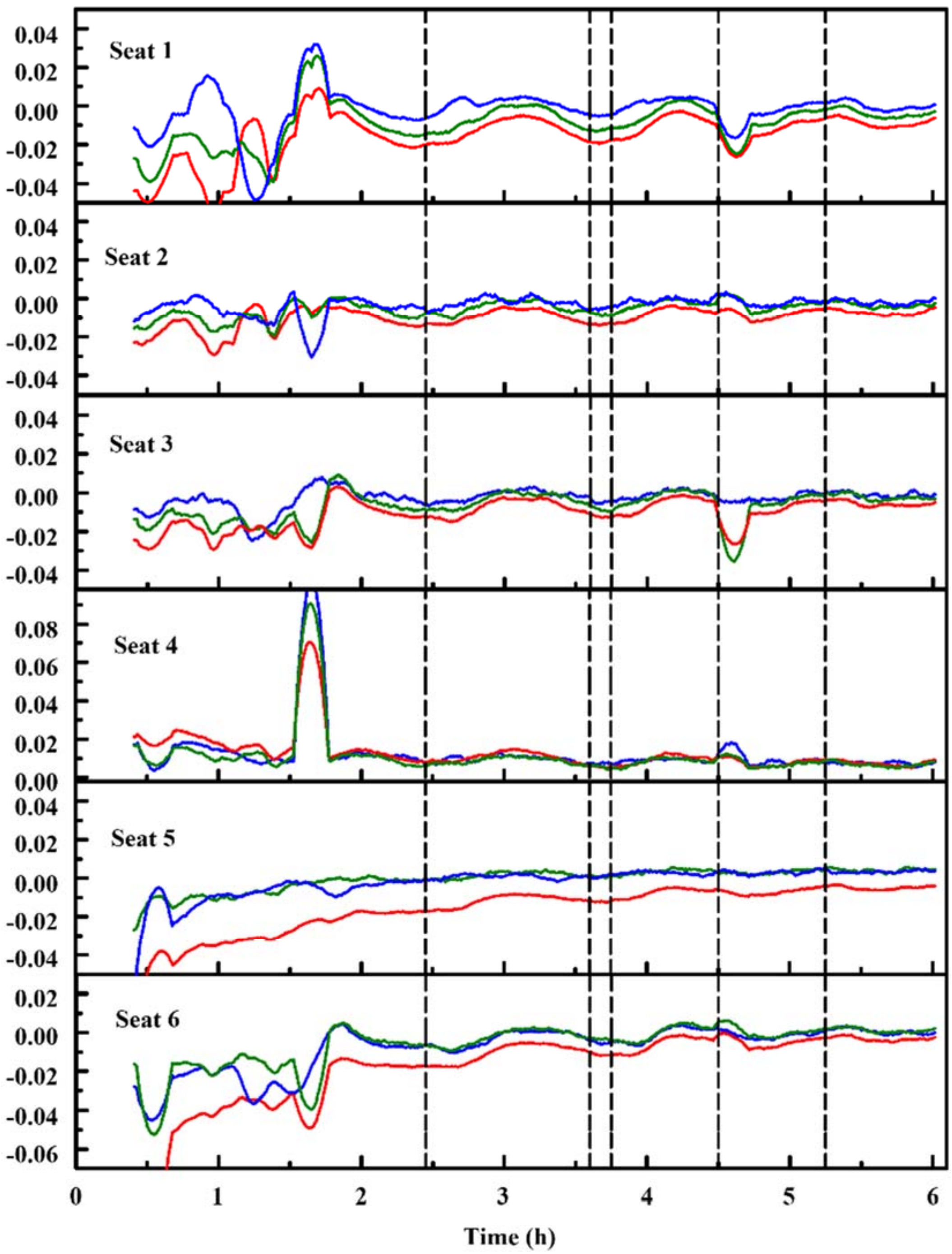

Fig. 46 — Slopes for Ethylene Oxide Exposures. This data was collected on 19 November 2018 between 09:38 and 15:41. Here, a 30 point sliding window is applied to calculation of the slope. Prior to slope calculation, intensity values are normalized to the first intensity value for each color of each indicator. Dashed lines indicate the beginning of chemical stream flow, 78 ppm ethylene oxide. Filename: parallax_temp_9.txt

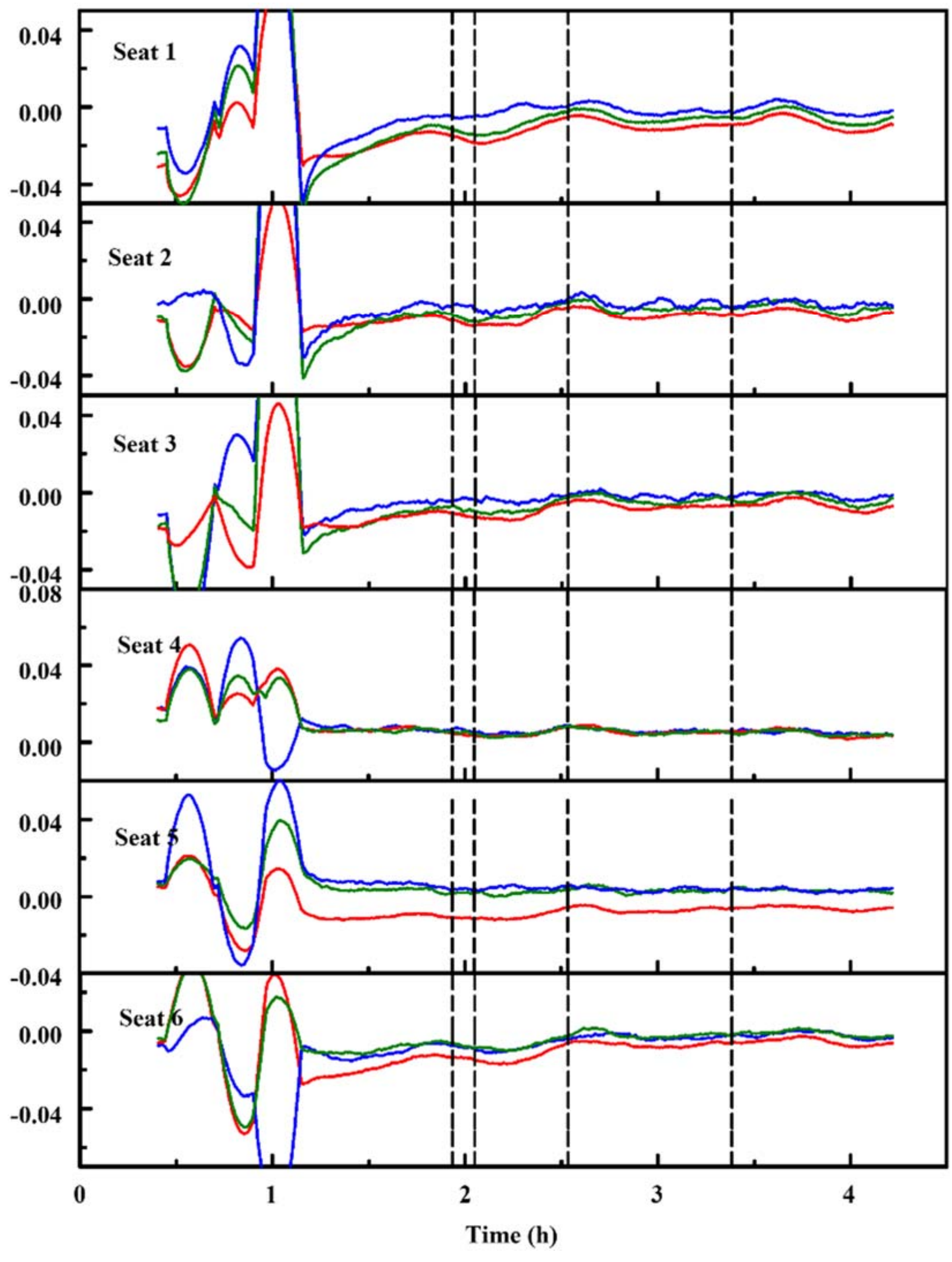

Fig. 47 — Slopes for Ethylene Oxide Exposures. This data was collected on 20 November 2018 between 08:45 and 13:00. Here, a 30 point sliding window is applied to calculation of the slope. Prior to slope calculation, intensity values are normalized to the first intensity value for each color of each indicator. Dashed lines indicate the beginning of chemical stream flow, 78 ppm ethylene oxide. Filename: parallax_temp_10.txt

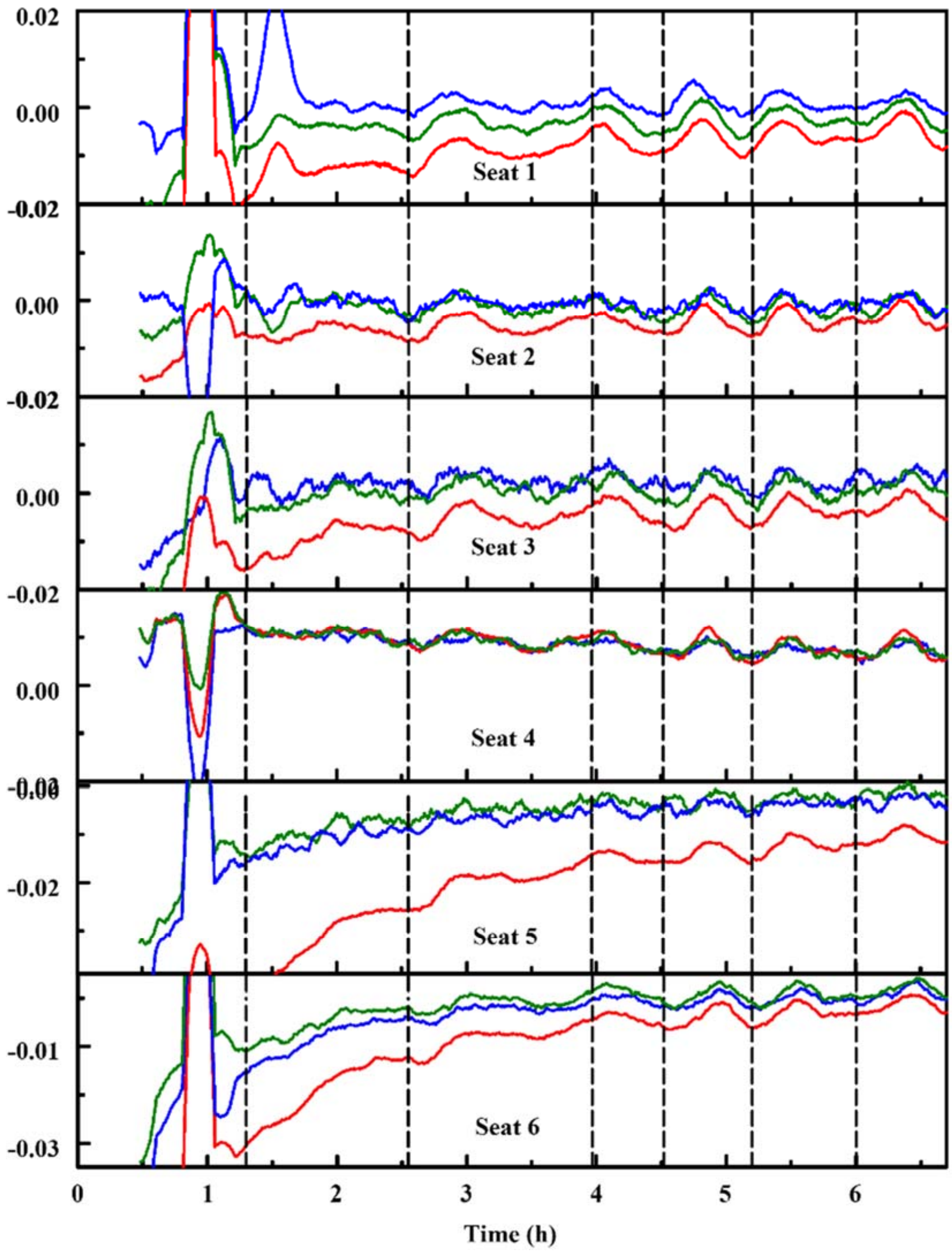

Fig. 48 — Slopes for Ethylene Oxide Exposures. This data was collected on 26 November 2018 between 09:18 and 16:02. Here, a 30 point sliding window is applied to calculation of the slope. Prior to slope calculation, intensity values are normalized to the first intensity value for each color of each indicator. Dashed lines indicate the beginning of chemical stream flow, 361 ppm ethylene oxide. Filename: parallax_temp_11.txt

Figure 49 presents the slopes from data collected during exposure to Simple Green. Post experiment application of the algorithm indicated positive responses following the first three exposures. All responses were triggered by seat 4 only. The graph does not show a characteristic pattern for these responses or responses to any other target exposures. Figure 50 presents the slopes from data collected during exposure to GB with Simple Green. The graph of the data (Figure 26) shows little variation resulting from exposures. Here, the behavior following the first exposure is again mixed with the changes due to chamber equilibration. This was the only positive exposure associated event reported during post experiment application of the algorithm. While there are behaviors noted in the slopes (Figure 50), there are no patterns noted.

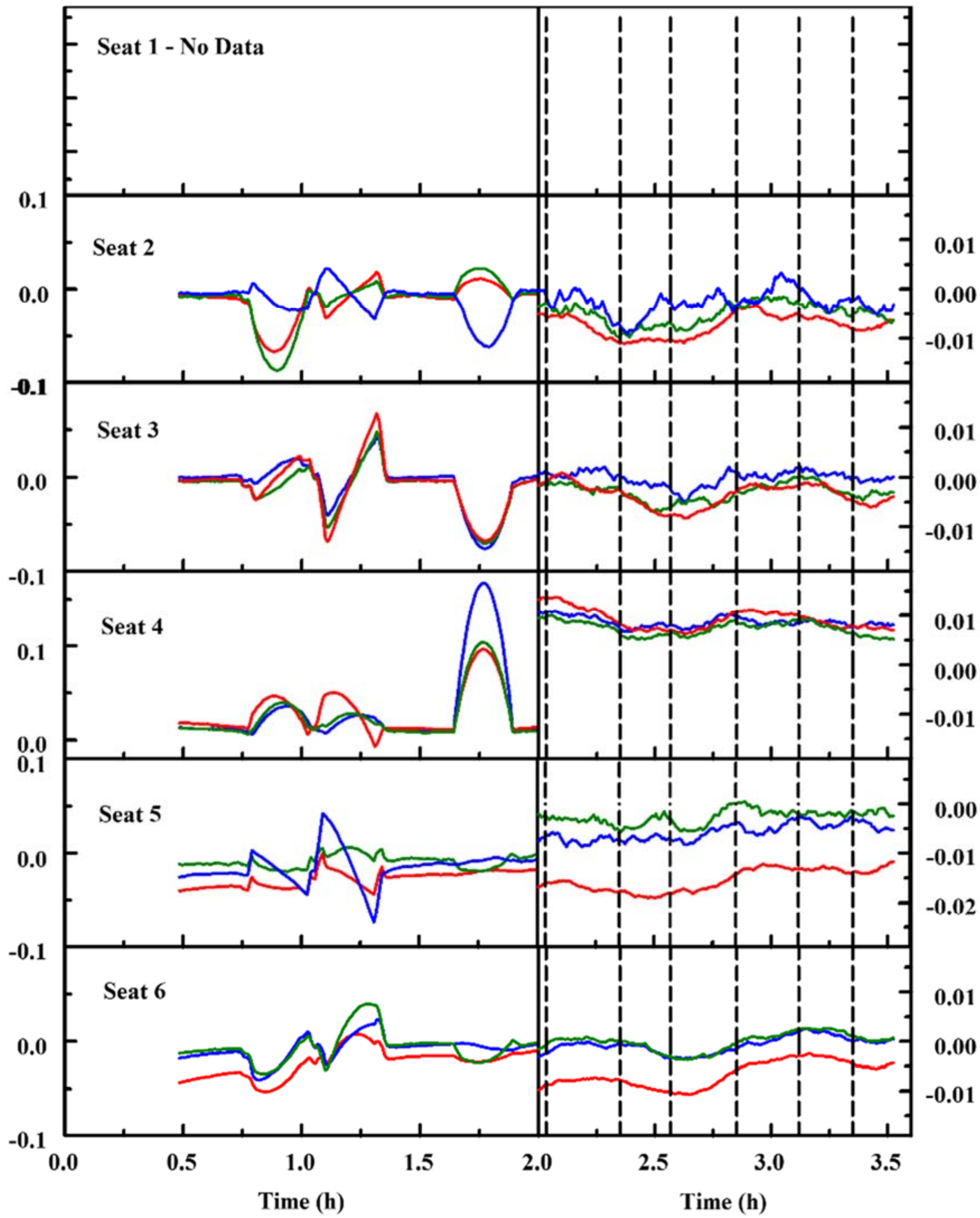

Fig. 49 — Slopes for Simple Green Exposures. This data was collected on 04 December 2018 between 12:30 and 16:02. Here, a 30 point sliding window is applied to calculation of the slope. Prior to slope calculation, intensity values are normalized to the first intensity value for each color of each indicator. Dashed lines indicate the beginning of chemical stream flow from headspace. Filename: parallax_temp_21.txt

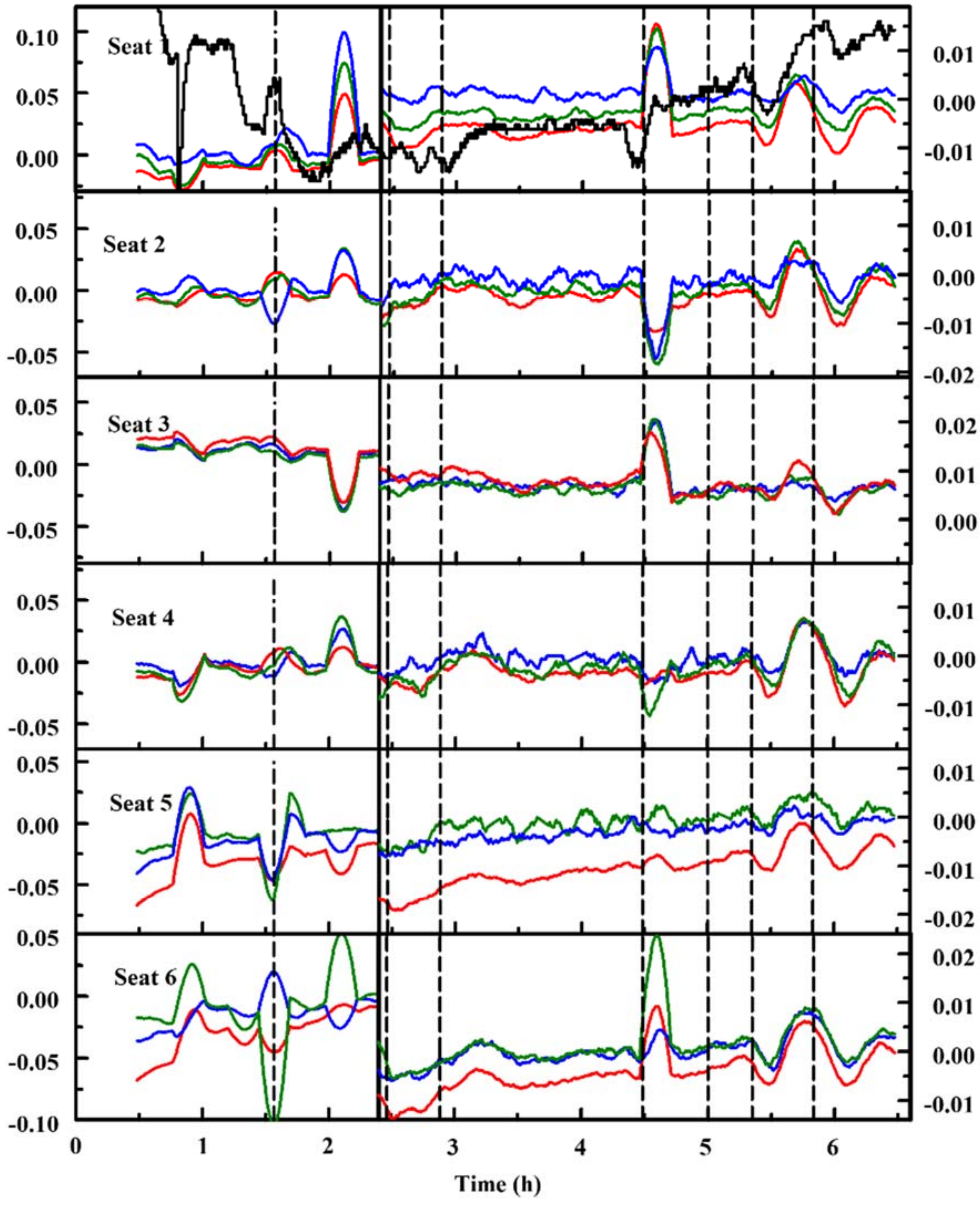

Fig. 50 — Slopes for GB with Simple Green Exposures. This data was collected on 06 December 2018 between 08:43 and 15:12. Here, a 30 point sliding window is applied to calculation of the slope. Prior to slope calculation, intensity values are normalized to the first intensity value for each color of each indicator. Dashed lines indicate the beginning of chemical stream flow, 0.22 mg/m^3 GB. The black line overlaying the top frame is the humidity collected during these exposures. Filename: parallax_temp_22.txt

Figures 51 and 52 present the slopes from data collected during exposure to HD. Reponses to the low concentration exposures were not reported during the experiment and are not seen in Figure 51. While the humidity event at occurring at exposure 4 complicates analysis (described in the Results section), seats 2, 3, and 4 show a characteristic response at exposures 2, 4, 5, and 7. VX exposures did not produce characteristic responses on the device (Figure 53). Simulant exposures did not produced characteristics responses at the low concentration. A response pattern does emerge for seats 2, 3, 5, and 6 for the high concentration exposures.

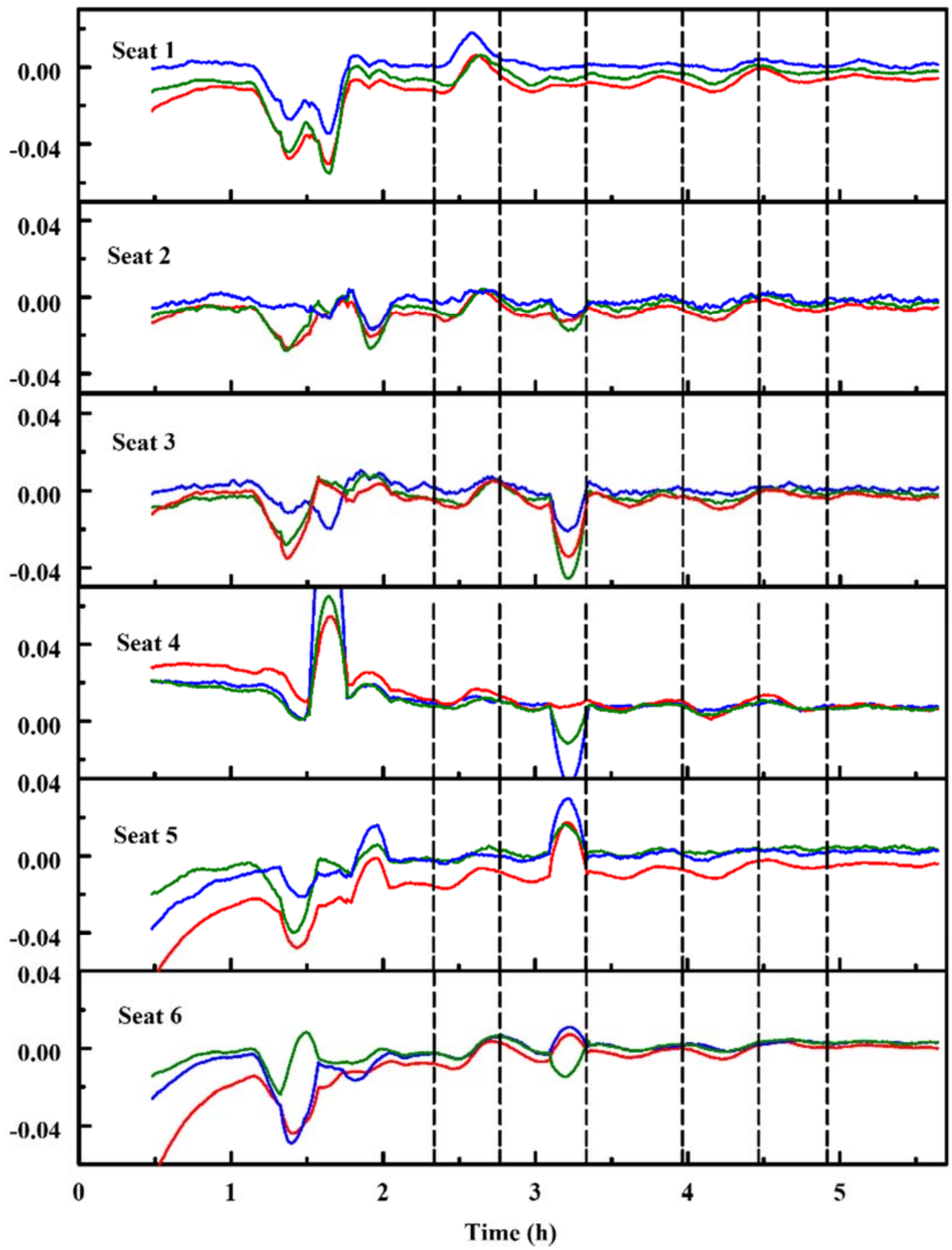

Fig. 51 — Slopes for HD Exposures. This data was collected on 07 December 2018 between 10:47 and 16:26. Here, a 30 point sliding window is applied to calculation of the slope. Prior to slope calculation, intensity values are normalized to the first intensity value for each color of each indicator. Dashed lines indicate the beginning of chemical stream flow, 1.2 mg/m^3 HD. Filename: parallax_temp_23.txt

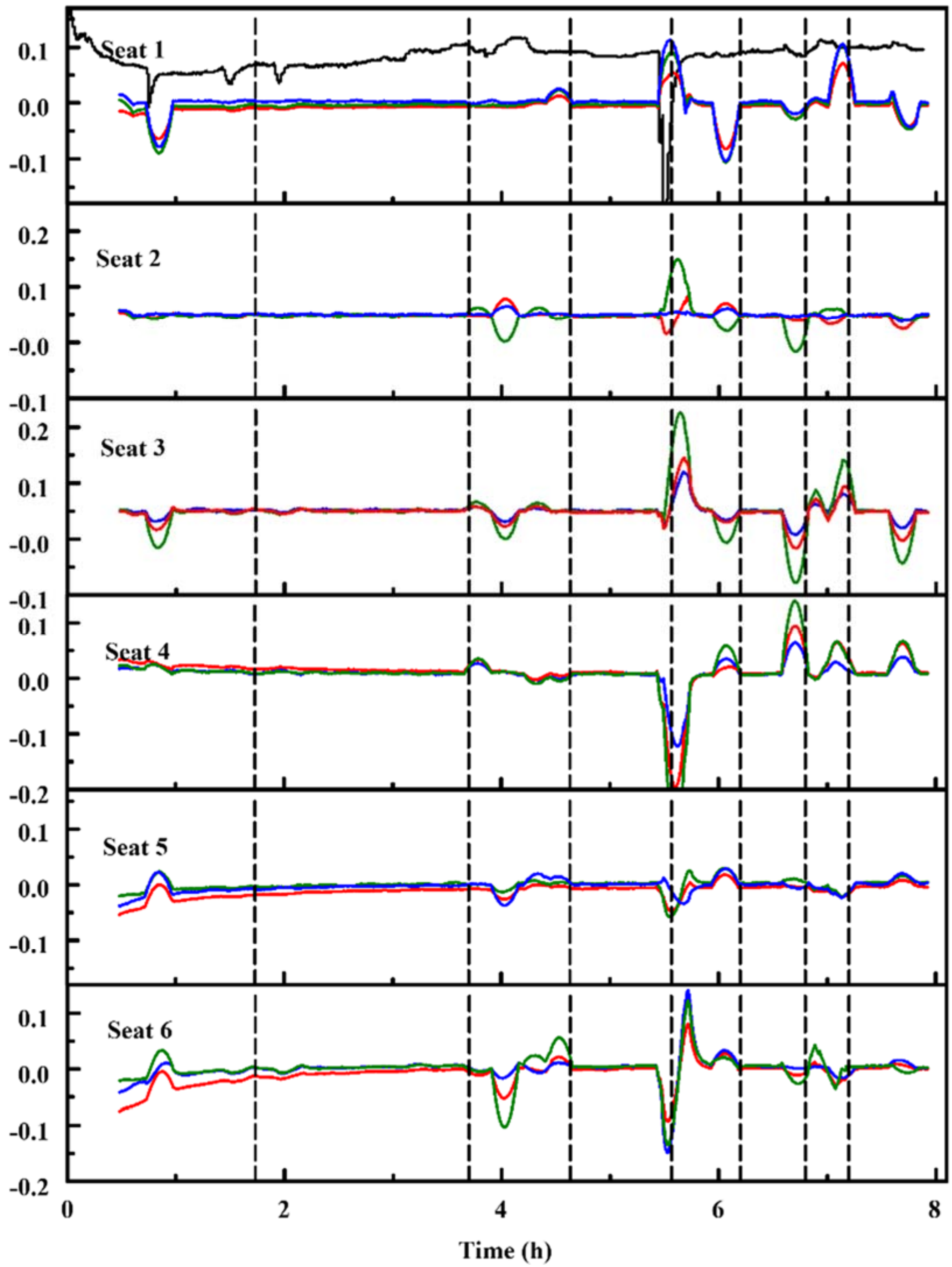

Fig. 52 — Slopes for HD Exposures. This data was collected on 10 December 2018 between 09:38 and 17:34. Here, a 30 point sliding window is applied to calculation of the slope. Prior to slope calculation, intensity values are normalized to the first intensity value for each color of each indicator. Dashed lines indicate the beginning of chemical stream flow, 2.5 mg/m^3 HD. The black line overlaying the top frame is the humidity collected during these exposures. Filename: parallax_temp_24.txt

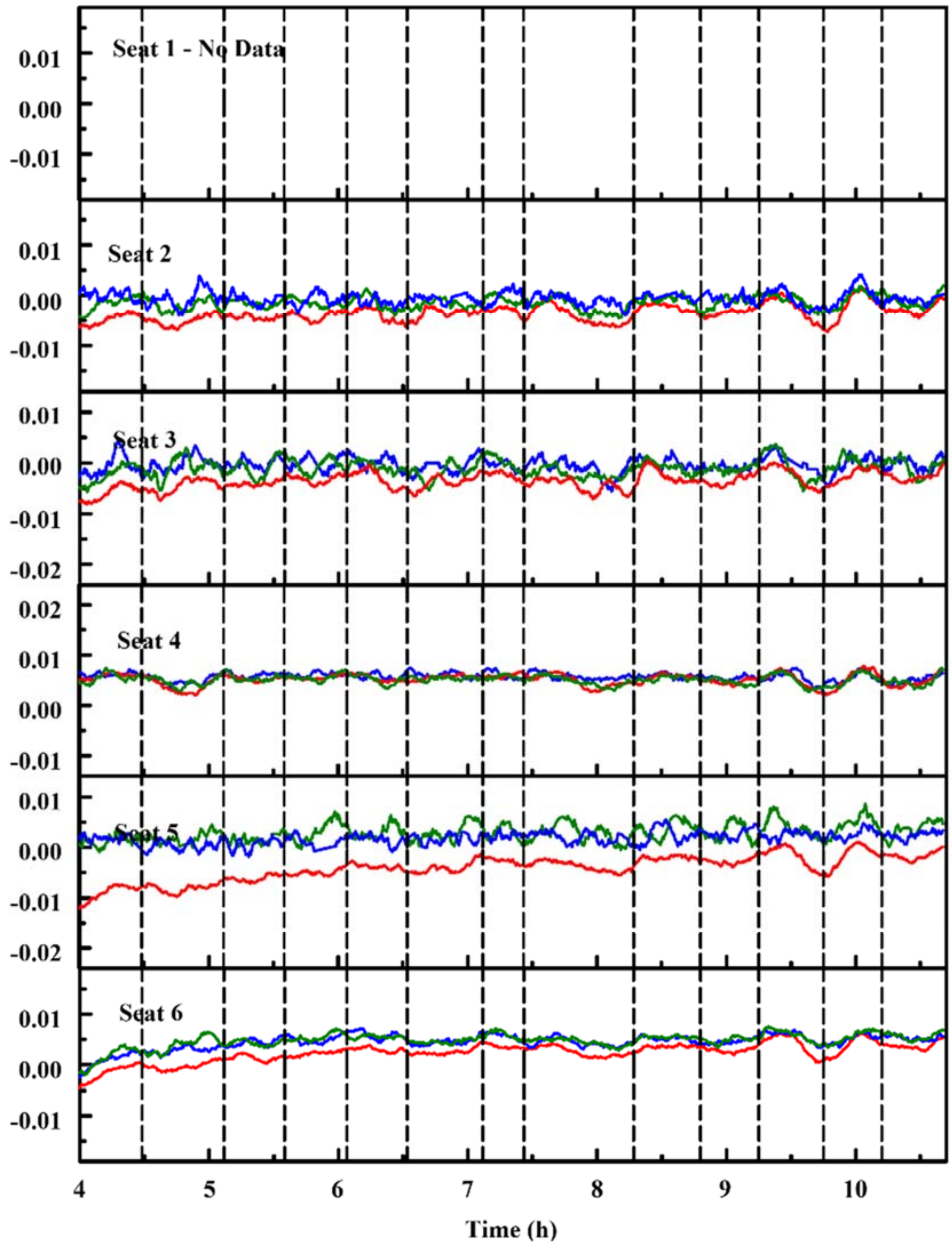

Fig. 53 — Slopes for VX Exposures. This data was collected on 13 December 2018 between 08:25 and 19:06. Here, a 30 point sliding window is applied to calculation of the slope. Prior to slope calculation, intensity values are normalized to the first intensity value for each color of each indicator. Dashed lines indicate the beginning of chemical stream flow, 0.013 and 0.022 mg/m^3 VX. Humidity and temperature are provided in Figure 35. Filename: parallax_temp_30.txt

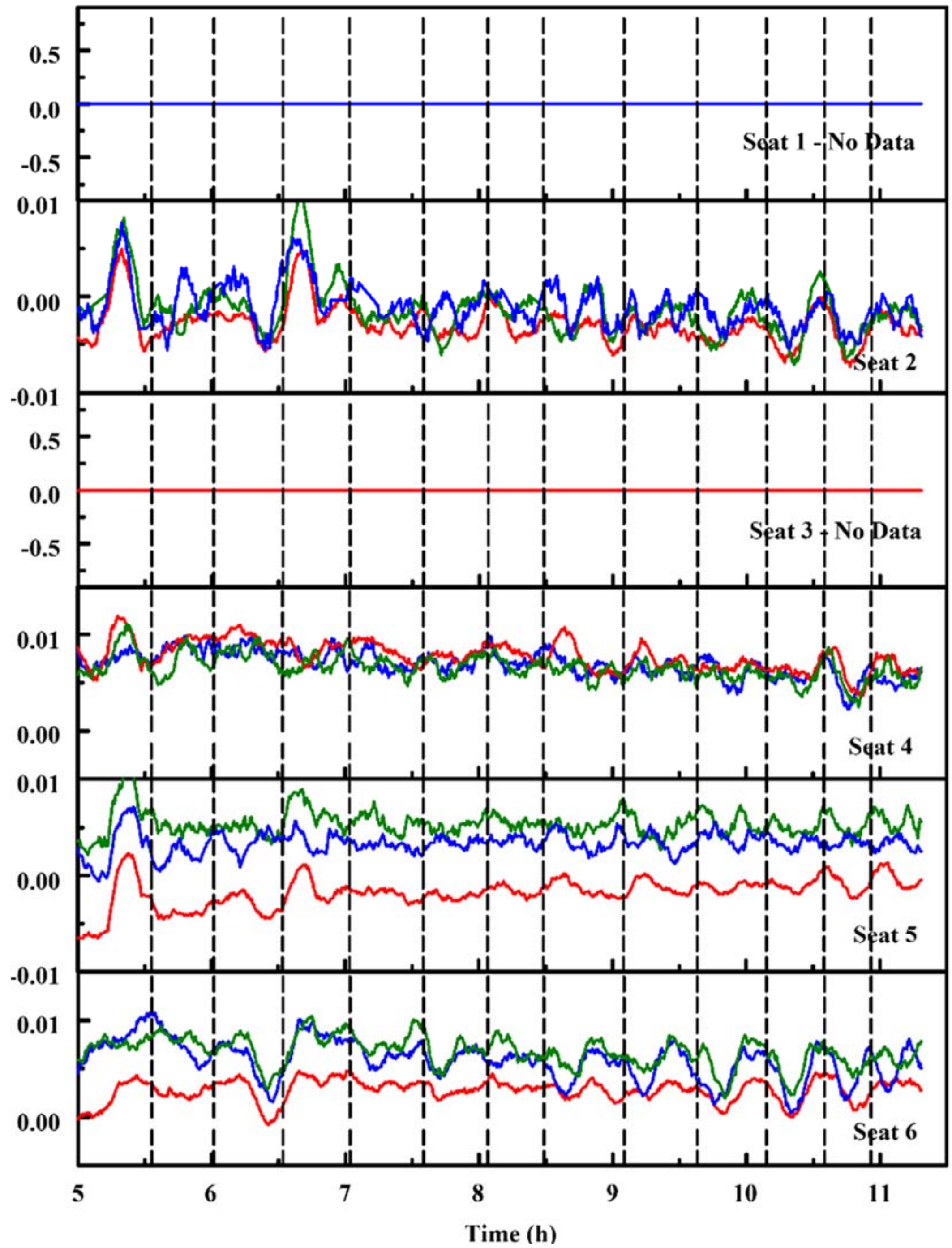

Fig. 54 — Slopes for Simulant Exposures. This data was collected on 14 December 2018 between 08:15 and 19:34. Here, a 30 point sliding window is applied to calculation of the slope. Prior to slope calculation, intensity values are normalized to the first intensity value for each color of each indicator. Dashed lines indicate the beginning of chemical stream flow, 0.013 and 0.022 mg/m^3 Simulant. Humidity and temperature are provided in Figure 39. Filename: parallax_temp_31.txt

While the automated version of the algorithm in the current form does not provide target identification, this is a planned component under ongoing development. While the final device implementation (see Conclusions) should offer a larger number of array elements, the potential of the device for target identification using a "fingerprint" type response can be demonstrated using the current dataset from the six element array. The slope responses have been binned to provide color maps of the responses (Tables 14 and 15). Data collected at the 5 s sample increment have been handled separately from that collected at the 30 s sampling increment. As shown in Table 14, there were no specific responses noted for exposures to the low concentration SO_2. At the high concentration, a pattern of response emerges with positive responses to six of the seven exposures. This pattern is distinct from that of the response to phosgene where we see seven positive responses to eight exposures at low concentration and seven positive responses to seven exposures at high concentration.

In Table 15, responses to Cl_2 exposure can be observed for four out of six low concentration exposures and four of four high concentration exposures. Recall, the device failed during the high concentration trials. This response pattern is distinct from that noted for responses to high HD concentrations (four of seven exposures detected). Low HD concentrations were not detected. This handling of the data did not yield positive responses for ethylene oxide, Simple Green, GB with Simple Green, VX, or Simulant.

Table 14 –Binned Response Summary from Post Experiment Slope Analysis, 5 s data. Bins used here are <0.025, 0.025 to 0.035, 0.035 to 0.045, 0.045 to 0.055, and >0.055.

Target	Exposure	N_4TPP	AgN_4TPP	ZnN_4TPP	AuDIX	TlDIX	YDIX
Sulfur dioxide (low)	1*	1	1	2	0	4	0
	2	0	0	0	0	0	0
	3	0	0	1	0	0	0
	4	0	0	0	0	0	0
	5	0	1	0	0	0	0
	6	0	0	0	0	0	0
Sulfur dioxide (high)	1*	1	2	1	1	2	3
	2	0	1	1	1	0	0
	3	0	1	1	0	0	1
	4	0	1	1	1	0	1
	5	0	0	0	0	0	0
	6	0	1	1	1	0	1
	7	0	1	1	1	0	0
Phosgene (low)	1*	3	0	0	0	0	0
	2	3	1	2	0	0	0
	3	4	4	4	2	3	3
	4	4	4	4	2	2	3
	5	3	4	3	1	1	2
	6	3	3	3	0	1	1
	7	2	3	2	0	0	0
	8	2	3	3	0	0	0
Phosgene (high)	1*	4	4	4	2	2	4
	2	4	4	4	4	4	4
	3	2	3	2	0	1	0
	4	3	3	2	0	1	1
	5	4	3	3	2	1	3
	6	3	3	3	4	1	1
	7	3	3	3	4	0	1

*First exposure of series compromised by background variations

Table 15 – Binned Response Summary from Post Experiment Slope Analysis, 30 s data. Bins used here are <0.043, 0.043 to 0.053, 0.053 to 0.063, 0.063 to 0.073, and >0.073.

Target	Exposure	N_4TPP	AgN_4TPP	ZnN_4TPP	AuDIX	TlDIX	YDIX
Ethylene oxide (low)	No Responses						
Ethylene oxide (high)	No Responses						
Simple Green	No Responses						
GB with Simple Green	1[ε]	4	1	1	1	2	2
	2 - 7	No Responses					
HD (low)	2	0	0	1	1	0	0
	1, 3 - 7	No Responses					
HD (high)	1	0	0	0	0	0	0
	2	0	1	1	1	0	3
	3	4	1	2	4	0	4
	4[ε]	4	2	4	4	4	4
	5	0	1	3	4	0	0
	6	4	0	3	2	0	2
	7	4	1	4	2	0	0
Cl_2 (low)	1	4	4	4	0	2	4
	2	2	2	2	0	2	4
	3	1	1	1	0	1	2
	4	0	0	1	0	0	0
	5	2	1	1	0	1	1
	6	0	0	0	0	0	0
Cl_2 (high)[*]	1	4	3	3	0	1	1
	1[ε]	4	4	4	3	2	4
	2	4	4	4	0	2	3
	3	4	4	4	0	4	4
VX (low)[†]	No Responses						
VX (high)[†]	No Responses						
Simulant (low)[γ]	No Responses						
Simulant (high)[γ]	No Responses						

[*]Exposures after device failure have been omitted. [†]Completed with five indicators due to board damage. [γ]Completed with four indicators due to board damage. [ε]Exposure compromised by background variations.

In Table 16, 30 s data has been reprocessed using a different set of bins. In this analysis, ethylene oxide is detected in five of nine low concentration exposures and five of six high concentration exposures with a clear pattern emerging for this response. Simple Green is detected by a single seat in two of six exposures (seat #2). GB with Simple Green produces positive responses in six of seven exposures, though a clear pattern of responses is not noted. Positive responses are noted for three of six low concentration HD exposures and seven of seven high concentration HD exposures. Positive responses are noted for all of the Cl_2 exposures. The events for HD and Cl_2 tend to involve all of the indicators in the array. VX is detected in four of six low concentration and five of six high concentration exposures and produces a pattern distinct from that of the other targets including the Simulant. Simulant is detected in five of six low concentration and four of six high concentration exposures.

Table 16 – Binned Response Summary from Post Experiment Slope Analysis, 30 s data. Bins used here are <0.006, 0.006 to 0.016, 0.016 to 0.026, 0.026 to 0.036, and >0.036.

Target	Exposure	N_4TPP	AgN_4TPP	ZnN_4TPP	AuDIX	TlDIX	YDIX
Ethylene oxide (low)	1^{ε}	1	1	1	0	0	1
	2	0	0	0	0	0	0
	3	1	1	1	0	0	1
	4	2	1	2	0	0	1
	5	0	0	0	0	0	0
	1	0	0	0	0	0	0
	2	1	1	1	0	0	1
	3	1	1	1	0	0	0
	4	1	1	1	0	0	0
Ethylene oxide (high)	1^{ε}	2	1	1	0	2	2
	2	1	1	1	0	0	1
	3	1	0	0	0	0	0
	4	1	1	1	0	0	1
	5	1	1	1	0	0	0
	6	1	1	1	0	0	1
Simple Green	1^{ε}	0	1	0	0	0	0
	2	0	1	0	0	0	0
	3 - 6	No Responses					
GB with Simple Green	1^{ε}	4	4	4	4	4	4
	2	0	1	0	0	1	0
	3	0	1	1	1	1	0
	4	2	2	2	1	0	1
	5	0	0	0	0	0	0
	6	1	1	1	2	1	1
	7	1	1	1	2	1	1
HD (low)	1	2	1	1	1	1	1
	2	1	1	4	3	3	2
	3	0	0	0	1	0	0
	4	1	1	1	1	1	0
	5	0	0	0	1	0	0
	6	0	0	0	0	0	0
HD (high)	1	0	0	1	1	1	1
	2	3	3	4	4	3	4
	3	4	3	3	4	4	4
	4^{ε}	4	3	4	4	4	4
	5	3	2	4	4	1	2
	6	4	2	4	4	2	4
	7	4	2	4	4	3	2
Cl_2 (low)	1	4	4	4	2	4	4
	2	4	4	4	2	3	4
	3	4	2	2	2	2	4
	4	3	2	2	1	2	3
	5	4	3	3	2	2	3
	6	3	2	2	1	2	2

Cl_2 (high)*	1	4	4	4	3	3	4
	1ε	4	4	4	3	4	4
	2	4	4	4	3	3	4
	3	4	4	4	2	4	4
VX (low)†	1		1	1	0	0	0
	2		0	1	0	0	0
	3		0	1	0	1	0
	4		0	0	0	0	0
	5		0	1	0	1	0
	6		0	0	0	0	0
VX (high)†	1		1	1	0	1	0
	2		0	0	0	1	0
	3		1	1	0	1	0
	4		1	1	0	1	0
	5		1	1	0	1	0
	6		1	1	0	1	0
Simulant (low)γ	1		1		0	0	1
	2		1		0	0	1
	3		1		0	0	0
	4		1		0	0	1
	5		1		0	0	0
	6		0		0	0	0
Simulant (high)γ	1		1		0	0	1
	2		0		0	0	0
	3		1		0	0	1
	4		1		0	0	1
	5		1		0	0	1
	6		0		0	0	0

†Completed with five indicators due to board damage. γCompleted with four indicators due to board damage. εFirst exposure of series compromised by background variations.

CONCLUSIONS

The prototype device used for this series of evaluations was designed for long term environmental monitoring, rather than for use in a wearable format. The automated detection algorithm applied with the device was focused on meeting the needs of this long term application rather than those of the CVCAD program. Only minimal changes were made to accommodate the goals of the evaluations described here. While the test methodology employed represented an efficient use of time and resources, these types of serial exposures complicated analysis and may not reflect a typical device usage scenario. A final complication in the datasets results from the use of the fans onboard the prototype device to drive air flow through the entire experimental module. This type of additional load on the device was not tested previously and may have altered observed behaviors. It certainly impacted the data used to populate the Background windows within the onboard algorithm. Nevertheless, the sensor device with previously designed algorithm was able to achieve detection of some of the targets evaluated. Post experiment analysis of the data was able to capture behaviors that were not captured by the onboard algorithm. This analysis significantly improved the overall performance of the device under these evaluations (Table 17).

Table 17. Post Processing Performance Summary

Target	**Total Exposures**	**Original Algorithm Report**	**Post-Analysis Detection**
100 ms integration, 5 s sampling increment			
SO_2, 1.5 ppm	6	1	0
SO_2, 30 ppm	7	0	6
Phosgene, 1.2 ppm	8	6	7
Phosgene, 7.4 ppm	8	5	7
500 ms integration, 30 s sampling increment			
Ethylene oxide, 78 ppm	9	1	5
Ethylene oxide, 361 ppm	6	0	5
Simple Green	6	3	0
GB, 0.22 mg/m^3 (Simple Green)	7	1	6
HD, 1.2 mg/m^3	6	0	3
HD, 2.5 mg/m^3	7	5	7
Cl_2, 5 ppm	6	6	6
Cl_2, 100 ppm	4	4	4
VX, 0.013 mg/m^3	6	0	4
VX, 0.022 mg/m^3	6	0	5
Simulant, 0.013 mg/m^3	6	0	5
Simulant, 0.022 mg/m^3	6	0	4

This post experiment analysis does not lend itself to the type of time to response calculations used with the automated algorithm, so no values are reported here. It should be noted that the time to detection is not limited by the indicator materials in this device. Time to detection can be altered through changing the frequency of sampling (using 15 s or 5 s, rather than 30 s). Moving forward in prototype iterations, NRL is considering hardware that allows for simultaneous sampling of all of the indicators. This would provide the increased integration time desired without an associated sampling time increase. The number of time points used in the algorithm also impact the time to detection and the sensitivity. Use of more time points increases sensitivity but lengthens the time to detection.

A follow-on iteration of the prototype device is currently being evaluated by NRL. This iteration provides isolation of the electronics from the environment as well as from targets. This type of isolation would have prevented the failure of the prototype during Cl_2 exposures and would be expected to extend overall device durability. While device failures within the evaluations described here represent missed opportunities, they are not entirely unexpected for a prototype device at this engineering iteration. Beyond protection of the electronic components, the new device iteration being evaluated provides an array of 15 indicators, occupying a footprint of 2.5” x 7” x 3.25” at a weight of 293 g (1,290 g with battery pack; Figure 55). For comparison, the prototype used under the current study was 10.8” x 3” x 3” and weighed 1,585 g as well as requiring an external power source. Incorporation of 15 indicators provides the potential for greater target discrimination through expansion of the number of array elements. For example, indicators with greater sensitivity to VX and Simulant could improve performance against those targets. Indicators with lesser sensitivity to Cl_2 and HD could be used to provide improved distinction between those targets.

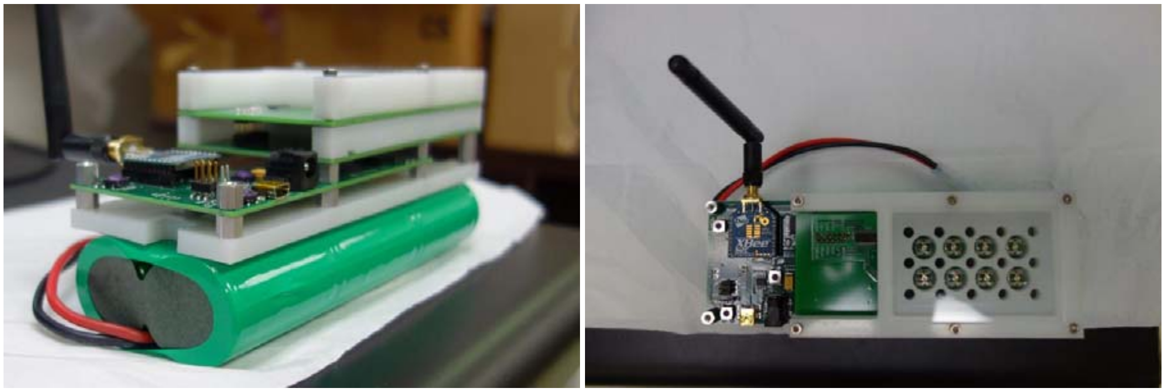

Fig. 55 — The new iteration prototype device includes fifteen surface mount color sensors with custom control board and can be powered using a battery pack.

ACKNOWLEDGEMENTS

Development of prototype and algorithms was sponsored by the Office of Naval Research through NRL base funding (WU#69-6A27, 69-6A26, and 69-6954). Evaluation of the device was supported by the Joint Project Manager for Nuclear, Biological and Chemical Contamination Avoidance (JPM NBC CA; Solicitation Number W911SR-18-R-CVCA). The authors would like to thank M.B. Tabacco and H. Huang of Smiths Detection, Inc (Edgewood, MD) for their support through this process. Data presented here was collected by the JPM / ECBC team; their support and cooperation throughout this process is greatly appreciated.

REFERENCES

1. Johnson, B.J.; Erickson, J.S.; Kim, J.; Malanoski, A.P.; Leska, I.A.; Monk, S.M.; Edwards, D.J.; Young, T.N.; Verbarg, J.; Bovais, C.; Russell, R.D.; Stenger, D.A. Miniaturized reflectance devices for chemical sensing. *Meas. Sci. Technol.* **2014**, *25*.
2. Johnson, B.J.; Liu, R.; Neblett, R.C.; Malanoski, A.P.; Xu, M.; Erickson, J.S.; Zang, L.; Stenger, D.A.; Moore, M.H. Reflectance-based detection of oxidizers in ambient air. *Sens. Actuator B-Chem.* **2016**, *227*, 399-402.
3. Erickson, J.; Malanoski, A.; White, B.; Stenger, D.; Tankard, E. Practical Implementation of Detection Algorithm for Reflectance-Based, Real-Time Sensing; US Naval Research Laboratory, Washington, DC, **2018**, NRL/MR/6930--18-9812.
4. Johnson, B.J.; Malanoski, A.P.; Erickson, J.S.; Liu, R.; Remenapp, A.R.; Stenger, D.A.; Moore, M.H. Reflectance-based detection for long term environmental monitoring. *Heliyon* **2017**, *3*, e00312.
5. Malanoski, A.P.; Johnson, B.J.; Erickson, J.S.; Stenger, D.A. Development of a Detection Algorithm for Use with Reflectance-Based, Real-Time Chemical Sensing. *Sensors* **2016**, *16(11)*, 1927.